UTAH GEOLOGY

UTAH GEOLOGICAL AND MINERAL SURVEY
a division of the
UTAH DEPARTMENT OF NATURAL RESOURCES

Vol. 5, No. 1, Spring, 1978

Utah Geology

Vol. 5, No. 1, Spring, 1978

STATE OF UTAH
Scott M. Matheson, Governor

DEPARTMENT OF NATURAL RESOURCES
Gordon E. Harmston, Executive Director

UTAH GEOLOGICAL AND MINERAL SURVEY
Donald T. McMillan, Director

Utah Geology

Vol. 5, No. 1 Spring, 1978

CONTENTS

Cover scenes from photos of old Gold Hill Mining camp. "What's Next Dr. Peck" by Joseph H. Peck, M.D., 1959, Prentiss-Hall. Sketches by Greg McLaughlin.

INFORMATION FOR CONTRIBUTORS

UTAH GEOLOGY is published two times a year and contains short scientific papers dealing with some aspect of the geology of Utah.

The Utah Geological and Mineral Survey invites authors to submit their papers for publication in UTAH GEOLOGY. Manuscripts should be submitted to the Editor, UTAH GEOLOGY, 606 Black Hawk Way, Salt Lake City, Utah 84108.

Papers should be not more than 60 pages in length, typewritten and double-spaced, with no words split at the ends of lines. The form should be that generally accepted by the U. S. Geological Survey, the Geological Society of America, or that in a recent issue of UTAH GEOLOGY. Include a table of contents and lists of tables and illustrations, with captions and the page number on which each is first mentioned, in the order of their appearance.

All illustrations and tables must be complete and clearly labeled, be on separate pages, and be referred to in the text. The place at which they are to appear in the text should be indicated. Plan illustrations to fit page size (18.5 x 22 cm or 7¼ x 9½ inches), single column width (5.75 cm or 2 5/16 inch), or two column width (12.2 cm or 4 13/16 inch). Extreme reduction should be avoided.

Photographs should be oversized, good quality, black and white glossy prints. Any lettering or lines should be made on an attached transparent overlay.

Measurements should be given in the metric system, with English equivalents given in parentheses. Exceptions are original data with many measurements made in English units, such as drill hole data.

All material not the original work of the author must be properly credited and necessary permission obtained for its use. The list of references to writings or maps of other authors must be complete and accurate, with the names of the publications spelled out.

The author should retain a copy of his manuscript and illustrations, as the Utah Geological and Mineral Survey can not be responsible for material lost in the mails. Original illustrations and photos will be sent at the owners risk; they will be carefully handled and returned on request, but the Utah Geological and Mineral Survey can not assume liability for loss or damage.

Papers will be read for scientific content, originality, and clarity of presentation, and may be returned to the author for his approval of any suggested changes or for necessary revision. Once both the author and editor are satisfied with the paper, it will be considered correct, complete, and ready for printing. A galley proof will be prepared and returned to the author, who should read it carefully for any errors or omissions in the text, tables, illustrations, legends, and bibliographic references. The author should make necessary corrections on the galley and return it to the editor. Since changes are costly and time-consuming, the cost of additions or changes not the responsibility of the editorial office must be assumed by the author.

Twenty five reprints will be provided free of charge for each published paper. Additional copies can be ordered from the publisher at cost; information will be provided to the authors before publication.

SUBSCRIPTION INFORMATION

Subscriptions to UTAH GEOLOGY are $7.00 per year (for two issues); $13.00 for two years, and $18.00 for three years. Single issues are available for $4.00. Send orders for subscriptions to:

Publication Sales Office
Utah Geological and Mineral Survey
606 Black Hawk Way
Salt Lake City, Utah 84108

A LEAD AND STRONTIUM ISOTOPIC STUDY OF IGNEOUS ROCKS AND ORES FROM THE GOLD HILL MINING DISTRICT, UTAH

J. S. Stacey[1] *and R. E. Zartman*[1]

ABSTRACT

A multistage model is presented to account for the different lead isotopic compositons of the northern and southern parts of the Gold Hill stock. The stock was found actually to be two bodies of different ages - Oligocene in the north (38 m. y.) and Jurassic in the south (152 m.y.). Initial $^{87}Sr/^{86}Sr$ ratios computed from measurements made on the intrusive rocks are 0.715 ± 0.001 for the north and 0.709 ± 0.001 for the south.

Lead in the northern intrusion at Gold Hill and 100 km eastwards in the Oquirrh Mountains region is shown by the model to have originated in an Archean upper crustal environment (determined $\mu = {}^{238}U/{}^{204}Pb \approx 12$) from 2.7 b.y. to 1.65 b.y. ago. Subsequently, this lead was incorporated in 1.65 b.y. lower crust and subjected to granulite or higher rank metamorphism (determined $\mu \approx 4$ to 7), and remained there until being remobilized in the Oligocene by plutonic activity.

The ore and feldspar lead in the southern intrusion at Gold Hill, however, seems to have remained in upper crustal environments ($\mu \approx 12$) continuously since 2.7 b.y. ago (e.g., there was no high rank metamorphism of this material in the Precambrian) until being remobilized in Jurassic time. By implication, this must apply to much of the miogeosynclinal material of similar lead isotopic composition found westwards in Nevada.

INTRODUCTION

The purpose of this paper is to examine the lead and strontium isotopic characteristics of rocks and ores from the Gold Hill mining district in west- central Utah. Supplemental to the study of isotopic composition, we report some new radiometric ages that provide insight into the timing of igneous activity. The Gold Hill district lies near the western edge of the North American craton, within the transition zone between a shelf-type sedimentary environment and the substantially thicker miogeosynclinal rocks of the Cordilleran geosyncline existing to the west. The craton in this vicinity contains the boundary between two major Precambrian age provinces — a feature that provides further complications to the lead isotopic systematics.

It has been apparent for some years that regional patterns of lead isotopic composition are exhibited by the rocks and ores of the western United States (Doe, 1967; Stacey and others, 1968). More recently Zartman (1974) has synthesized the available data and has delineated the boundaries between several regions of differing isotopic behavior, (inset, figure 1). Table 1 summarizes the geologic and isotopic characteristics of each region that form the basis of his classification. Subsequently, Doe and Zartman (1978) have derived a model to interpret lead isotopic behavior in terms of the geochemical cycle of uranium, thorium and lead in a dynamic evolving earth. Some of the concepts of that work will be utilized in our interpretation of the Gold Hill data.

The Gold Hill mining district was chosen because available data had indicated that it occurs in a transition zone between two important types of lead behavior. Lead isotope data from the ores in the Oquirrh Mountains and Tintic mining districts to the east in central Utah exhibit linear arrays on both the $^{207}Pb/^{204}Pb$ and $^{208}Pb/^{204}Pb$ - $^{206}Pb/^{204}Pb$ plots (Stacey and others, 1968). Immediately to the west of Gold Hill, ores from White Pine County, Nevada, show a much more uniform composition (Rye et al., 1974). Thus, somewhere between these localities the linear array representing two-stage lead isotope behavior of Area I degenerates into an essentially uniform isotopic composition that is characteristic of Area II. Also, because the lead in igneous rocks and major ore bodies in the Oquirrh Mountains and Tintic Districts is distinctly less radiogenic than the corresponding lead in White Pine County, Nevada, there must exist a fundamental difference between the source materials of these two areas.

Throughout this study we have relied heavily on published geologic literature of the area, especially Nolan (1935) and El-Shatoury and Whelan (1970), to which the reader is referred. At Gold Hill the sedimentary rocks, which are predominantly limestones, sandstones, and shale, have a thickness in excess of 10,000 m and range in age from Cambrian to Triassic. They have been strongly deformed in several stages during Late Jurassic through Late Tertiary times. Nolan (1935) concluded that it was towards the end of this period that the sedimentary rocks were intruded by the quartz monzonite Gold Hill stock.

A wide variety of mineral deposits, including base and precious metals, beryllium, and tungsten, are associated with this igneous activity. Post-dating the intrusion are a series of Pliocene volcanic and pyroclastic rocks ranging from rhyolites to basalts. One of the purposes of this paper is to investigate further the relationship between the igneous rocks and the lead-bearing deposits in this mining district.

REGIONAL GEOLOGY

Throughout much of Utah, the existence of crystalline Precambrian basement is well established from outcrops in a number of basin ranges. These rocks maintain much of their original Precambrian textures essentially free of subsequent recrystallization. In contrast, little evidence exists to indicate an equivalent preservation of basement structure under Nevada. Where Precambrian rocks may exist in Nevada, such as in the Snake

[1]U. S. Geological Survey
Denver Federal Center
Denver, Colorado 80225

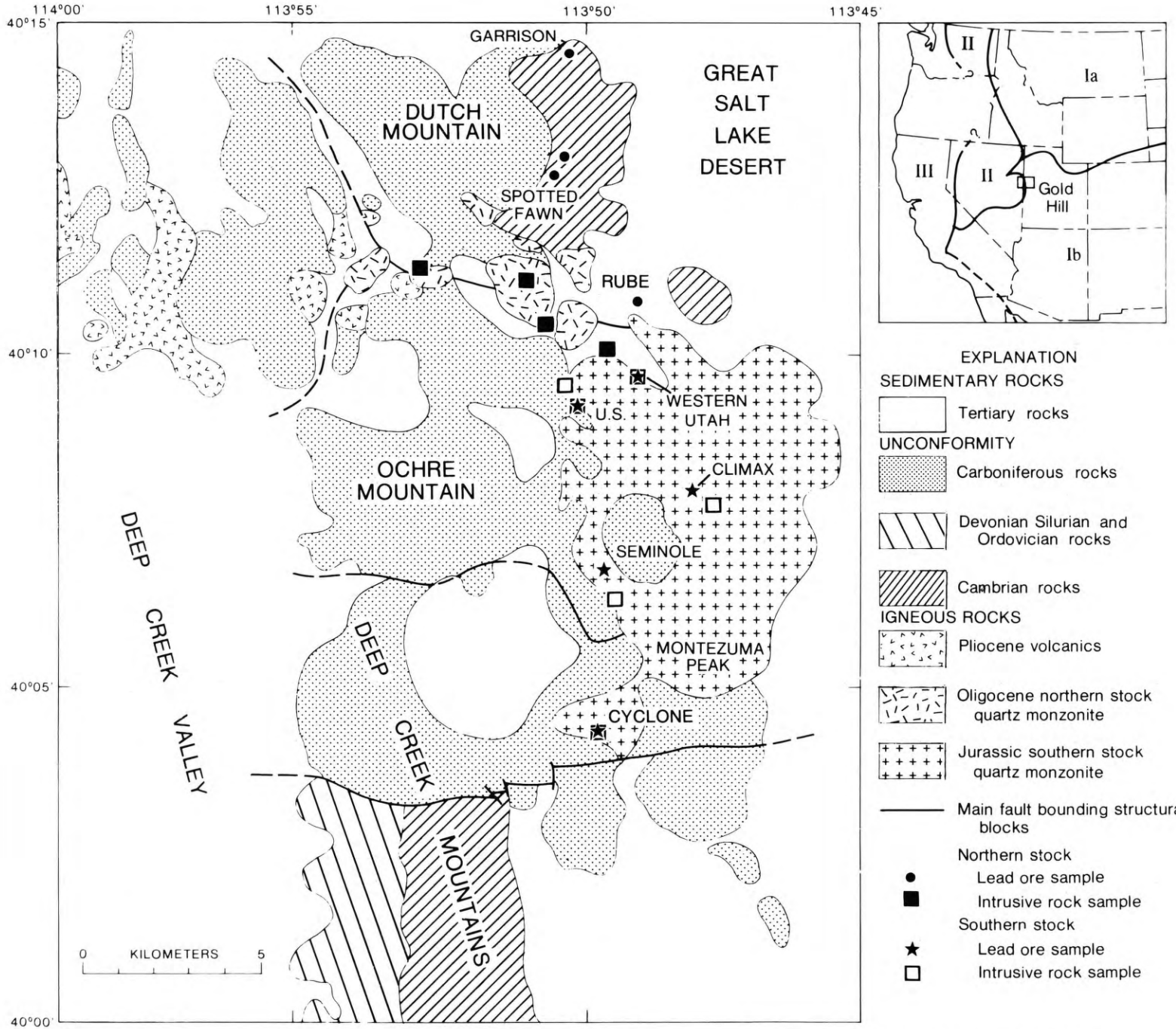

Figure 1. Outcrop map of the Gold Hill mining district, simplified from Nolan (1935). Inset shows location of the district and the boundaries of Areas I, II, and III--each of which exhibit fundamentally different lead isotope characteristics. Area Ia - "continental" 2700 m.y. or older; Area Ib - "continental" 1800 m.y. or younger; Area II - "miogeosynclinal"; Area III - "eugeosynclinal".

Table 1: Lead Isotopic Characteristics for a Regional Classification of the Western United States, from Zartman (1974).

Province and type	Normal isotopic range $^{206}Pb/^{204}Pb$	$^{208}Pb/^{204}Pb$	Lead isotope characteristics	Source material
Area I				
Rocks	16.2-18.8	36.5-39.9	Comparatively unradiogenic; fairly wide range in isotopic composition	Precambrian crystalline basement rocks of the lower crust or, possibly, the mantle.
Ores	16.6-24+	36.8-42+	Extreme range in isotopic composition. Linear arrays within mining districts on $^{206}Pb/^{204}Pb$ vs. $^{207}Pb/^{204}Pb$ diagrams Large, hypothermal deposits are least radiogenic; small or peripheral deposits are most radiogenic	As above, with variable amount of radiogenic lead addition from upper crustal rocks.
Area II				
Rocks	19.1-19.7	38.9-40.3	Comparatively radiogenic; small range in isotopic composition.	Isotopically homogenized miogeosynclinal sedimentary rocks eroded from the adjacent Precambrian sialic upper crust.
Ores			Similar to the rocks.	Similar to the rocks.
Area III				
Rocks	18.7-19.4	38.2-39.1	Intermediate between lead of Areas I and II; small range in isotopic composition.	Eugeosynclinal plutonic, volcanic, and sedimentary rocks, possibly associated with subduction processes.
Ores			Only a few analyses of ore lead available, apparently similar to the rocks.	

River and the Ruby Mountains, they have undergone extensive recrystallization during one or more periods of Phanerozoic deformation.

To the east of Gold Hill, the Ordovician to Mississippian sedimentary rocks are predominantly carbonates with minor amounts of quartzites and shales, having a typical aggregate thickness of approximately 10,000 m. Such shelf type rocks grade westwards into a miogeosynclinal sequence with increasing thickness up to 20,000 m along the axis of the Cordilleran geosyncline in central Nevada. There, the miogeosynclinal rocks, by facies change and tectonic superposition, give way to a eugeosynclinal sequence of graywackes, cherts, sandstones, and intercalated volcanics.

The area comprising western Utah and much of Nevada has been the site of repeated orogeny since early Paleozoic time (Gilluly, 1965). Major thrusting and telescoping of lower and middle paleozoic rocks took place during the Late Devonian to Early Mississippian Antler orogeny in Nevada (Roberts and others, 1958). Deformation also occurred during the Late Jurassic through Cretaceous (Sevier) and the Late Cretaceous to Paleocene (Laramide) orogenies in eastern Nevada and western Utah. Since Oligocene time, this terrane has been subjected to tensional forces, possibly due to the counter-clockwise rotation of the Sierra Nevada Mountains away from the continental interior (Hamilton and Meyers, 1966). The resulting crustal extension has formed the complex north-south trending system of block-faulting that comprises the present Basin and Range province. Although this faulting has added further complexity to the region, it has yielded some three-dimensional glimpses of the structures at scattered points throughout the area.

Volcanic and plutonic rocks occur ubiquitously throughout western Utah and Nevada. Extensive geochronologic work in recent years has greatly increased our knowledge of the timing of igneous activity (Armstrong, 1970; Armstrong and others, 1969). We now know that this activity spanned much of Mesozoic and Cenozoic time, and produced a complex spatial-temporal pattern throughout the western U.S.A. Even within restricted areas such as the one under study here, it is not unusual to find several periods of intrusion and/or volcanism represented.

Much of the mineralization in the Basin and Range province has been considered to be related in a general way to the igneous activity. However, only a few detailed isotopic and dating studies have sought to verify specific associations (Stacey and others, 1968; Moore and others, 1968).

From the brief preceding discussion it is apparent that the transition zone in lead isotopic composition between eastern Nevada and western Utah roughly coincides with the westward disappearance of a continental basement, and the facies changes in the overlying sedimentary rocks. Other features such as the

structural complexities of the rocks resulting from Phanerozoic tectonism and the distribution of igneous rocks cannot yet be clearly related to this transition.

ANALYTICAL TECHNIQUES

All feldspar lead and uranium–thorium chemical separations were made using standard ion column procedures. In the case of lead, these were followed by an electroplating step. Feldspar lead was analyzed in the mass spectrometer using the single filament, silica gel method (Cameron and others, 1969) and galena was analyzed by the triple filament procedure originated by Catanzaro (1969). All samples were analyzed twice in a 30 cm radium, 68° sector mass spectrometer, yielding precisions of less than ± 0.1 percent for all ratios with respect to ^{204}Pb at the 95% level of confidence. All isotope ratios have been normalized to absolute values by comparison with the NBS common lead standard SRM 981 (Catanzaro and others, 1968).

PETROLOGIC RELATIONS AND ISOTOPIC DATA

Very early in our study, it became apparent that the Gold Hill stock might be a composite intrusion formed from two different magma sources. K-feldspar was separated from samples of igneous rocks that were representative of the whole exposed area of the stock. Isotopic analyses were made on the lead from these feldspars, and the data were found to form two distinct groups (figure 2; table 2). These groups correspond to a geographical division in which the least radiogenic feldspars are from the north. Lead isotope analyses of galenas from across the district also suggest a north–south dichotomy (table 3; figure 2).

These results prompted us to examine more closely the assumption of earlier workers that the Gold Hill stock did, in fact, represent a single magmatic episode. Our suspicions that this might not be so were reinforced by a distinctly bimodal appearance of the hand specimens that also corresponds to the two different lead isotopic groups. Nolan (personal communication) noticed this difference in appearance during his original work in the area, but at that time there were no analytical techniques available to further differentiate the groups. In all aspects of the investigation, both in the field and the laboratory, this dichotomy in the intrusive rocks became a prime element of the study.

Nolan (1935) assigned a post–Eocene, pre-Late Pliocene age to the Gold Hill stock because it metamorphozed the White Sage Formation and is overlain uncomformably by younger volcanic rocks. These observations were made in the northwest part of the stock and might not necessarily apply elsewhere. Therefore, in our study, K-Ar biotite and Rb-Sr whole rock analyses were made on some of the granitic rocks to determine if an age difference exists between the northern and southern parts of the district. Two K-Ar biotite analyses yielded an average of 38.5± 1 m.y. for the northern quartz monzonite (table 4). Two samples from the south, however, yield an average K-Ar biotite age of 152± 4 m.y. (table 4). Thus there are actually two stocks present in the district that have quite different ages, Jurassic in the south and Oligocene in the north.

Whole rock samples from both intrusions, while having Rb/Sr ratios too low to provide meaningful ages, did define average initial $^{87}Sr/^{86}Sr$ values for the two groups. Whole rocks from the north have an initial $^{87}Sr/^{86}Sr$ value of 0.715 ± 0.001 and those from the south yield 0.709 ± 0.001 (table 5, figure 3).

The northern ore lead data, table 3, exhibit a linear trend on each plot of figure 2, which we interpret as indicating a genetic relationship between all four samples, a relationship typical for Area 1 type ore lead derived from continental Precambrian basement. The least radiogenic of these ore samples is from the Garrison mine in the northeast corner of the district (figure 1). This ore lead itself belongs to Area I type, as does the feldspar lead from the northern intrustion. However, the higher $^{207}Pb/^{204}Pb$ and especially the higher $^{208}Pb/^{204}Pb$ ratios from the feldspars (figure 2) indicate that the ores cannot be directly derived from the northern stock. Thus it is not surprising to find that none of the "northern" deposits is actually emplaced in the northern intrusion itself. Rather, there seems to be a broad halo of hydrothermally altered rock that extends for several kilometers east and north of the Gold Hill district. Only scattered porphyry dikes offer evidence of igneous activity as far north as the Garrison mine.

In the southern portion of the district, the lead isotope ratios from both ores and intrusive feldspars exhibit a homogeneous pattern that is typical of Area II type lead. Here indeed the ores do seem to be directly related to the intrusion. In addition, because the southern ore data lie above the linear trend for the northern ores on each of the plots in figure 2, no direct genetic relationship can be inferred from lead isotopes between the southern and northern ore deposits. [1] The lead isotopic composition of sample 42 is significantly more radiogenic than is the lead in the other southern feldspars (figure 4). This sample is situated close to the boundary with the Oligocene stock, and also close to the Rube mine that we associate with Oligocene mineralization. It would therefore seem that radiogenic lead in the total rock of sample 42 was redistributed into the feldspar at the time of the Oligocene intrusion.

The most probable location of a boundary between the two intrusive bodies can be interred from figure 4. The actual contact is apparently not exposed, but must closely follow the alluvium–filled wash that runs northeast from Gold Hill. In addition to the isotopic and radiometric criteria distinguishing the two bodies, we have come to recognize several petrologic features useful to field mapping. The dominant rock in the northern body is a light-to-medium pinkish gray, medium-grained quartz-monzonite. It possesses a distinct mottling due to ferromagnesium minerals. Not uncommonly, the quartz monzonite has suffered some deuteric alteration with the feldspars taking on a chalky appearance, and the hornblende and biotite altering to chlorite and sericite. As was noted by Nolan (1935), abundant aplite dikes are associated with the northern body but rarely continue beyond the margins of the intrusion into the country rock.

Except for some local variants, the southern body is comprised of a medium to dark gray, medium-grained granodiorite. The distinctly deep violet color of the potassium feldspar in this rock is a diagnostic characteristic of the older intrusion. Although the same ferromagnesium minerals hornblend and biotite, occur in both bodies, they are generally more abundant in the southern body. Unlike the mineralization accompanying the northern body, the major ore fluids here appear to have been confined to the intrusion and immediate wall rocks, which have been altered by contact metamorphism. In the vicinity of mineralized areas, extensive aureoles of silicified, sericitzed, and chloritized rock surround the ore deposits.

---

[1] Although the shift in the $^{207}Pb/^{204}Pb$ ratios is comparatively small, this ratio is a very sensitive indicator of the genetic history of lead samples. In this case the difference shown in the lower plot of figure 2, together with the much larger difference in the $^{208}Pb/^{204}Pb$ in the upper plot of the same figure, precludes any direct relationship.

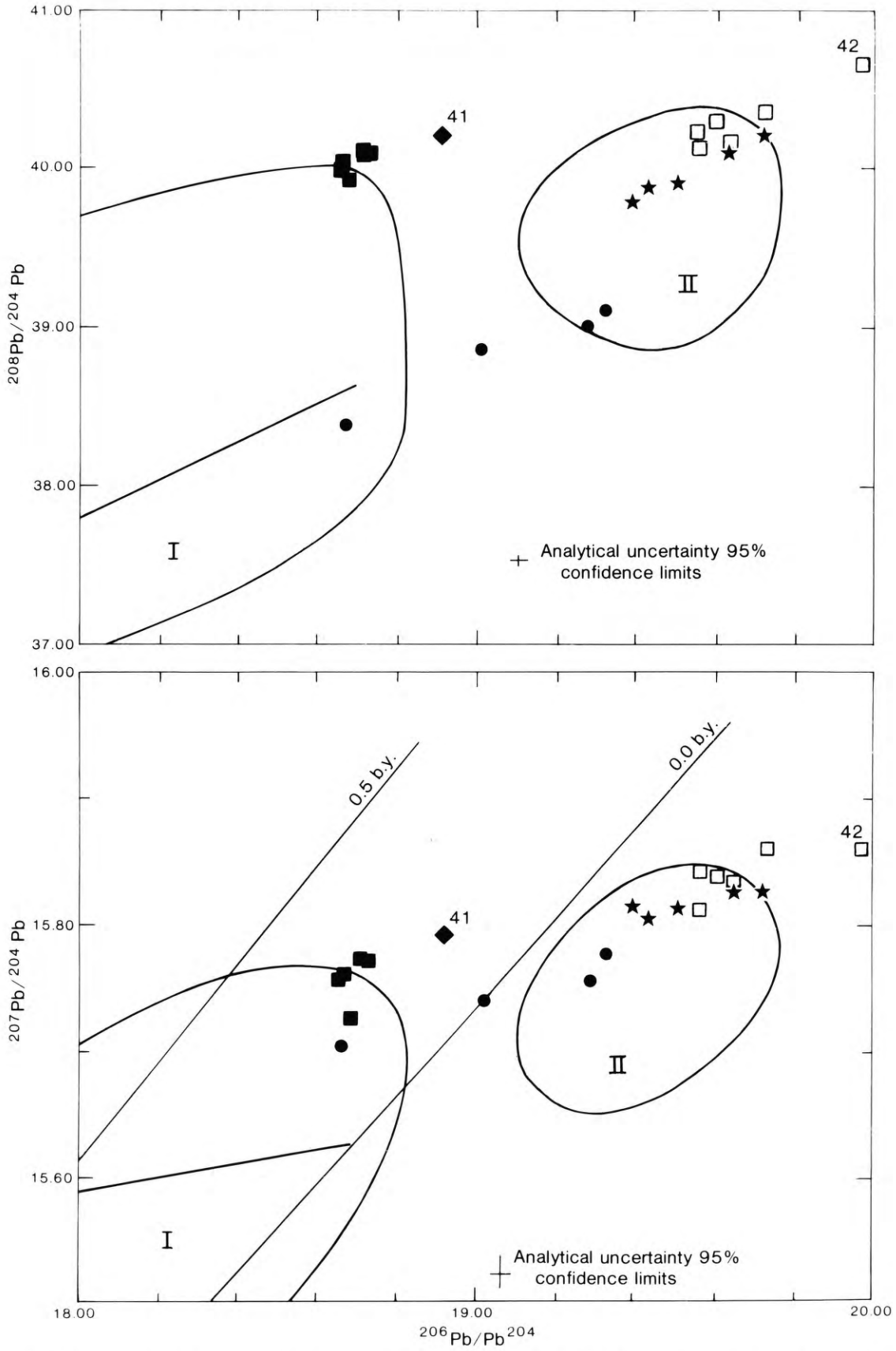

Figure 2. Lead isotope data from ores and feldspars of plutonic rocks from the Gold Hill mining district. Also shown are the fields for Areas I and II that represent characteristically different lead isotope behavior and part of the average lead isotope growth curve of Stacey and Kramers (1975). Northern group: ■ feldspars; ● ores; ♦ feldspar from porphyry dike intruding southern stock. Southern group: □ feldspars; ★ ores.

Table 2. Isotopic analyses of some feldspar leads from granitic rocks of the Gold Hill Stock, Utah

	Sample No. and Latitude, Longitude	Concentrations, ppm			$\frac{^{206}Pb}{^{204}Pb}$	$\frac{^{207}Pb}{^{204}Pb}$	$\frac{^{208}Pb}{^{204}Pb}$
		Pb	U	Th			
	Northern Group						
68-2-F	40°10.5'N, 113° 49.5'W	58.7	0.15	0.13	18.668	15.761	40.028
70-2-F	40°11.3'N, 113° 52.8'W				18.713	15.774	40.079
5A-F	40°10.6'N, 113° 49.9'W				18.685	15.726	39.908
6-F	40° 11.3'N, 113° 50.9'W				18.658	15.758	39.996
38B-F	40°10.3'N, 113° 49.2'W				18.731	15.772	40.075
41-F	40°09.9'N, 113° 48.5'W				18.915	15.791	40.194
	Southern Group						
68-1-F	40° 9.6'N, 113° 49.5'W	43.0	0.65	1.69	19.537	15.812	40.170
10-F	40°09.8'N, 113° 48.6'W				19.733	15.860	40.366
13A-F	40°09.3'N, 113° 49.9'W				19.645	15.832	40.173
15A-F	40°04.5'N, 113° 49.5'W				19.566	15.841	40.230
18-F	40°06.6'N, 113° 49.1'W				19.611	15.838	40.302
19-F	40°07.9'N, 113° 47.1'W				19.568	15.812	40.139
42-F	40°10.8'N, 113° 48.9'W				19.976	15.862	40.682

Table 3. Lead isotope analyses of some ore leads from Gold Hill, Utah

Mine or Prospect	Mineral Analyzed	Coordinates Latitude, Longitude	$\frac{^{206}Pb}{^{204}Pb}$	$\frac{^{207}Pb}{^{204}Pb}$	$\frac{^{208}Pb}{^{204}Pb}$
Northern Group					
Garrison	Cerussite	40° 14.7'N, 113° 50.3'W	18.670	15.707	38.375
Rube	Cerussite and galena	40° 10.9'N, 113° 48.5'W	19.015	15.741	38.856
Spotted Fawn	Galena	40° 13.1'N, 113° 50.4'W	19.325	15.776	39.060
Dutch Mountain prospect	Galena	Near Spotted Fawn	19.289	15.756	39.003
Southern Group					
U. S. Mine	Galena	40° 09.4'N, 113° 49.8'W	19.395	15.814	39.778
Western Utah	Plumbo-jarosite	40° 09.7'N, 113° 48.3'W	19.435	15.804	39.860
Cyclone	Galena	40° 04.5'N 113° 49.5'W	19.510	15.812	39.892
Climax	Galena	40° 08.2'N, 113° 47.4'W	19.641	15.830	40.115
Seminole	Galena	40° 07.0'N, 113° 49.3'W	19.724	15.827	40.216

Table 4. K-Ar age data for biotite concentrates from four quartz monzonite samples from the Gold Hill Stock, Utah

Sample No.	% K_2O	$*Ar^{40}$ (10^{-10} moles/gm)	% $*Ar^{40}$	$\frac{*Ar^{40}}{K^{40}}$	Age m.y. $\pm 2\sigma$
Northern Group					
1. 70-2	6.29	3.499	78	0.00220	37.4±1.3
2. 6	7.95	4.702	73	0.00234	39.7±1.4
Southern Group					
3. 15A	7.73	17.93	93	0.00919	151 ±5
4. 18	6.40	15.06	94	0.00932	153 ±5

Potassium determinations were made using flame photometer with a lithium internal standard. Constants used: K^{40} $\lambda_\epsilon = 0.585 \times 10^{-10}$ yr^{-1}

Atomic abundance: $K^{40} = 1.19 \times 10^{-4}$ * radiogenic argon $\lambda_\beta = 4.72 \times 10^{-10} yr^{-1}$

Table 5. Rb-Sr analyses for 11 whole rock granitic samples from the Gold Hill Stock, Utah

Sample	Average K-Ar Age m.y.	Rb ppm	Sr ppm	Rb/Sr	$\frac{^{87}Rb}{^{86}Sr}$	$\frac{^{87}Sr}{^{86}Sr}$	$\frac{^{87}Sr}{^{86}Sr}$
Northern Group							
68-2	38.2^{a1}	228	411	0.555	1.61	0.7165	0.715
70-2	38.2^{m2}	233	263	0.884	2.56	0.7155	0.714
5A	38.2^{a}	258	251	1.030	2.98	0.7172	0.715
6	38.2^{m}	205	318	0.646	1.87	0.7163	0.715
Porphyries Intruding Southern Stock							
37 40° 10.1'N, 113° 49.3'W		212	278	0.76	2.20	0.7161	
41		179	386	0.46	1.33	0.7150	
Southern Group							
10	152^{a}	172	694	0.247	0.715	0.7111	0.709
13A	152^{a}	203	725	0.280	0.61	0.7115	0.710
15A	152^{a}	158	653	0.242	0.70	0.7113	0.709
18	152^{m}	196	785	0.250	0.72	0.7104	0.708
19	152^{a}	168	791	0.213	0.62	0.7095	0.708

Rb and Sr concentrations were determined by x-ray fluorescence measurements; isotopic compositions by mass spectrometry
The ($^{87}Sr/^{86}Sr$) values were computed using the rubidium decay constant $\lambda = 1.42 \times 10^{-11}$ yr^{-1}

a^1 = assumed age; m^2 = measured age.

Table 6. Summary of data to compare characteristics of northern and southern components of the Gold Hill Stock

		Northern Component (Oligocene)	Southern Component (Jurassic)
Isotopic compositions of lead in feldspars from granitic rocks (excluding samples 41 and 42)	$^{206}Pb/^{204}Pb$	18.66 -18.73	19.54 -19.73
	$^{207}Pb/^{204}Pb$	15.73 -15.77	15.81 -15.86
	$^{208}Pb/^{204}Pb$	39.91 -40.08	40.15 -40.37
Isotopic composition of lead in ore deposits	$^{206}Pb/^{204}Pb$	18.67 -19.32	19.40 -19.72
	$^{207}Pb/^{204}Pb$	15.71 - 15.78	15.80 -15.83
	$^{208}Pb/^{204}Pb$	38.38 -39.06	39.78 -40.22
K-Ar biotite ages from quartz monzonites		38.5 ±1m.y.	152 ±4m.y.
Granitic whole rocks	($^{87}Sr/^{86}Sr$) initial	0.715±0.001	0.709±0.001
	(Rb/Sr)	0.56 -1.03	0.21 -0.28

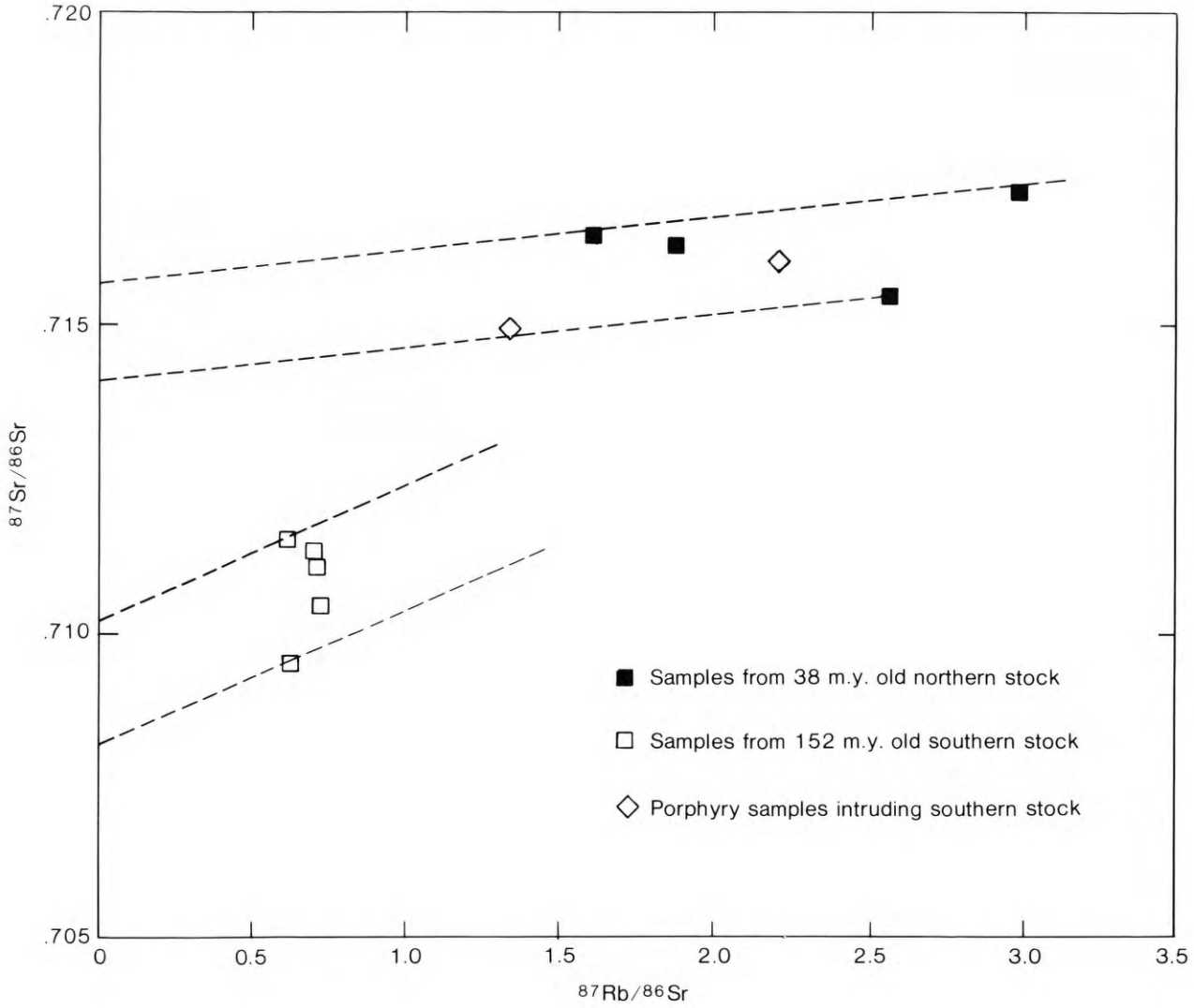

Figure 3. Rubidium-strontium whole-rock data for 11 granitic samples. Note the separate groupings that yield different ($^{87}Sr/^{86}Sr$) initial values 0.715± .001 for the northern stock and 0.709± .001 for the southern stock.

Perhaps the most striking feature along the contact zone is the occurrence of rounded xenoliths of a darker granodioritic rock, having the appearance of inclusions of the older southern unit, in the quartz monzonite of the northern body. These xenoliths, ranging in size from centimeters to tens of centimeters, increase in abundance as the contact is approached, and seem locally to have produced a hybridized rock by reacting with the younger magma.

Various porphyritic dikes cut both the Oligocene and Jurassic intrusions, as well as the country rocks for some distance beyond the border of the main plutons. Two prominent dikes of leucocratic granite porphyry were found in the contact zone between the two intrusive bodies. The dikes cut the southern body and its adjacent wall rocks, but seem to follow a fracture system parallel to that of aplites associated with the younger, northern body (see figure 4).

Samples of the two leucocratic porphyry dikes were collected for isotopic study (Nos. 37 and 41). Lead isotope data for both samples show a northern association for the feldspar lead, although in Sample 41 there does appear to be some addition of a more radiogenic component. This suggests slight assimilation of southern-type material by the porphyry as it intruded the southern body (see, particularly, the $^{208}Pb/^{204}Pb$—$^{206}Pb/^{204}Pb$ plot of figure 2). Whole-rock rubidium-strontium analyses reveal that the Rb/Sr ratios of both samples are too low to be used for dating (see table 5). However, their $^{87}Sr/^{86}$ Sr ratios, plotted in figure 3, also support a genetic relationship with rocks of the northern group. As a consequence, we doubt that the eastern dike (locality 41) is associated with ore deposition in the Western Utah mine even though it is south of the boundary between the two stocks. A description of this dike in the underground workings of the mine is given by Nolan (1935), who contrasts its relatively unaltered condition with that of the granodiorite. This in turn supports our field and laboratory observation indicating a postmineralization (i.e. post—Jurassic) age for the dike.

LEAD ISOTOPE MODELS

The plumbotectonics model of Doe and Zartman (1978) provides us with a generalized picture of lead isotope evolution throughout geologic time. Isotopic evolution results from the radioactive decay of the isotopes of uranium and

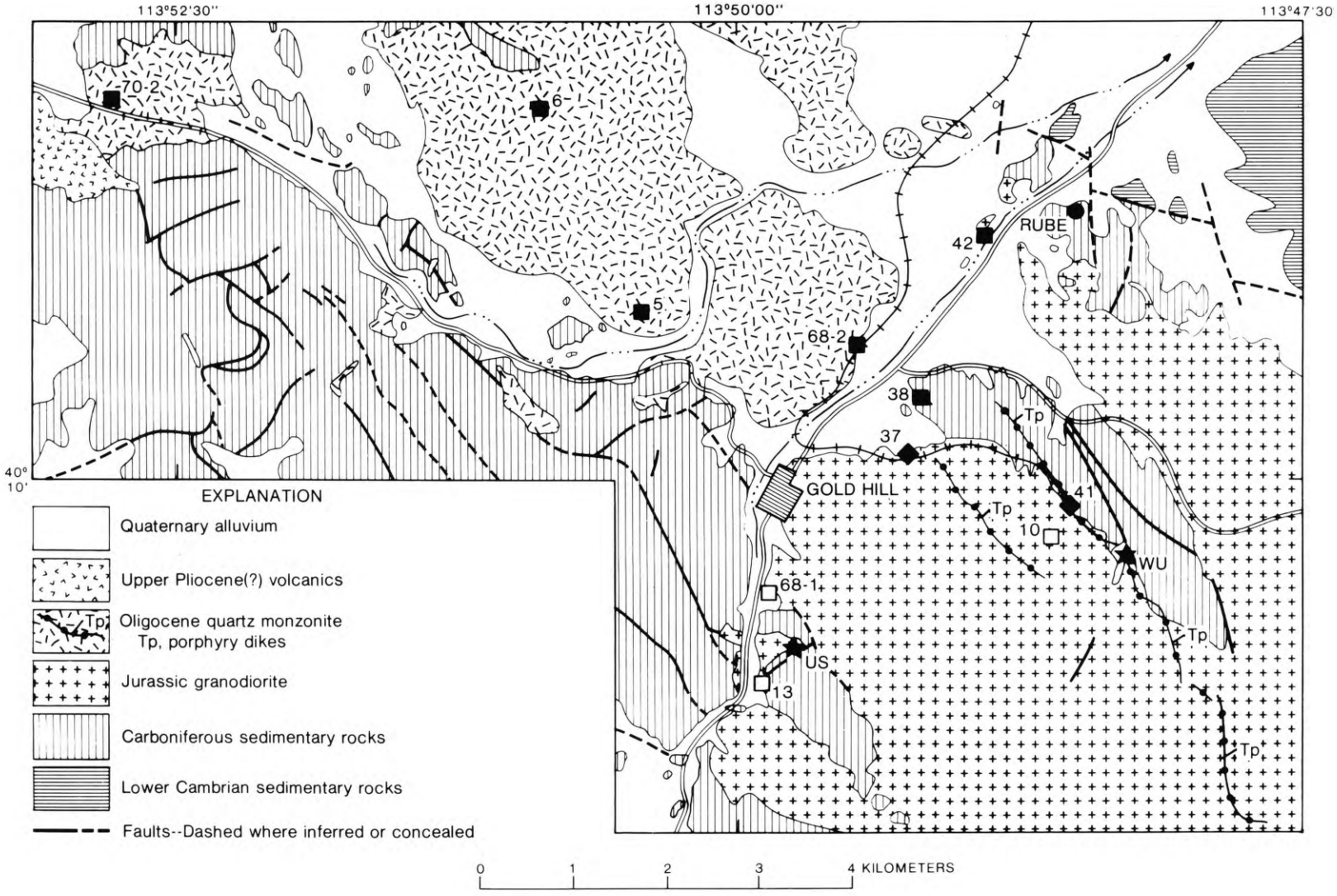

Figure 4. Geologic map showing sample locations within the boundary zone between northern and southern stocks at Gold Hill. The map is from Nolan (1935). Northern samples: ■ feldspars; ● ores; ◆ feldspar from porphyry dike intruding southern stock. Southern samples: □ feldspars; ★ ores.

thorium, but further constraints on resulting lead isotopic compositions are provided by orogenic mixing processes occurring in continental evolution. The model considers that new crustal material has been forming more or less continuously during the past 4 billion years by mixing portions of mantle and pre-existing crustal materials in orogenic environments. Newly formed crust is differentiated into lower crustal and upper crustal rocks, fractions of which subsequently become involved in further orogenies.

The domains taking part in such continental evolution are the mantle, the upper crust, the lower crust, and the orogene. Since each domain maintains its own limited range of uranium-to-lead and thorium-to-lead ratios, distinct evolution curves can be generated, and those calculated by Doe and Zartman are shown in figure 5. The orogene curve corresponds approximately to the average evolution curve for many conformable ore deposits and granitic rocks throughout the world. Such evolution has been discussed by many authors as the concepts in lead isotope studies have developed. (c.f., Russell and Farquhar, 1960; Patterson and Tatsumoto, 1964; Russell, 1972; Gancarz and Wasserburg, 1977).

Metamorphism of the continental crust causes uranium to be differentiated upward preferentially with respect to lead, increasing the production of ^{207}Pb and ^{206}Pb isotopes in the upper crust. Consequently, in the $^{207}Pb/^{204}Pb$ – $^{206}Pb/^{204}Pb$ plot of figure 5, an average development curve for the upper crust lies above that of the orogene. Conversely, depletion of uranium in the lower crust retards the generation of ^{207}Pb and ^{206}Pb, causing the curve for an average lower crust to lie below that of the orogene on the same plot.

Thorium, however, is less affected by metamorphism than is uranium, and therefore the thorium-derived ^{208}Pb isotope is more equally partitioned between the upper and lower crust than are the uranium-derived isotopes ^{206}Pb and ^{207}Pb. Thus, in figure 5, the $^{208}Pb/^{204}Pb$ - $^{206}Pb/^{204}Pb$ crustal evolution curves deviate from that of the orogene largely because of their changed $^{206}Pb/^{204}Pb$ values. This causes the characteristic curve for the lower crust to lie above that of the orogene. In contrast, that for the upper crust may lie below the orogene curve as shown in figure 5.

Stacey and Kramers (1975) showed that the development of conformable lead ore deposits and some granitic rock systems seem each to have followed effectively single-stage [1] development since about 3.7 b.y. ago until the time of their final emplacement. The significance of the 3.7 b.y. figure is that it probably marks the beginning of formation of the permanent crust. Although there may have been a continuum of uranium to lead (μ) ratios for the world-wide orogene development, an average μ of 9.74 is indicated over the past 3.7 b.y. It was to this average curve that the plumbotectonics orogene curve was originally fitted quite closely. Since the single-stage curve, generated entirely by radioactive decay, is easier to manipulate mathematically than the combination of mixing and decay processes in plumbotectonics, we have used the Stacey-Kramers curve as a basis for constructing a multi-stage model to explain the data from the Gold Hill region.

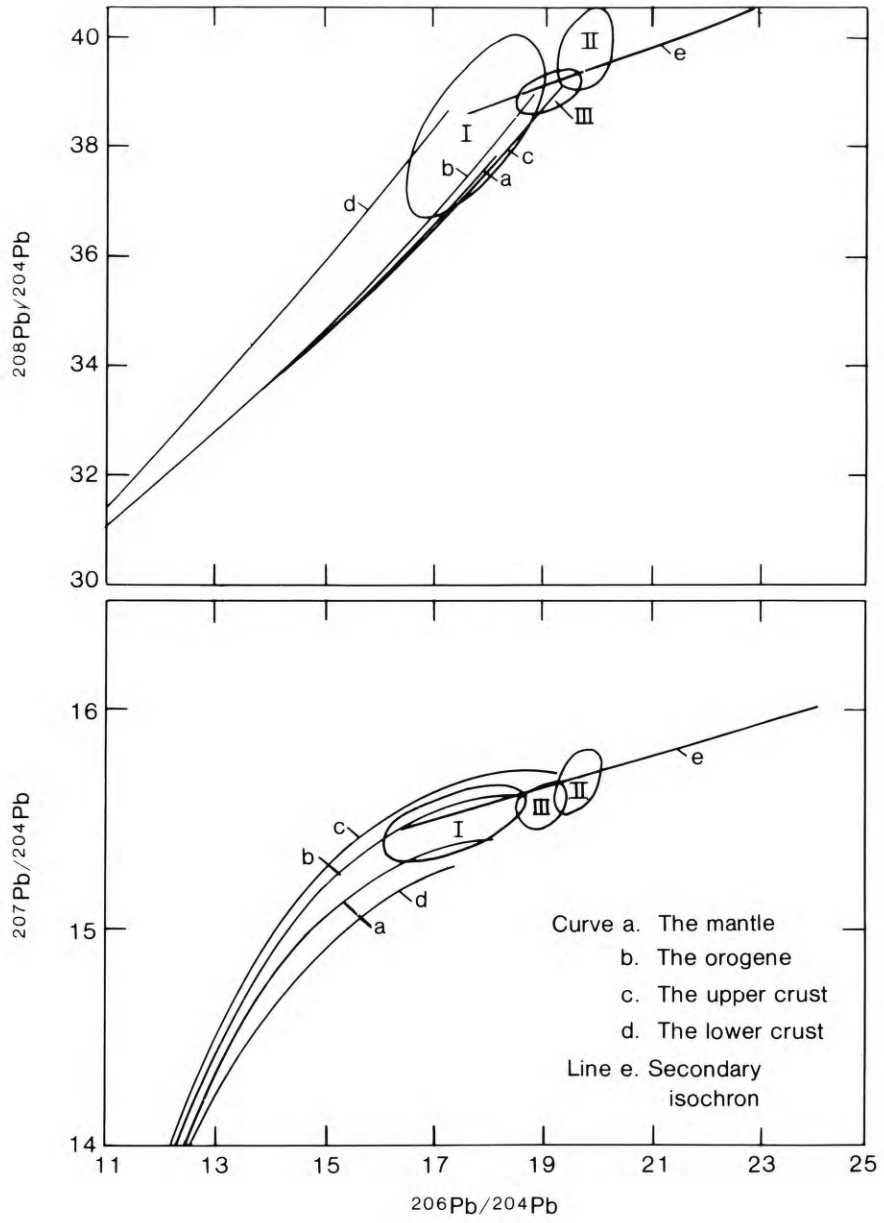

Figure 5. The generalized lead isotope evolution curves generated by the plumbotectonics model of Doe and Zartman (1977). The straight line (e) on each plot represents a secondary isochron formed by ore data taken across a mining district in an Area type I environment. The slope of the line in the lower graph is a function of both the age of the basement rocks and the time of mineralization. Fields are also shown for modern lead isotopic compositons for Areas type I, II and III of Zartman (1974).

[1] The term "single-stage" is taken to indicate a rock system which is closed with respect to uranium, thorium and lead since the time of its formation.

At the time of orogenesis a lead sample may become incorporated into either the upper or lower crustal rocks and the μ value of its new environment (μ_2) may then differ radically from 9.74, and a second stage of lead isotopic development begins. After passage of a further period of geologic time (several hundred million years), a lead sample will have an isotopic composition which, relative to the average growth curve, will be diagnostic of the nature of its second stage of evolution. If the data point lies below the growth curve then $\mu_2 > 9.74$, and we would attribute this to residence in the lower crust. However if the data point lies above the growth curve, then $\mu_2 > 9.74$ and an upper crustal residence is inferred for the period of its second stage of development.

One can envisage that subsequent uplift and erosion might involve the lead sample in another orogenic event that would provide a third stage of development, in which the uranium-lead ratios might assume yet a third value, μ_3. Again, after passage of further geologic time, the lead isotope composition would have evolved, but the relative values of $^{207}Pb/^{204}Pb$ and $^{206}Pb/^{204}Pb$ could still be quite definitive of its history.

In processes of ore formation, fluids containing lead with a homogeneous isotopic composition from an igneous source may traverse local basement rocks. In doing so these fluids are likely to become increasingly contaminated by a radiogenic lead component leached from those rocks as they travel outwards and upwards. "Near source" deposits remain comparatively unchanged in lead isotopic composition, but in smaller "far-from-source" deposits, this radiogenic component may be quite significant. In continental, Area I type environments where old basement rocks exist, the data from such a suite of samples across any one mining district often form a linear secondary isochron on each of the $^{207}Pb/^{204}Pb$ - $^{206}Pb/^{204}Pb$ and $^{208}Pb/^{204}Pb$ - $^{206}Pb/^{204}Pb$ plots (see figure 5). In the lower plot, the slope of the line is a function of both the age of the basement rocks and the time of mineralization. In the upper plot it is a function of the thorium - uranium ratio of the basement rocks (for further discussion of secondary isochrons, see Stacey and others, 1968, p. 800). We envisage such a process for the formation of the linear arrays for the northern ore lead data at Gold Hill.

DISCUSSION

The main isotopic characteristics of the igneous rocks and ores from the two parts of the Gold Hill district are summarized in Table 6. Several conclusions can be immediately drawn from these data. (1) The Gold Hill stock is really comprised of two different intrusions, differing in age by more than 100 m.y. To the south the stock has been shown to have a 152 ± 4 m.y., or Jurassic, age, while a 38 ± 1 m.y., or Oligocene, age obtains to the north. Both lead and strontium isotopic measurements indicate different source materials were involved in the formation of each of these bodies. (2) Since, in the Jurassic intrusion, the galena and feldspar leads have similar isotopic compositions, we conclude that the ore fluids were directly related to the igneous rocks, and mineralization probably took place during or shortly after emplacement and solidification of the magma. (3) The galena lead associated with the northern Oligocene intrusion however, has isotopic ratios that define trends distinctly displaced from the feldspar lead of that intrusion, especially on the $^{208}Pb/^{204}Pb$ vs $^{206}Pb/^{204}Pb$ graph of figure 2. Therefore, the ore lead cannot be straightforwardly derived from, or even mixed with material identical to that producing the igneous rock. It seems even less likely that the northern ore lead could be derived from the more radiogenic Jurassic lead. We do note however that the linear trend exhibited by the northern ore lead on the $^{207}Pb/^{204}Pb$ vs $^{206}Pb/^{204}Pb$ plot is a direct extension of the Oquirrh Mountain data from 100 km east of Gold Hill (see figure 6). Also, the radiometric age of the Last Chance stock at the Bingham Canyon mine, Oquirrh district is 38 m.y. (Moore and others, 1968), and was therefore contemporaneous with the northern intrusion at Gold Hill.

Before proceeding with model calculations, a brief account of the crustal development in this region seems desirable. The existence of 1600 to 1700 m.y. old basement rocks in Wasatch Mountains and elsewhere in central Utah has been verified by Damon and others (1966) and Hashad (1964). Further east in the Uinta Mountains (Hansen, 1965; Stacey and others, 1968), and to the north in the Raft River and Grouse Creek Ranges (Compton and others, 1977), an abrupt transition occurs to rocks of 2400 m.y. and older age. This terrane of Archean rocks (designated as Ia on figure 1) with an average age of 2700 m.y. represents an early period of cratonization to form continental crust. As we shall demonstrate, its presence to the east and north has left an indelible imprint on the lead isotopes in the vicinity of Gold Hill.

The souther Jurassic intrusion and related ore deposits at Gold Hill have the most radiogenic lead isotopic composition found in this study, and can be clearly identified as characteristic of Area II (see figure 2). The composition of the least radiogenic feldspar lead is $^{206}Pb/^{204}Pb = 19.54$ and $^{207}Pb/^{204}Pb = 15.81$. According to our interpretation, this lead has developed in an upper crustal environment with an almost constant μ value of approximately 12 since Archean time 2700 m.y. ago. The calculated values indicated by the model are: μ_1 averaged 9.74 from 3700 to 2700 m.y. ago, $\mu_2 = 11.7$ for the period 2700 to 1650 m.y., and $\mu_3 = 12.1$ for 1650 to 152 m.y. ago. During Phanerozoic time the preexisting crystalline basement rocks were transported as miogeosynclinal sediments into the Cordilleran geosyncline. In the process, a rather thorough mixing of detritus effected an isotopic homogenization, but did not appreciably alter the mean μ value. In reality, little detail of the geologic history of the precursor materials has survived, but evidence of their long residence in the upper continental crust has been firmly imprinted in the high $^{207}Pb/^{204}Pb$ ratios of the southern leads.

At the time of cratonization of the Archean crust, uranium, thorium, and lead were partitioned between lower and upper crustal rocks in such a way as to produce μ values of appreciably less than 9.7 in the lower crust and greater than 9.7 in the upper crust. Subsequently, much of the Archean upper crust was eroded, and it became a dominant component of sediments being deposited southwestward into a Proterozoic orogene. These sedimentary rocks were themselves eventually cratonized to form upper and lower crustal rocks, perhaps at various times, but in particular at about 1650 m.y. ago throughout the area of interest. The cycle was repeated again in Phanerozoic time, to shed material into the Cordilleran miogeosyncline west of the Utah-Nevada border. Here, near the edge of the orogene, the sediments were again dominated by a continental crustal component, this time derived from both the Archean and Proterozoic terranes. Finally, Mesozoic and Cenozoic igneous activity formed the intrusive rocks and their associated mineral deposits, reflecting in their lead and strontium isotopic composition the nature of the contributing source materials. In table 7 and figure 6 we present a multi-stage lead isotop model that uses the average growth curve of Stacey & Kramers (1975) for quantitative interpretation.

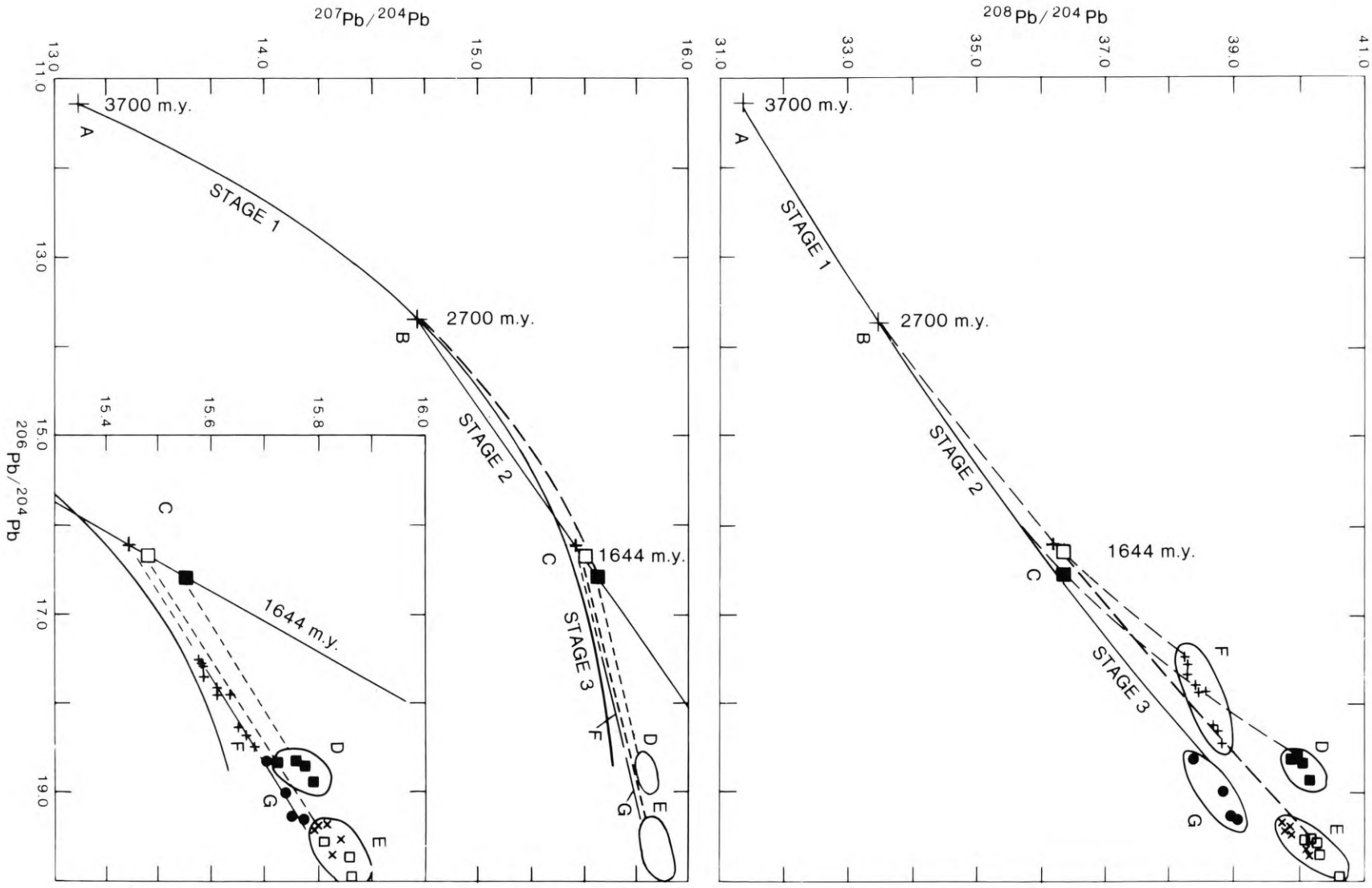

Figure 6. Multi-stage model for development of lead at Gold Hill, using the average evolution curves of Stacey and Kramers (1975).

3700 m. y. ago - A is the composition of average orogene lead.
2700 m. y. ago - B is the composition of average orogene lead.
1644 m. y. ago

C ■ - upper crustal material for Gold Hill Stock north.
C □ - upper crustal material for Gold Hill stock south.
C + - upper crustal material for Last Chance Stock, Oquirrh Mountains

Present day

D ■ - 38 m.y. Gold Hill stock north - feldspars.
E □, X - 152 m.y. Gold Hill stock south - feldspars and lead ores respectively
F + - 36-38 m.y. Oquirrh Mountains - galenas.
G ● - 36-38 m.y. Gold Hill north-lead ores.

Table 7. Multi-stage model data for lead isotopic development in the intrusions at Gold Hill and the Last Chance stock at Bingham Canyon, Oquirrh Mountains, Utah. Data are computed for the least radiogenic lead in each system. The following decay constants were used: $^{238}\lambda$=0.155125; $^{235}\lambda$= 0.98485; $^{232}\lambda$=0.049475. The present day value of $^{238}U/^{235}U$ = 137.88.

Stage	System	Times		Isotopic Compositions at end of Stage					
		Start m.y. ago	End m.y. ago	$^{206}Pb/^{204}Pb$	$^{207}Pb/^{204}Pb$	$^{208}Pb/^{204}Pb$	$^{238}U/^{204}Pb$	$^{232}Th/^{204}Pb$	Th/U
1	Av. Orogene Lead	3700	2700	13.637	14.690	33.366	9.74	36.84	3.78
2	Gold Hill Stock South	2700	1644	16.315	15.471	36.288	11.66	50.23	4.31
2	Gold Hill Stock North	2700	1644	16.563	15.544	36.328	12.74	50.91	4.31
2	Oquirrh Mtns. Last Chance Stock	2700	1644	16.229	15.446	36.197	11.29	48.66	4.31
3	Gold Hill Stock So.	1644	150	19.537	15.812	40.170	12.07	50.23	4.16
3	Gold Hill Stock No.	1644	38	18.658	15.758	39.996	7.36	44.27	6.01
3	Oquirrh Mtns. Last Chance Stock	1644	38	17.517	15.578	38.244	4.53	24.71	5.45

The lead in the feldspar of the northern Oligocene intrusion is also hypothesized to have been incorporated in the 2700 m.y. old upper crust, for which our model indicates μ_2 = 12.7 for the period 2700 to 1650 m.y. However, a μ_3 value of only 7.4 is calculated for subsequent development of this lead from 1650 m.y. ago until the Oligocene. In order to bring about this major change in rock chemistry, we infer that some Archean upper crustal rocks were eroded and transported southward to be incorporated into a 1650 m.y. old orogene. Metamorphic differentiation accompanying the cratonization of the Proterozoic rocks was responsible for the reduction of the uranium to lead ratio as these rocks became part of new lower crust. Between 1650 and 38 m.y. ago, the low μ_3 value of 7.4 retarded somewhat the further evolution of radiogenic lead isotopes. According to our hypothesis, the northern Gold Hill intrusion was derived from rejuvenated Proterozoic lower crust underlying the Gold Hill area, from which it acquired feldspar lead ratios of $^{206}Pb/^{204}Pb \approx 18.66$ and $^{207}Pb/^{204}Pb \approx 15.76$. Notice the relatively high $^{207}Pb/^{204}Pb$ value, which we regard as definitive evidence of residence in the upper crust for a long period of time prior to 1650 m.y. ago. These high $^{207}Pb/^{204}Pb$ values for the data actually were used to define the upper boundary of Area I type lead (figure 2).

Interpretation of the ore lead isotopic composition associated with the northern Gold Hill intrusion can be best accomplished by including the published results from the Oquirrh Mountains (Stacey and others, 1968). At Bingham Canyon, Utah the Oligocene Last Chance stock appears to record a similar genesis to the contemporaneous body at Gold Hill. It may have been generated at greater depth in the Proterozoic lower crust as indicated by its greatly retarded $^{206}Pb/^{204}Pb$ ratio of 17.52. While clearly labeled as a lead from Area I by this $^{206}Pb/^{204}Pb$ value, the comparatively high $^{207}Pb/^{204}Pb$ ratio of 15.58 again suggests an early residence in the upper crust. Assuming the same time parameters as applied at Gold Hill, our model yields μ_2 and μ_3 values of 11.3 and 4.53, respectively, for the Last Chance Stock. For the Oquirrh Mountains ore lead data, a well define secondary isochron is exhibited on each of the $^{207}Pb/^{204}Pb$ vs $^{206}Pb/^{204}Pb$ and $^{208}Pb/^{204}Pb$ vs $^{206}Pb/^{204}Pb$ plots. In addition the feldspar lead composition of the Last Chance Stock falls near the lower end of each of these lines. Stacey and others (1968) interpreted this to indicate that the ores were all derived from

similar material as the Last Chance Stock with different proportions of radiogenic lead added from higher levels of the 1650 m.y. basement at the time of mineralization.

In the north at Gold Hill, the feldspar lead data is not collinear with that of the ore lead (see figure 2), and therefore there can be no direct genetic relationship between ore and feldspar lead in that area. However, it is most interesting that the northern ore lead data do lie on an extension of the Oquirrh Mountain secondary isochron in the $^{207}Pb/^{204}Pb$ vs $^{206}Pb/^{204}Pb$ plot of figure 6. It seems unlikely that the ultimate source of the mineralizing fluids was as far away as the Oquirrh Mountains. More probably the fluids at Gold Hill were derived from basement rocks similar in age ($\approx$ 1650 m.y.) to those of the Oquirrh Mountains but shallower and nearer to Gold Hill. Indeed, a basement source different from and shallower than that for the Oquirrh Mountains deposits is suggested by the trend of the northern data in the $^{208}Pb/^{204}Pb$ vs $^{206}Pb/^{204}Pb$ plot in figure 6. This trend is apparently not collinear with that of the Oquirrh Mountains data. If the least radiogenic sample, that from the Garrison mine, is assumed to be of "near source" origin, then our model would indicate, for the source material, residence in a more nearly average crustal environment where $\mu_3 = 8.5$ during the period 1650 - 38 m.y. ago.

Moore and Lanphere (1971) measured the K-Ar age of hydrothermal biotite at Bingham Canyon mine to be 36.5 m.y., that is, about 2 m.y. after emplacement of the Last Chance stock. A similar age could well apply to the deposits in the northern part of the Gold Hill district. Although the lead isotopic data indicate similar source rocks for the ores at Gold Hill and at Bingham Canyon, it should not be assumed that the existence of a large Bingham Canyon type deposit is also indicated at Gold Hill. On the contrary, the comparitively high $^{206}Ph/^{204}Pb$ values for the ores at Gold Hill point to the presence of only minor deposits such as those already found there. For the use of lead isotopes as a prospecting tool the reader is referred to Doe and Stacey (1974).

In order to extend the calculations to include the thorium-derived isotope, ^{208}Pb, some arbitrary assumptions had to be made for the multistage model. It was noted that in the source material for the southern intrusion at Gold Hill, the uranium to lead ratio had remained almost constant during the entire period from 2700 to 152 m.y. ago - changing only from 11.7 to 12.1 in μ value at 1650 m.y. ago. Therefore, in the computations, we assumed that the thorium to lead ratio also remained constant over this period of time - with the result that for the southern intrustion the $^{232}Th/^{204}Pb$ value in stages 2 and 3 is 50.2. This value is considerably greater than 36.8 as allowed for in the average orogene, and explains why the curve for the southern intrusion lies above the orogene curve on the $^{208}Pb/^{204}Pb$ vs $^{206}Pb/^{204}Pb$ diagram in figure 6. The second arbitrary assumption made was that during the period 2700 to 1650 m.y. ago, the source materials for all three stocks considered in table 7 had the same thorium to uranium ratio, and this is computed to be 4.31.

Strontium isotopes offer us another means of identifying gross geochemical characteristics of the precursor material from which an igneous rock is derived. The $^{87}Sr/^{86}Sr$ ratio incorporated into a magma is a useful index of the source rock, with higher values indicating longer residence times in a more differentiated material. It is not generally possible, however, to establish for strontium isotopes time constraints for strontium evolution at different levels within the crust with the mathematical sophistication developed for the lead isotopes. Examination of the strontium isotopic data for the main phase of igneous rocks (see table 5 and figure 3) show initial $^{87}Sr/^{86}Sr$ values of 0.709 ± 0.001 and 0.715 ± 0.001 for the southern and northern intrusions, respectively. Several other studies have noted similar isotopic ratios for plutonic and volcanic rocks of western Utah and eastern Nevada (Scott and others, 1971; Best and others, 1974; Compton and others, 1977). Such values are appreciably greater than those attributable to most mantle rocks, and therefore, support the hypothesis of a continental source for the material of igneous rocks in the area.

While a general consensus exists that $^{87}Sr/^{86}Sr$ values higher than about 0.706 are usually diagnostic of an older underlying sialic crust (Hedge, 1966; Doe, 1968; Armstrong and others, 1977), little progress has been made toward further subdividing continental terranes on the basis of strontium isotopes. Apparently, the dichotomy between older continental crust and younger, mantle-dominated eugeosynclinal environments is a more fundamental determinant of the strontium isotopes than any difference between, for example, upper and lower crust. Accordingly, the remarkably sharp change in lead isotopic patterns at the boundary of Areas I and II is not obviously reflected in the strontium isotopes. Both lead and strontium have been used successfully, however, to delineate a boundary between Areas II and III (Armstrong and others, 1977).

We might have expected that the southern intrusion-- interpreted to have had the longest upper crustal identity -- would reveal a higher $^{87}Sr/^{86}Sr$ ratio than the northern intrusion. But this expectation is not borne out by either the initial isotopic composition or by the Rb/Sr ratio of the rocks. Although we have no assurance that this latter ratio was not changed at the time of magma generation, the data do suggest that the northern intrusion may derive from a higher Rb/Sr source material than the southern intrusion. This feature can be used to strengthen our argument for a northern derivation for the two porphyry dikes extending into the southern intrusion. Such a correlation is strongly supported both in terms of initial ratio and Rb/Sr ratio (see table 5 and figure 3).

ACKNOWLEDGEMENTS

Our thanks are due to many people who have made this study possible. Thomas B. Nolan was particularly helpful in providing samples from his collection, which is now in the Smithsonian Institute in Washington. In addition, two of the Dutch Mountain galena samples were supplied by Mr. Cecil Woodman, a long time resident of Gold Hill. We have also had valuable discussions with our colleague Zell Peterman.

Mineral separations were made for us by Gerry Cebula and Jack Groen. Potassium argon analyses were performed by Dick Marvin and Harald Mehnert, and the strontium analyses by Kiyoto Futa and Bob Hildreth. Lead isotope chemistry and mass spectrometry were carried out by Maryse Delevaux.

Retrieval and plotting of the lead isotope data from the U.S.G.S. lead isotope data bank (Doe and Rohrbough, 1977) were made possible for us by Randy Rohrbough (Rohrbough and Stacey, 1976).

REFERENCES

ARMSTRONG, R.L., 1970, Geochronology of Tertiary igneous rocks, eastern Basin and Range Province, western Utah, eastern Nevada, and vicinity. U.S.A.: Geochimica et Cosmochimica Acta, v. 34, p. 203-232.

ARMSTRONG, R.L., E.B. Ekren, E. H. McKee, and D.C. Noble, 1969, Spacetime relations of Cenozoic silicic volcanism in the Great Basin of the western United States: American Journal of Science v. 267, p. 478-490.

ARMSTRONG, R.L., W. H. Taubeneck, and P. O. Hales, 1977, Rb-Sr and K-Ar geochronometry of Mesozoic granitic rocks and their Sr isotopic composition, Oregon, Washington, and Idaho: Geological Society of America Bulletin v. 88, p. 397-411.

BEST, M.G., R.L. Armstrong, W. C. Graustein, G. F. Embree, and R. C., Ahlborn, 1974, Mica granites of the Kern Mountains pluton, eastern White Pine County, Nevada: Remobilized basement of the Corilleran miogeosyncline?:Geological Society of America Bulletin v. 85, p. 1277-1286.

CAMERON, A.E., D. H. Smith, and R. L. Walker, 1969, Mass spectrometry of nanogram size samples of lead: Analytical Chemistry, v. 41, p. 525-526.

CATANZARO, E. J., 1967, Triple filament method for solid sample lead isotope analysis: Journal of Geophysical Research, v.72, p. 1325-1327.

CATANZARO, E. J., T. J. Murphy, W. R. Shields, and E. L. Garner, 1968, Absolute isotopic ratios of common, equal atom, and radiogenic lead isotope standards: Journal of Research, National Bureau of Standards, v. 72A, no. 3, p. 261-267.

COMPTON, R. R., V. R. Todd, R. E. Zartman and C. W. Naeser 1977, Oligocene and Miocene metamorphism, folding, and low-angle faulting in northwestern Utah: Geological Society of America Bulletin v. 88, p. 1237-1250.

DAMON, P. E., P. W. Gast, A. Hashad, T. Sayyah, and J. A. Whelan, 1966, Geochronology of the Precambrian of northern Utah; *in* Abstracts for 1966: Geological Society of America Special Paper 101.

DOE, B. R., 1967, The bearing of lead isotopes on the source of granitic magma: Journal of Petrology v. 8, no 1, p. 51-53.

DOE, B. R., 1968, Lead and strontium isotopic studies of Cenozoic volcanic rocks in the Rocky Mountain region - A summary. *In* Cenozoic Volcanism in the Southern Rocky Mountains: Colorado School of Mines Quarterly v. 63, p. 149-174.

DOE, B. R., J. S. Stacey, 1974, The application of lead isotopes to the problems of ore genesis and ore prospect evaluation: A review: Economic Geology v. 69, p. 757-776

DOE, B. R., and R. E. Zartman, 1978, Plumbotectonics I, the Phanerozoic: Geochemistry of hydrothermal ore deposits, H. Barnes, editor, New York, John Wiley and Sons.

DOE, B. R., and R. Rohrbough, 1977, Lead Isotope Data bank, U. S. Geological Survey Open File Report, 77-418

El --SHATOURY, H. M., and J. A. Whelan, 1970, Mineralization in the Gold Hill Mining District, Tooele County, Utah: Utah Geological and Mineralogical Survey Bulletin 83, 37 p.

GILLULY, J., 1965, Volcanism, tectonism and plutonism in the western United States: Geological Society of America, Special paper no. 80, 69 p.

GANCARZ, A. J. and G. J. Wasserburg, 1977, Initial Pb of the Amitsoq gneiss, West Greenland, and its implications for the age of the Earth: Geochimica and Cosmochimica Acta v. 41, p. 1283-1301.

HAMILTON, W. B. and B. M. Meyers, 1966, Cenozoic tectonics of the western United States: Reviews of Geophysics v. 4, p. 509-549.

HANSEN, W. R., 1965, Geology of the Flaming Gorge Area, Utah-Colorado-Wyoming: U.S. Geological Survey Professional Paper 490, 196 p.

HASHAD, A. H. 1964, Geochronological studies in the central Wasatch Mountains, Utah: Utah University unpublished Ph.D. thesis.

HEDGE, C. E., 1966, Variations in radiogenic strontium found in volcanic rocks: Journal of Geophysical Research v. 71, p. 6119-6126.

MOORE, W. J., M. A. Lanphere, and J. D. Obradovich, 1968, Chronology of intrusion, volcanism and ore deposition at Bingham, Utah: Economic Geology v. 63, p. 612-621.

MOORE, W. J., and M. A. Lanphere, 1971, The age of porphyry-type copper mineralization in the Bingham mining district, Utah - a refined example: Economic Geology v. 66, p. 331-334.

NOLAN, T. B., 1935, The Gold Hill mining district, Utah: U. S. Geological Survey Professional Paper no. 177, 172 p.

PATTERSON, C. C., and M. Tatsumoto, 1964, The significance of lead isotopes in detrital feldspar with respect to chemical differentiation within the Earth's mantle: Geochimica et Cosmochimica Acta, v. 28, 1-22.

ROBERTS, R. J., P. E. Totz, J. Gilluly, and H. G. Ferguson, 1958, Paleozoic rocks of north-central Nevada: American Association of Petroleum Geologists, Bulletin v. 42, p. 2813-2857.

ROHRBOUGH, R., and J. S. Stacey, 1976, The lead isotope data bank Part II: Retrieval and Plotting, U.S. Geological Survey Open File Report 76-763.

RUSSELL, R. D., and R. M. Farquhar, 1960, Lead isotopes in geology: New York, Interscience Publishers, Inc., 243 p.

RUSSELL, R. D., 1972, Evolutionary model for lead isotopes in conformable ores and in ocean volcanics: Reviews of Geophysics Space Physics v. 10, p. 529- 549.

RYE, R. O., B. R. Doe, and J. D. Wells, 1974, Stable isotope and lead isotope studies of the Cortez, Nevada, gold deposit and surrounding area: U.S. Geological Survey Journal of Research v. 2, p. 13-23.

SCOTT, R. B., R. W. Nesbitt, E. J. Dasch, and R. L. Armstrong, 1971, A strontium isotope evolution model for Cenozoic magma genesis, eastern Great Basin, U.S.A.: Bulletin of Volcanology v. 35, p. 1-26.

STACEY, J. S., R. E. Zartman, and I. T. Nkomo, 1968, A lead isotope study of galenas and selected feldspars from mining districts in Utah: Economic Geology 63, v. 7. p. 796-814.

STACEY, J. S., and J. D. Kramers, 1975, Approximation of terrestrial lead isotope evolution by a two-stage model: Earth and Planetary Science Letters v. 26, p. 207-221.

ZARTMAN, R. E., 1974, Lead isotopic provinces in the Cordillera of the western United States and their geologic significance: Economic Geology v. 69, p. 792-805.

Meadow near the headwaters of the Weber River above Smith and Morehouse Reservoir, Summit County. Unnamed peak in center is 10,369 feet (3,168 meters) high. Sparse snow cover remaining in early June 1976 reflects the beginning of the warm dry spring and summer of 1976 which then led into the extreme drought of 1976-77.

Photo by J.H. Rathbone

WIND TIDES OF THE GREAT SALT LAKE

by Anching Lin[1] *and Po Wang*[2]

ABSTRACT

Essential features of hydrographic and meteorological characteristics of wind tides on Great Salt Lake are described. Three major modes of seiching are found; and the fundamental mode has a period of 6.13 hours. The implications of these forces on the geomorphology of the lake are also discussed.

INTRODUCTION

In his study of Lake Bonneville, Gilbert (1890) discussed the importance of the forces exerted by waves as primary agents in the shaping of the shores of the lake. The waves, together with the action of their currents, eroded, transported, and deposited shore and bottom materials; waves were and are, largely responsible for the formation of the bars, spits, and embankments visible today including the benches that ring Utah's mountain valleys. These geological features of the ancient shores of Lake Bonneville were clearly recognized by Gilbert.

The present Great Salt Lake (figure 1) is the remnant of Lake Bonneville, which probably went through more than 10 sizable cycles of rise and fall of lake level during the past 70,000 to 100,000 years (Morrison, 1966). At its maximum Lake Bonneville covered about 20,000 square miles and had depths to 1,000 feet. By comparison, the Great Salt Lake is relatively small and shallow, with 1,500 square miles in area and 35 feet in maximum depth. Because of its shallowness and its small total volume of water mass, The Great Salt Lake should be more responsive to wind action than Lake Bonneville. The resulting wave forces play an essential role in many present day problems of Great Salt Lake; the maintenance of beach facilities against flooding by waves, the up-keep of the causeways, the current systems (associated with the waves of various sizes) and the resulting distribution of minerals in the lake, the possible mixing of brines in the two-layer South Basin, etc.

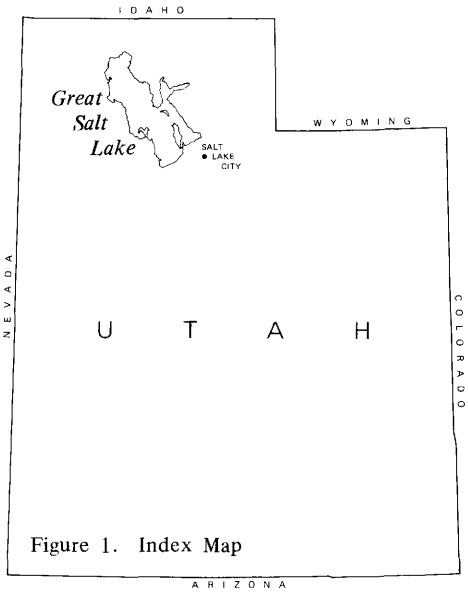

Figure 1. Index Map

In an enclosed basin of a moderate size, such as the Great Salt Lake, the waves and the associated coastal currents are the principal forces that shape the shores of the lake. Unlike basins of a much larger size, the tidal forces caused by the gravitational attractions among the moon, the sun, and the earth, and the effects of the earth's rotation may be ignored in Great Salt Lake. Therefore, this leaves the wind, possibly accompanied by moving pressure centers, as the primary source of energy that agitates the lake. The wind generates two kinds of water waves. These wind-generated water waves may best be described as: (1) short waves with each wave cycle lasting from a few seconds to several minutes, and (2) long waves with each cycle extending over hours. In this report we are interested in various phenomena associated with the long waves of the lake, referred herein as wind tides.

In the contemporary Great Salt Lake, the wave action is now forming a spit to the west of Antelope Island. Recent soundings of the lake have revealed its growth, although at a small enough rate to have escaped the visual observations. The formation of such a spit could very well add unexpected and heavy costs to the industrial operations that are dependent on the lake. The adverse results of littoral erosion, the transportation and redeposition of shore materials, are constant threats to those who invest in facilities around the lake. Three incidents that took place in the last ten years demonstrate the magnitude of the forces involved:

Example 1: In 1965, a test jetty was begun between Silver Sands and Saltair to determine the feasibility of using mill tailings from Kennecott Copper Corporation as road base and dike material (Suekawa, 1970). Among the many findings from the test, it was learned that the power of the wave action had been grossly underestimated; the rapid erosion of the jetty hastened the completion of the tests. The construction of the jetty was completed in December, 1966, and by May of 1967, over 600 feet of the jetty had been wiped out by the wave and currents. The study concluded that a 20:1 degree side slope could not withstand the action of the waves. (It should be noted here that most of the beaches on the south shore have a natural slope of less than 200:1).

Example 2: The Syracuse Causeway which provides the only access road to Antelope Island State Park was planned in the early 60's, when the lake level was at a low point in its fluctuating cycle and the lake was generally believed to be drying up. Since the completion of the causeway, however, the lake has been rising. Because this eventuality was not considered, the causeway has been severely damaged several times requiring extensive and expensive maintenance to keep it open and the park accessible to the public. There is no question that the high level of the lake caused the flooding and washed out the causeway, making it necessary to rebuild the road several times; however, the constant action of the waves also contributed to the erosion of the unprotected embankment even when flooding was not present. The impact of wave action has not yet been sufficiently determined to plan maintenance requirements properly.

Example 3: Regular maintenance of the Southern Pacific Railroad causeway has been necessary to keep the track open. The sheer force of the waves may be illustrated by the fact that the two

[1] Associate Professor, Department of Civil Engineering, University of Utah, Salt Lake City, Utah 84112.
[2] Graduate Student, Department of Civil Engineering, University of Utah, Salt Lake City, Utah 84112

culverts, which were constructed to allow an exchange between the two basins, are often plugged by rocks of considerable size from the fill material of the causeway. Just how these are transported through the culverts has yet to be determined. Perhaps the most plausible assumption is to attribute it to "wind set-up": the waves and currents caused by strong wind. As the wind acts on the lake for a long enough period of time, the lake surface tends to become tilted, setting up large differences in the lake level on either side of the causeway. On a calm day, the lake level may typically differ by about 18 inches, with the strongest currents running about 15 feet per second through the culvert. When there is a strong wind, an additional 18 inches in lake difference is not uncommon; the resultant flushing power of the currents through the culverts is considerable. Thus, the transportation of sizable pieces of rock through the culverts is not unlikely.

This paper is an expository report on the nature of wind tides in the South Basin; for detailed accounts of wind tides on Great Salt Lake we refer the readers to Lin (1976) and Wang (1977). The authors will base their discussion on (1) lake level records that were collected at Silver Sands and Promontory Point, (2) the wind, barometric pressure records, and radar echoes that were collected at the Salt Lake Airport, and (3) the data from the computation of these records.

The turmoil created when a wind storm strikes the lake, as evidenced by the short waves, is obvious to even the most casual observer; yet few people are aware of the long waves which are caused by the wind, for these are not readily discernible. A wind tide normally consists of wind surge and seiching which are associated with various species of long waves and generally involve the movement of the whole water mass. The two phases of a wind tide should be distinguished; "surging" denotes the phase when the wind is effectively acting on the surface of the lake and "seiching" refers to the vertical oscillation phase when the wind is no longer an effective force on the lake. During surging the wave forms are complex; however, even among the complex waves a prevailing, 6-hour oscillation pattern is recognizable. During seiching, after the wind has dropped, the wave forms are "clean" and simpler; only a single component of the long wave then survives.

Although long waves can reach exceptional wave heights, it usually takes about 6.0 hours for one wave to travel from Silver Sands to Promontory Point and back to Silver Sands. Since the rate of oscillation is very slow, it is necessary to use the records of lake-level fluctuations to identify long waves. From lake level measurement records as well as from theoretical calculations, it has been found that among the various species of long waves, the one that is most likely to occur in the Great Salt Lake has a period of about 6.0 hours. The 6-hour oscillation period is then used as a criterion to identify the presence of wind tides.

Referring to the calendar in figure 2 (Lin, 1976), the period of time during which wind tides occurred on Great Salt Lake was shaded for the two gaging stations; the records of the two stations have been placed alongside each other for ready comparison. Thus we see that the oscillation of long waves was observed simultaneously at the two stations, indicating that the water mass of the lake was oscillating as a whole. That is, the whole body of water underwent some form of sloshing back and forth, completing a cycle in about 6 hours.

Lake level data indicate that the months of September and November appear to be the time favored for major wind tides to take place. One major episode of wind tide is to be expected for each of these months. This indicates that the occurrence of wind tides is somewhat seasonal and that they are closely related to the frontal weather activities in the area.

METEOROLOGICAL ASPECTS OF WIND TIDES

Many facilities, both private and public, around the lake collect meteorological data. Only the records that are made at the Salt Lake City Airport are comprehensive enough to be readily usable and were extensively used in this study. The meteorological tower recently erected on the lake by the UGMS should produce very useful information in the future, but data available from the tower at this time are still too limited.

Two types of meteorological data are used for this study. (1) ground-level records of wind speeds and barometric pressures and (2) radar echoes. The airport makes a continuous record of radar echoes on an hourly basis for the Intermountain Area. These echoes register the atmospheric conditions at elevations between 20,000 to 35,000 feet; they offer good indications of the general direction and the speed of movement of storms. The ground-level wind and barometric condition data relates the forces that are directly responsible for the formation of wind tides and are therefore most pertinent in this wind tide study.

Twenty five episodes of wind tides were selected for study. The authors traced the histories of these storms from the records of radar echoes collected by the U.S. Federal Aviation Administration. These records indicate that the storms which are responsible for the major wind tides usually approach the lake from two directions: (1) from Tooele Valley, moving over the lake in a northerly direction, and (2) from the west of the lake, moving in an easterly direction over the lake. These echoes normally dissipate as they move across the Wasatch Front and reform in new storm cells after they have lifted over the mountains.

To determine if movement of pressure systems alone contributes to wind tides, the movement of a storm system was studied. If a low pressure center (such as a squall line), moves across the surface of the lake at a speed that is close to the natural speed of wave propagation on the lake, then resonance may be triggered. This phenomenon was reported in Lake Erie by Harris (1955). With an average depth of 20 feet in the Great Salt Lake, the speed of wave propagation is about 15 knots (or 25.37 feet per second).

Radar records show that it is possible that the squall lines which are associated with some of the observed wind tides may move with a speed that is close to 15 knots, and thus just this movement of pressure center alone, without wind action, could create high levels of surge. Unfortunately, it is not possible to make enough pressure measurements at various points around the lake to monitor the ground level speed of the low-pressure lines as they advance. While the movement of a pressure center may be an important factor in a wind tide, it is probably more incidental than a fundamental requirement; in the case of Great Lakes only three episodes were found in a decade (Harris, 1955).

A southerly wind appears, as a general rule, to be associated with a wind tide on the lake. Most of the wind tides were generated by a southerly wind; this appears to be the prevailing storm pattern in the area and a typical example is given in figure 3a. From the study of the radar echoes, it was apparent that all major wind tides were caused by various forms of synoptic scale weather systems, including winter cyclones, fronts, squalls and severe thunderstorms. Among all these possible weather systems, the winter cold fronts and cyclones are by far the most frequent causes of major wind tides. It suffices to note that a front entering the lake area normally possesses some consistent features; front lines usually

Figure 2. Occurrence of wind tides in the South Basin of Great Salt Lake, 1970-1975. (Lin, 1976)

approach the lake from the northwest (see figure 3b); therefore, the storm front usually moves over the lake stretching in a north-to-south direction. Such a front is always preceded by strong southerly winds blowing parallel to the front line. Behind the front, the wind intensity is reduced substantially, and the directions of the wind become less predictable. This sequence of events is shown in the wind and pressure data of figure 3a and 3b. The prefrontal southerly wind is peculiar to the general area of northern Utah, because as a front approaches the lake, the center of the lowest pressure is usually situated somewhere in southern Idaho or Wyoming.

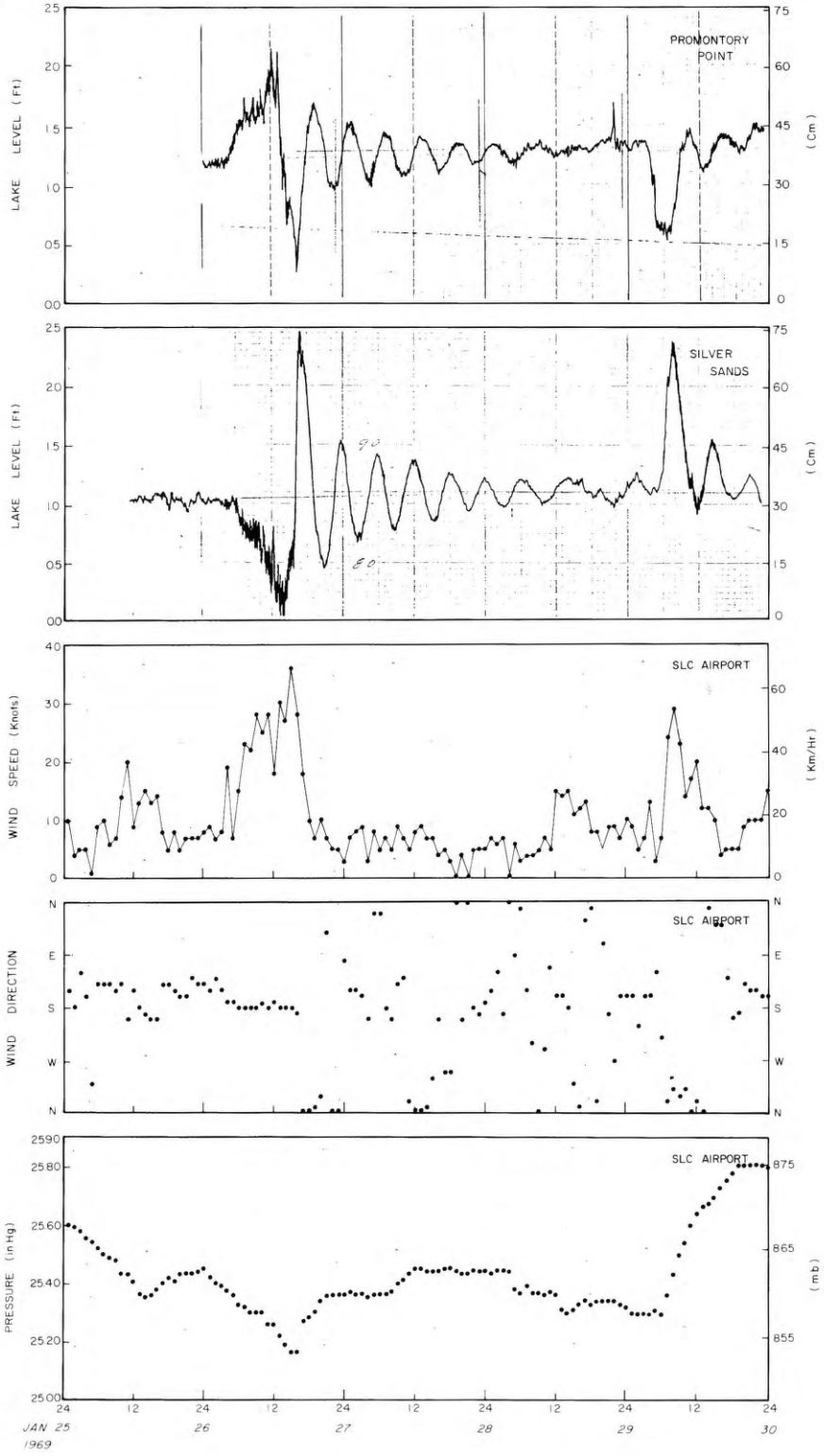

Figure 3a. Selected magrigram in the South Basin of Great Salt Lake and associated meteorological records, January 1969.

Local thunderstorms and local low pressure systems are all capable of generating major wind tides, but not as effectively as the winter frontal storms. Local thunderstorms consist of storm cells with diameters that range from 5 to 30 miles; a squall line consists of a series of such cells. A typical feature of thunderstorms is that the wind direction is unpredictable. A wind tide generated by a thunderstorm is depicted in figures 4a and 4 b.

HYDROGRAPHIC ASPECTS OF WIND TIDES

The nature of the wind tides on the Great Salt Lake is determined from a study of the hydrographic records, in conjunction with the associated meteorological records. While records of the lake levels have been measured by the U.S. Geological Survey, Salt Lake District Office at Silver Sands since 1939, the station at Promontory Point was not installed until 1968. The authors have selected for this study 25 episodes that show prominent wind tides that occurred from 1968 to date. Figure 3a and 4a present two typical episodes of major wind tides.

Each lake has its own inherent system of long waves. Once the geometry of a lake, including its depth, shape, and bottom topography, has been set, the system of long waves is fixed. The underlying principles that describe the normal modes are analogous to the other vibration systems in the physical world. Just as the natural frequency of a pendulum is dependent upon its physical make-up, the natural frequency (of a normal mode) of a lake depends on the water depth, shape, and bottom topography of the lake. The system of long waves includes an infinite number of species of waves, usually called the normal modes; the fundamental mode refers to the wave with the longest wave length. Theoretically, it can be shown that the fundamental mode is easier to excite and more difficult to damp out than any of the normal modes. In practice one can often observe the fundamental mode both during surging and seiching. Before the construction of the railroad causeway, the period of the fundamental mode was closer to 9.0 hours (Lin, 1976); after the construction of the causeway, the period of the fundamental mode of the South Basin is 6.0 hours.

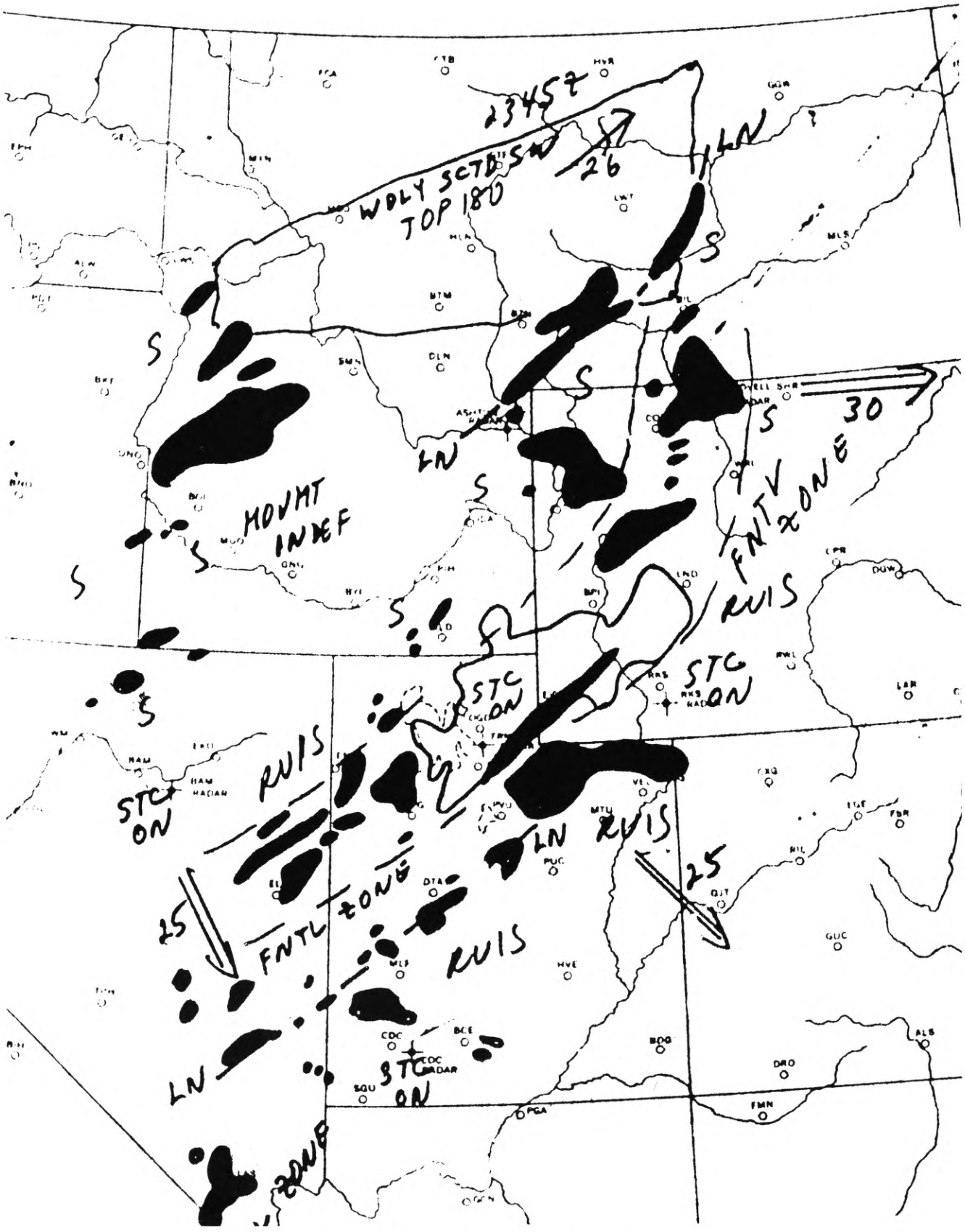

Figure 3b. Typical radar echo, associated with wind tide example I.

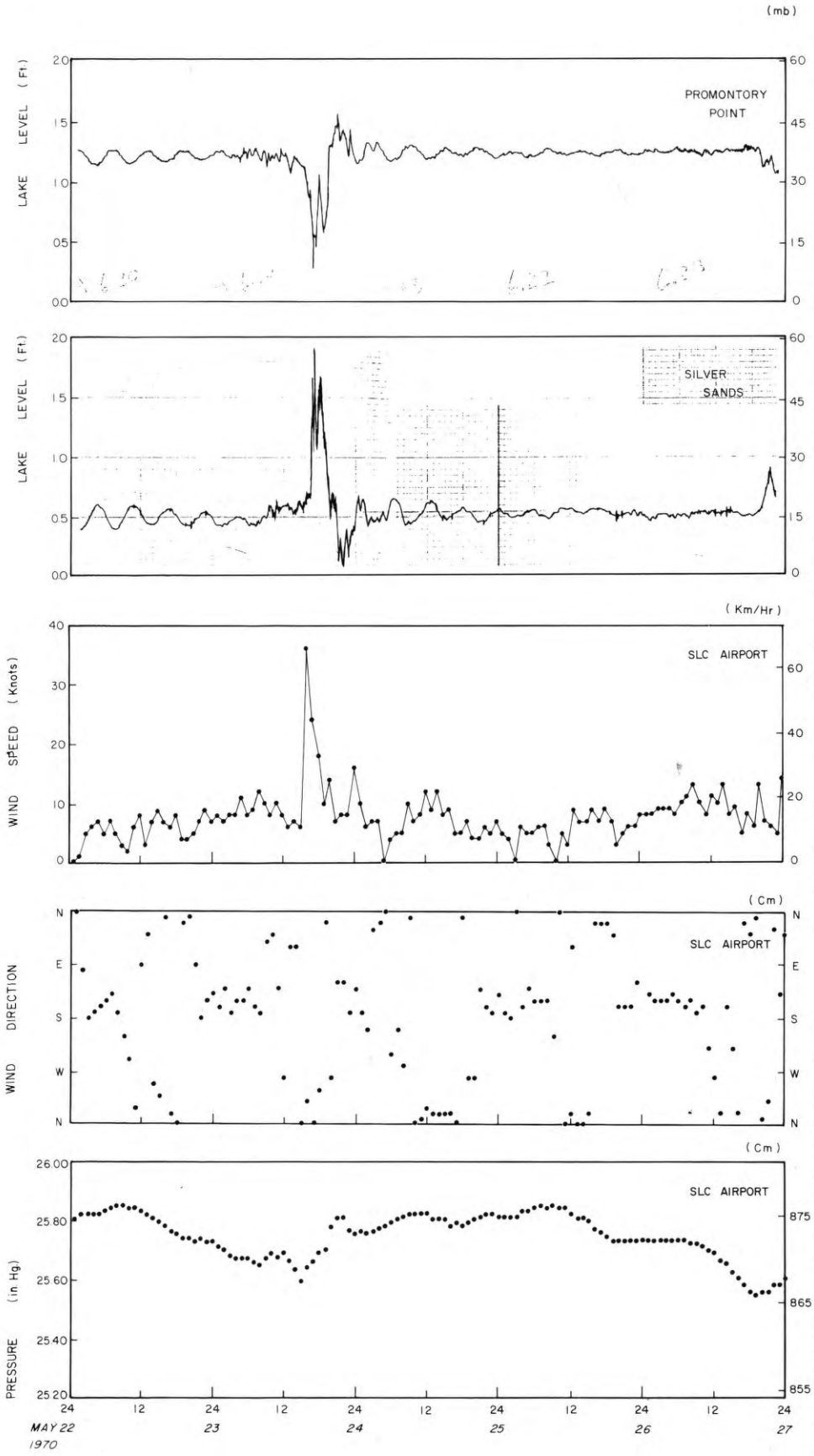

Figure 4a. Selected magrigram in the South Basin of Great Salt Lake and associated meteorological records, May 1970.

To compute the normal mode, the standard techniques of eigen value computation may be used. Usually this same computation will also reveal the associated currents and the relative range of oscillation at all the other points on the lake. The first three modes of the South Basin were computed; their periods were found to be 5.43, 2.09, and 1.53 hours (Wang, 1977). (These computations were carried out without any consideration for the bottom resistance). Inspection of figures 3 and 4 shows that there is a 6-hour wave component instead of the 5.43 hour component as computed. Spectral analysis (Wang, 1977) actually shows that the three major modes have periods of 6.33, 3.13 and 1.79 hours respectively. This discrepancy can be accounted for by the bottom resistance factor (Lin, 1976; Wang, 1977).

For the episodes selected, the lake level at Silver Sands at the climax goes up by at least one foot and may go as high as two feet above the mean level of the lake; the corresponding lake level at Promontory Point then goes down by about 80 percent of the rise at Silver Sands. Whatever the storm pattern on the lake, a definite ratio for the range of lake level fluctuations between Silver Sands and Promontory Point may be calculated. In fact, the relative range of wind tides (at its seiching phase) for any location along the lake shore is fixed; that is, the range for a wind tide at the west end of the Syracuse Causeway is always a fixed fraction of that at Silver Sands. In some locations on the lake, there are no appreciable wind tides; the line connecting these locations is called the nodal line.

Given the shape, a water level of 4200 feet, and the bottom topography of the South Basin, the relative range of the seiching can be computed fairly accurately; the results for the fundamental mode are presented in figure 5. The ranges of seiching at various locations along the lake shore are indicated as fractions of the range at Silver Sands. Figure 5 shows that the south shore is generally subject to higher waters, and that a line connecting the north end of the Antelope Island and the north end of Stansbury Island makes up a nodal line along which range of seiching is practically negligible. The sloshing motion also has an associated oscillatory current pattern, as is shown in figure 6.

A typical wind tide episode usually begins with a wind blowing from the south. To create a wind tide of major magnitude, wind speeds must exceed 10 knots for at least 12 hours. This general

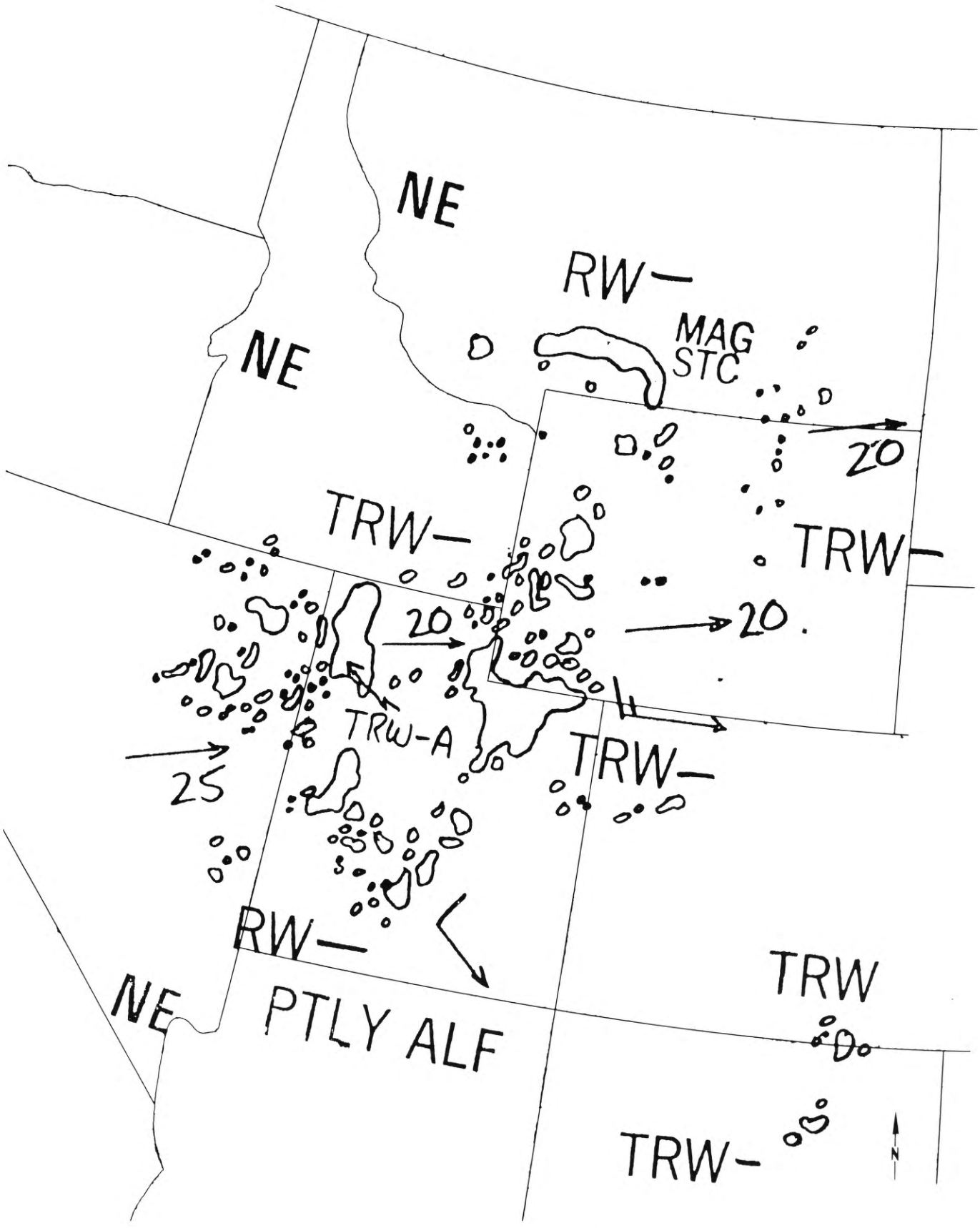

Figure 4b. Typical radar echo, associated wtih wind tide example II.

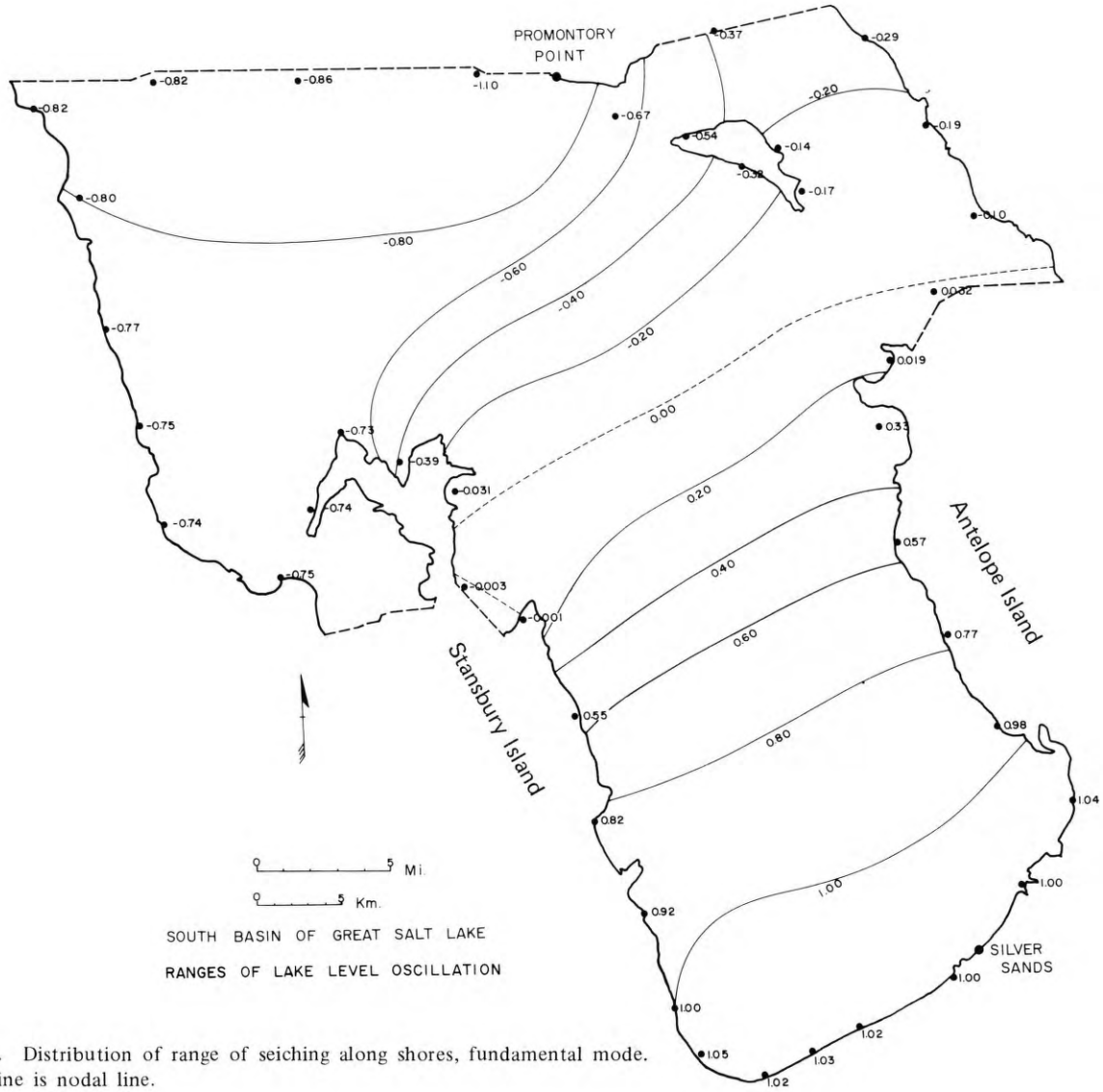

Figure 5. Distribution of range of seiching along shores, fundamental mode. Dotted line is nodal line.

rule was found to hold consistently for the 25 wind tides selected for analysis in this paper. As the wind continues to work on the surface of the lake, the surface of the lake begins to pile up (wind set-up); the lake level becomes lower at Silver Sands and at the same time higher at Promontory Point. When the wind stops, or drops below 10 knots, the seiching phase begins and then the sloshing motion follows as the lake gradually resumes its normal levels. The seiching phase usually lasts for about two days. Several such wind tides may overlap one another.

CONCLUSIONS

Wind tides on the Great Salt Lake occur frequently and involve considerable energy. The resulting sloshing motion is most effective for transporting bottom materials and thus creating and recreating the bottom topography and beach structures of the lake. This motion may also upset the balance of two-layer brines in the south basin. The effect of forces of wind on the water level may accentuate the temporary differences in lake levels between the two sides of the railroad causeway and result in extremely strong currents under the culverts, moving rock from the causeway foundations and possibly clogging the culverts.

Two feet of flooding must be expected along the south shores as a consequence of wind tides, in addition to free board designed for regular wind waves. Any installation of beach facilities must consider this flooding. The full impact of the waves on the slope stability of embankments on the lake has yet to be assessed.

Most modelling that has been done on the Great Salt Lake in connection with its water and mineral balances has not considered the implications of wind tides. Considering their importance to industry and the State of Utah, additional study is warranted.

ACKNOWLEDGEMENTS

This work is supported jointly by the Utah Geological and Mineralogical Survey and the Division of Great Salt Lake. The authors are indebted to Ted Arnow, Leon Jensen and Kidd Waddell of the U. S. Geological Survey for their cooperation in providing the hydrographs and to the Federal Aviation Administration for the meteorological data.

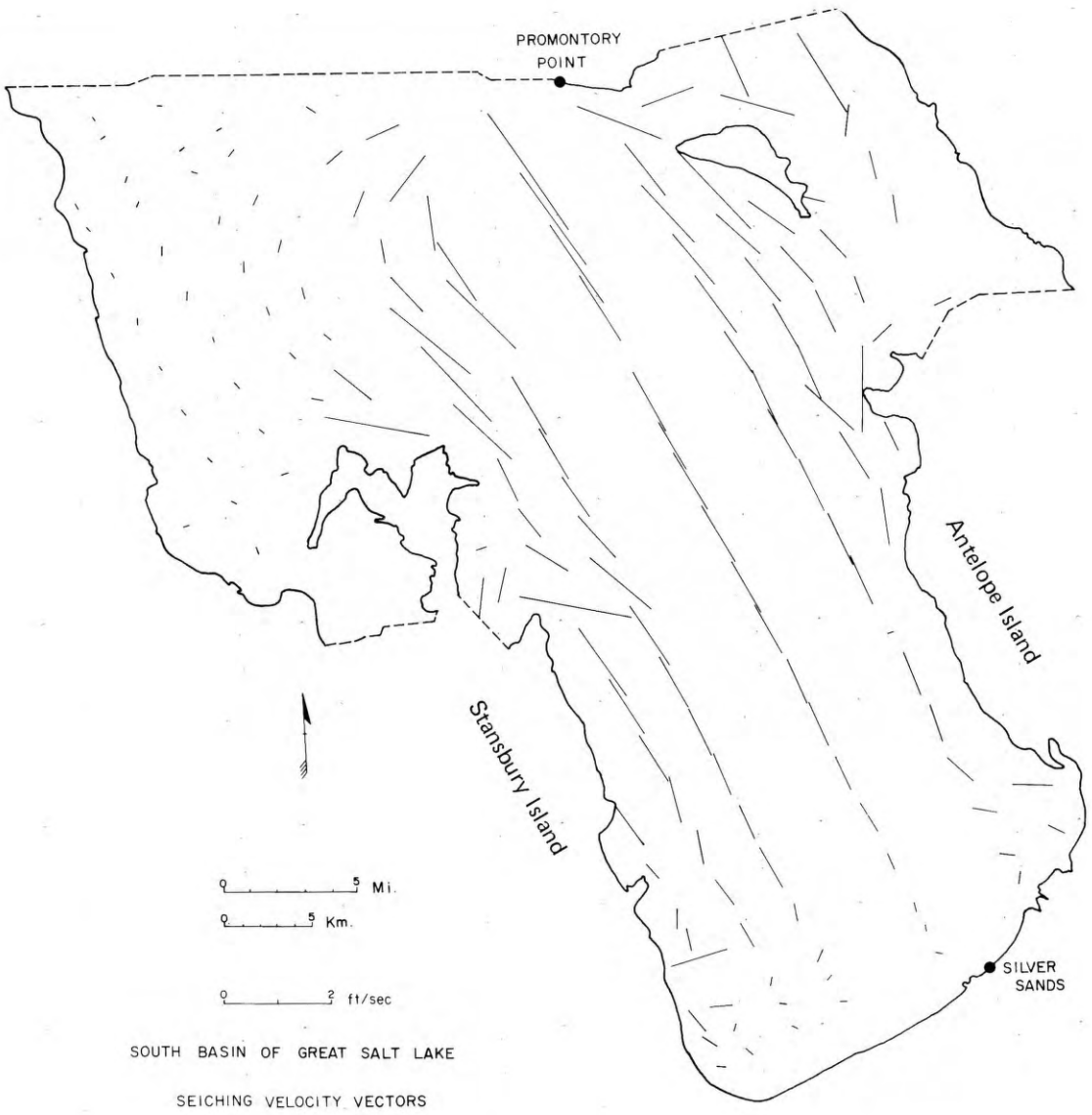

Figure 6. Current pattern of seiching, fundamental mode.

REFERENCES

HARRIS, D. L. 1955, The effect of a moving pressure disturbance on the water level in a lake (abstract): Transactions American Geophysical Union, v. 36 (3), p. 512-513; also paper in American Meteorological Monograph v. 2 no. 10, p. 46-57 (1959).

LIN, A. 1976. Survey of physical limnology of the Great Salt Lake: Utah Division of Water Resources, Technical Report. 82 p.

MORRISON, R.B., 1966, Predecessors of Great Salt Lake. *In* the Great Salt Lake, W. L. Stokes, editor: Utah Geological and Mineral Survey, Publication No. 20, p. 77-104.

SUEKAWA, Harry S., 1970, Study of the Kennecott Copper Corporation - Great Salt Lake Authority tailings test: Utah Geological and Mineral Survey Special Studies No. 28, 41 p.

WANG, Po, 1978, Wind tides of Great Salt Lake: unpublished Ph. D. Dissertation, University of Utah.

Petrolgyphs in Nine-Mile Canyon, Uinta Basin, dating from the Fremont culture, approximately 400 - 800 A.D.

Photo by UGMS Staff

MANGANESE, MOLYBDENUM AND SELENIUM IN THE GREAT SALT LAKE

by Paul L. Tayler [1], Lynn A. Hutchinson[2], and Melvin K. Muir[3]

ABSTRACT

The behavior of manganese, molybdenum and selenium in the Great Salt Lake was investigated. These elements occur in inflowing streams, both from natural and industrial origins. The brines and sediments of the Great Salt Lake were sampled and analyzed to determine the disposition of the elements in the lake. It was found that manganese, molybdenum and selenium are not concentrating in the brines as are other soluble salts but are being precipitated into the sediments.

INTRODUCTION

The behavior of copper, zinc, cadmium, mercury, lead, and arsenic ions in Great Salt Lake brines was investigated during the summer of 1976 and reported in the spring of 1977 (Tayler, Hutchinson, and Muir, 1977). To assist in understanding the behavior of these elements, pH, specific gravity, temperature, carbonate, bicarbonate, dissolved oxygen, and soluble sulfide concentrations were measured. In general, it was concluded that heavy metals do not concentrate in the brines as soluble salts but are precipitated to the sediments, along with clays, organics, and carbonates.

Not included in the original investigation but subsequently determined to be of interest are the elements manganese, molybdenum and selenium.

Manganese minerals are widely distributed in the earth's crust primarily as oxides, silicates and carbonates. Analyses of natural streams flowing into the Great Salt Lake between the years 1970 and 1974 indicate that the average concentration of manganese in the major streams is about .005 mg/ℓ. Manganese is important in industrial usage as an alloy improving the properties of steels, and therefore is widely found associated with man and his waste materials. Minute quantities of manganese are also solubilized in mineral processing such as copper ore flotation. The C-7 ditch which drains the Magna industrial area to the Great Salt Lake contained an average of .175 mg/ℓ during the 1970 to 1975 period (Utah State Division of Health 1970-1974).

Molybdenum is a relatively rare but very useful material. It is alloyed with steels for high strength and high temperature uses. It is often found associated with copper-bearing porphyry ore bodies and is a significant commercial by-product at the Bingham Mine. It is recovered as molybdenite concentrate during the flotation of the Bingham Mine ores. Small amounts may be solubilized during coppre ore flotation and will occur in concentrator waste streams. Molybdenum is not a parameter routinely monitored in streams flowing into the Great Salt Lake by the Division of Health of the State of Utah, and therefore normal concentrations in inflowing streams are not available.

Selenium is also a by-product of Kennecott Copper mining operations and, being a transition element, is used for its photovoltaic and photoconductive properties. It is recovered in smelting and refining activities and also occurs in industrial waste streams. Analysis of streams flowing into the Great Salt Lake indicates concentrations from .001 to .003 mg/ℓ in the streams and .018 mg/ℓ in the industrial C-7 ditch (Utah Division of Health 1970-1974).

To investigate the effect of the natural and industrial inputs of manganese, molybdenum, and selenium to the Great Salt Lake a sampling procedure was developed which could be coordinated with the earlier studies on the behavior of metals in the Great Salt Lake.

PROCEDURE

Nine sampling sites were chosen in the south arm of the Great Salt Lake. The sample sites were near the south shore in the vicinity of industrial and recreational areas as well as in deeper water near Antelope Island and the Utah Geological and Mineral Survey research tower. The sample station locations are identified in figure 1.

Samples were taken, with a pump, near the surface, at an intermediate level and near the bottom of each sampling site. Also, sediment samples were obtained at each site (table 1). Due to the high salt content of the samples, it was necessary to modify routine analytical techniques to avoid interference from the salts. This was done by extracting the metals of interest from the brine using a chelating agent as described in the former article (Tayler, Hutchinson, and Muir, 1977).

The samples were analyzed both for total and dissolved concentrations of manganese, molybdenum, and selenium. For total concentration the sample was analyzed as received including suspended materials. For dissolved analyses the sample was first filtered using a Teflon coarse filter followed by a 0.45 micron paper filter. The term "soluble metals" in these comments is defined as the metals that pass through the 0.45 micron paper. Soluble metals are, therefore, either physically dissolved or are contained in submicron particulates that pass through the filter.

RESULTS

The analytical results for manganese, molybdenum, and selenium both on the filtered and unfiltered portion of the samples collected are reported as a function of depth in table 2.

The presence of a very turbid, anaerobic, deep brine layer found at sample stations 1, 3, 7, 8, and 9 is again noted. This brine layer with an associated high concentration of hydrogen sulfide underlies the bulk of the lake south arm waters below the 22 foot depth and is described in great detail in Utah Geology (Tayler, Hutchinson, and Muir, 1977).

The average concentration of manganese, molybdenum, and selenium determined at the five lake depths in this sampling are summarized in table 3. Included in the table for comparative purposes are

[1] Metallurgist, Utah Copper Division, Kennecott Copper Corporation, Salt Lake City, Utah.
[2] Associate Scientist, Research Center, Kennecott Copper Corporation, Salt Lake City, Utah.
[3] Assistant Scientist, Research Center Kennecott Copper Corporation, Salt Lake City, Utah.

Table 1. Samples taken for Kennecott Copper Corporation by the Utah Geological and Mineral Survey

Station Location and No.	Depth	Temp. F°	Specific Gravity
1. ESE of American Salt Intake about 4 miles	surface	46	1.082
	15′	44	1.084
	30′7″ bottom	52	1.180
	1 sample of bottom muds		
2. 300 feet N. of Black Rock	surface	48	1.080
	5′6″	45	1.082
	11′ bottom	45	1.082
	1 sample of bottom muds		
3. Research tower	surface	47	1.084
	12′9″	44	1.084
	25′8″	47	1.174
	1 sample of bottom muds		
4. Canal N. of Silver Sand Marina	Surface	50	1.078
	7′8″	44	1.084
	15′6″ bottom	45	1.084
	1 sample of bottom muds		
5. N. end of C-7 Ditch	surface	49	1.080
	3′6″	48	1.082
	7′ bottom	46	1.086
	1 sample of bottom muds		
6. .75 mile N. of Hardy Salt Intake	surface	47	1.080
	7′	44	1.082
	14′3″ bottom	44	1.082
	1 sample of bottom muds		
7. 4 miles N. of Hardy Salt Intake	surface	48	1.080
	11′	44	1.084
	22′3″ bottom	44	1.086
	1 sample of bottom muds		
8. 2.5 miles S of Ant. Isl. S. tip	surface	47	1.080
	13′	44	1.084
	25′6″ bottom	47	1.176
	1 sample of bottom muds		
9. 2 miles W of Mollies Nipple Ant. Is.	surface	45	1.084
	16′	43	1.084
	32′ bottom	52	1.182
	1 sample of bottom muds		

the average manganese, molybdenum, and selenium concentrations in major inflowing streams and in the Magna area industrial and residential discharge (C-7 ditch) into the Great Salt Lake.

The bulk of the Great Salt Lake waters are characterized by the manganese concentrations in the surface and intermediate layers. In these layers the manganese concentration is below the level of detection of .005 mg/ℓ or 5 parts per billion and is below the concentration found in inflowing streams and particularly in industrial and residential discharges into the lake. The lake is concentrating soluble salts in its waters naturally; however, since manganese concentrations are below that found in inflowing streams, a self cleansing mechanism must be operating which has been effective for both natural and man-caused inputs. A similar effect, found for other metals studied previously, was attributed to co-precipitation with clays, organics, and carbonates which are constantly precipitating to the lake floor. This conclusion is supported by the high concentrations of these metals found in the lake sediments.

Although the concentration of molybdenum in the lake is below the detection level in all layers in the lake, significant concentrations are found in the sediments. It is evident the molybdenum is also being precipitated from the brime.

Selenium is detectable in all brines in very low concentrations. Relative to the lake water concentrations the amount of selenium in the sediments is small.

CONCLUSIONS

The average concentration of manganese, molybdenum, selenium, sodium, and chloride for inflowing streams and lake waters is give in table 4. The concentration factor for these parameters in the lake water is also given.

The concentration factors indicate the degree to which the concentration of various elements over background has occurred during the life of the present lake. Further, since the average inflow of water to the lake on a yearly basis is about 1/10 of its volume, the concentration factor can also be interpreted as the number of decades required to bring the lake to its present salt and metal concentrations if precipitation did not occur. As the lake is thousands of years old and itself the result of desiccation of a substantial portion of old lake Bonneville, the relatively few years of input required to bring the lake to the concentration of manganese and selenium to present levels, 18 and 25 years respectively, compared with 3,000 years for sodium and chloride, is indicative of the rapid precipitation of these elements relative to more soluble salt.

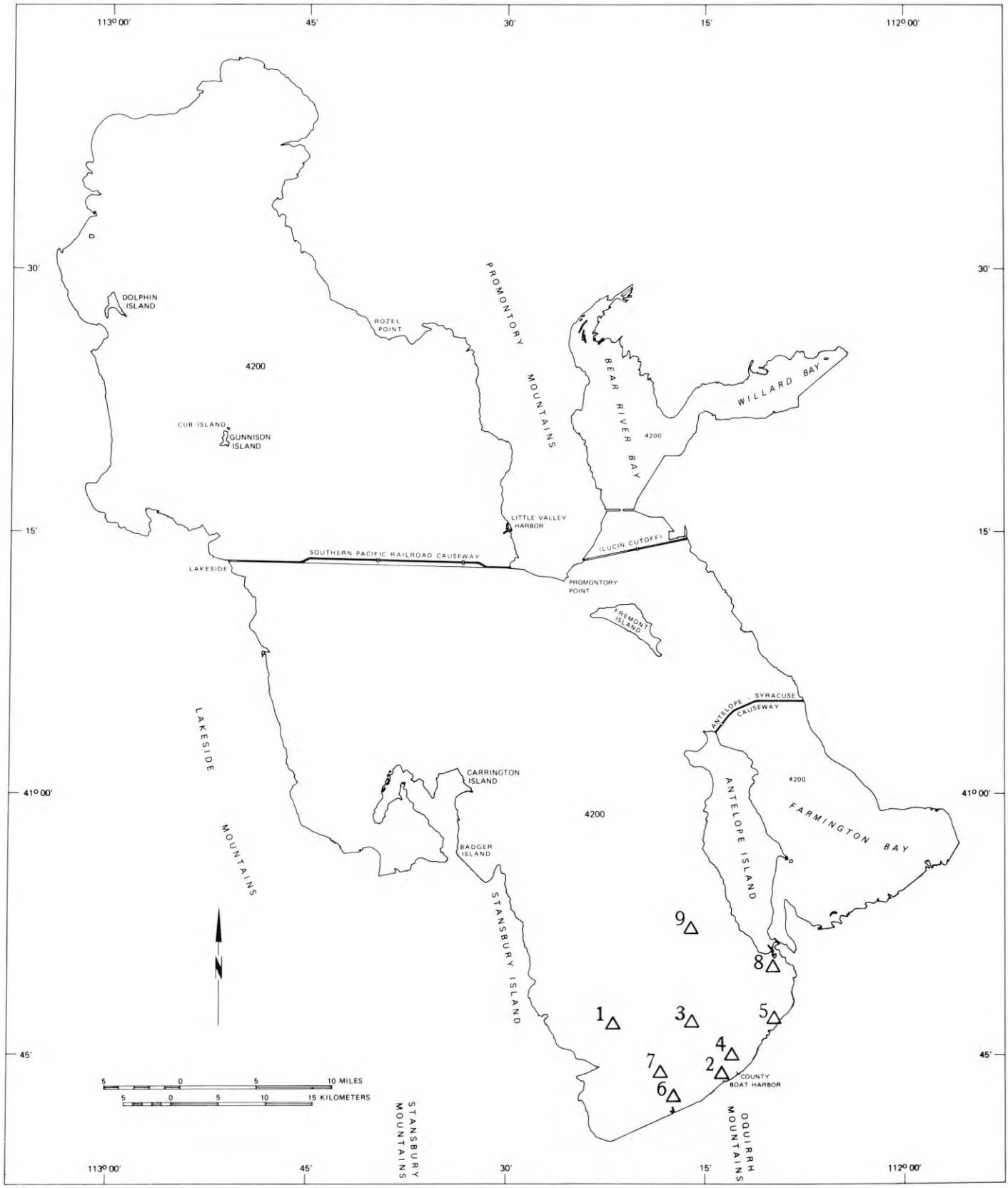

Figure 1. Great Salt Lake Chemical sampling points.

Table 2. Analytical results for Manganese, Molybdenum and Selenium on filtered and unfiltered portion of samples described in Table 1.

(All Values ppm)

Station No	Depth in feet	Manganese		Molybdenum		Selenium	
		Filtered	Unfiltered	Filtered	Unfiltered	Filtered	Unfiltered
1	0	<.005	<.005	<.010	<.010	.005	.005
	15	<.005	<.005	<.010	<.010	.003	.005
	31	.060	.210	<.010	<.010	.003	.010
	Sediment		150.		88.		0.33
2	0	<.005	<.005	<.010	<.010	.003	.007
	6	<.005	<.005	<.010	<.010	.005	.014
	11	.010	.020	<.010	<.010	.005	.007
	Sediment		80.		29.		0.16
3	0	<.005	<.005	<.010	<.010	.003	.025
	13	<.005	<.005	<.010	<.010	.003	.010
	26	.040	.190	<.010	<.010	.005	.025
	Sediment		150.		70.		0.33
4	0	<.005	<.005	<.010	<.010	.007	.014
	8	<.005	<.005	<.010	<.010	.007	.010
	16	.010	.010	<.010	<.010	.005	.017
	Sediment		265.		43.		0.16
5	0	<.005	<.005	<.010	<.010	.007	.014
	4	<.005	<.005	<.010	<.010	.003	.010
	7	.010	.010	<.010	.014	.005	.021
	Sediment		80.		24.		0.16
6	0	<.005	<.005	<.010	<.010	.005	.007
	7	<.005	<.005	<.010	<.010	.014	.014
	14	.010	.010	<.010	<.010	.007	.014
	Sediment		245.		28.		0.33
7	0	<.005	<.005	<.010	<.010	.007	.010
	11	<.005	<.005	<.010	<.010	.005	.007
	23	.010	.050	<.010	<.010	.005	.007
	Sediment		210.		17.		2.10
8	0	<.005	<.005	<.010	<.010	.005	.007
	13	<.005	<.005	<.010	<.010	.007	.007
	26	.100	.230	<.010	<.010	.014	.014
	Sediment		270.		26.		0.66
9	0	<.005	<.005	<.010	<.010	.007	.007
	16	<.005	<.005	<.010	<.010	.007	.007
	32	.080	.550	<.010	<.010	.014	.014
	Sediment		125.		32.		1.7

Table 3. Average concentration of Manganese, Molybdenum, and Selenium at five levels in Great Salt Lake, in major inflowing streams, and in the Magna Area industrial and residential discharge.

Depth	Manganese ppm	Molybdenum ppm	Selenium ppm
Surface			
Dissolved	<.005	<.010	.005
Total	<.005	<.010	.011
Intermediate			
Dissolved	<.005	<.010	.006
Total	<.005	<.010	.010
Bottom (above deep brine layer)			
Dissolved	.010	<.010	.005
Total	.020	<.010	.013
Bottom (below deep brine layer)			
Dissolved	.070	<.010	.009
total	.295	<.010	.016
Sediments			
Above Deep Brine layer	175.	28.	0.58
Below Deep Brine Layer	175.	54.	0.76
Major Inflowing Streams	.005		.002
Magna Industrial Flow (C-7 ditch)	.175		.018

Table 4. Average concentration of Manganese, Molybdenum, Selenium, Sodium and Chloride in stream inflow in Great Salt Lake.

Parameter	Stream Inflow ppm	Lake ppm	Concentration Factor
Manganese	.005	.009	1.8
Molybdenum		<.010	
Selenium	.002	.005	2.5
Sodium	300.	85,700.	285.
Chloride	490.	147,000.	300.

It appears that the manganese, molybdenum, and selenium are being continuously precipitated along with organic material, clays, and carbonates into the sediments of the lake and as a result large concentrations of toxic metals are not found in the lake waters. This concurs with the findings of the other metallic elements as reported in the previous article (Tayler, Hutchinson, and Muir 1977).

REFERENCES

TAYLER, Paul L., Lynn A. Hutchinson, Melvin K. Muir, 1977, "Heavy Metals in the Great Salt Lake". Utah Geology, vol 4, no. 1, p. 19 – 28.

Utah State Division of Health, "Water, Wastewater-Chemical and Radiological Analysis," 1970-1974.

Oil-impregnated high angle reverse fault in dark red, earthy Entrada Sandstone, north of Sweetwater Rim, NE¼ section 33, T. 26 S., R. 14 E., Emery County. Fault is seen in cross section from lower left to upper right. Geologist is seated on fault trace. Oil (and probably natural gas) moving up the fault zone and outward into permeable layers of the sandstone have bleached the dark red color to tan and white. The fault coincides with a sharp flexure which is seen at lower left. Beds are flexed opposite to that expected for a fault of this type. Displacement is estimated to be about 80 feet (25 meters).

Photo from 35mm color slide by H.R. Ritzma

A PRELIMINARY GEOLOGIC MAP OF THE WILDCAT CREEK AREA, EASTERN BEAVER COUNTY, UTAH

by Galen Haugh[1]

Although the area around Wildcat Creek in eastern Beaver County is shown on the Geologic Map of the State of Utah (Hintze, 1963) to be comprised of Tertiary Sevier River Formation, field investigation has revealed a variety of rock types, mostly igneous. In view of the geothermal potential near Cove Fort and Sulphurdale to the northeast, a geologic map correcting this discrepancy would be of vital interest to companies exploring the geothermal potential of the area. A preliminary geologic map of the Wildcat Creek area (figure 1) was made in August, 1976, using aerial photos at a scale of 1:36,500. The mapped area lies between the Mineral Mountains and Interstate 15 and encompasses about 14 x 23 km (8 x 14 miles). It is dominated by a series of north trending ridges and washes, influenced by Basin and Range block faulting, and by a line of silicic lava domes. The following rock types are found:

Granite

Granitic rocks crop out extensively in the southern part of the area and extend northward along Maple Flats. The outcrops form rounded boulders; grus is widespread and in areas of thick soil development the presence of granitic bedrock can be inferred by the granular consistency of the soil and occasional round granitic cobbles. Composition ranges from monzonite to quartz monzonite. Although rock textures are generally equigranular and fine to medium grained, local phenocrysts of feldspar up to 1 cm long are common. Alteration is moderate; the feldspar crystals are milky pink and white; the quartz phenocrysts appear slightly milky; and biotite, the predominant mafic mineral, has been partially oxidized.

Diorite

North of and adjacent to the area of granitic rocks is an area underlain by pyroxene diorite. The homogeneity and small size of this body indicate it could be a single intrusion. This body has undergone moderate alteration; the feldspar crystals are milky white and the pyroxenes are chloritized.

Rhyolite

Silicic extrusive rocks, predominately rhyolite, crop out in the northern part of the area. The presence of a number of silicic domes, for example Gillies Hill and Woodtick Hill, indicate individual eruptive centers. The rhyolite domes are outlined by a hachure pattern on the geologic map. Of particular interest is the association with the rhyolite of secondary quartz in joints and fractures and siliceous sinter, found along Interstate 15 at Mud Spring. The rhyolite on Gillies Hill contains numerous partially resorbed basaltic xenoliths.

Dacite and Andesite

Intermediate extrusive rocks predominate in the center of the area. Rock types include andesite and dacite. Alteration is locally extreme. Large areas of aphyric felsitic rocks up to hundreds of meters but generally tens of meters wide and containing quartz veins and stringers occur within the andesite and dacite. The occurrences of felsitic rocks are adjacent to the rhyolite domes, perhaps indicating an association with the rhyolite eruptions. The contacts of these altered rocks are highly variable and gradational and hence were not mapped.

Tuffs

Tuffaceous rocks are localized on Gillies Hill, apparently a volcanic center and the highest point in the area. The tuffs are foliated, poorly indurated and light tan in color.

Vitrophyre

Two outcrops of vitrophyre lie east of Gillies Hill. The outcrops are confined to separate hills in contact with rhyolite domes and apparently are separate bodies associated with the rhyolite eruptions. The vitrophyre is rhyolitic, with phenocrysts of quartz and sanidine.

Basalt

Basaltic rocks occur on the north and west sides of the mapped area. Morphologically the basalts are low-lying, lobate flows. Separate flows can be distinguished on the aerial photos as coming from several vents now covered by cinder cones, for example Crater Knoll.

Marble

In the middle of the mapped area are three small bodies of marble lying stratigraphically above the surrounding dacite and andesite. The origin and age of these bodies is unknown.

Quaternary alluvium

Alluvium, which skirts the area on practically all sides, can easily be separated into older and younger deposits. Older alluvium has flat erosional surfaces distinctly above the present drainage system (such as The Hogback). Younger alluvium is found in the present drainage system, predominately Cunningham Wash and the Wildcat Creek drainage. It appears that the two distinctly separate occurrences of alluvium reflect rejuvenation due to uplift of the area.

Age of the Rocks

Although definite ages of the rock types in the area have not been determined, approximate time relations can be assigned based upon structural and stratigraphic relations and by comparing these rocks with similar units for which the ages are known.

It is probable that the granite in the Wildcat Creek area and those in the Mineral Mountains are roughly of the same age, if not the same body. Granitic rocks in the Mineral Mountains, cropping out a mere two kilometers to the west, have been assigned several ages. Armstrong (1970) determined a K-Ar age of 9.2 ± 0.3 m.y., using biotite. Park (1968) used biotite and muscovite associated with beryllium mineralization contemporaneous with but slightly later than the crystallization of the pluton to calculate a K-Ar age of 15.5 ± 1.5 m.y. Stern (in Whelan, 1970) used zircon to obtain a lead-alpha age of 10 ± 10 m.y. The high uncertainty of this last determination is explained by low lead content of the sample, near the limit of detection.

While ages derived by the K-Ar method are much more precise than those derived by other methods, and are preferred, Ar concentrations record the last thermal event above 300° C. Waters of 300° C have been found by geothermal development at Roosevelt Hot Springs just west of the Mineral Mountains; there-

[1]Graduate Student, Department of Geology, Brigham Young University, Provo, Utah 84602

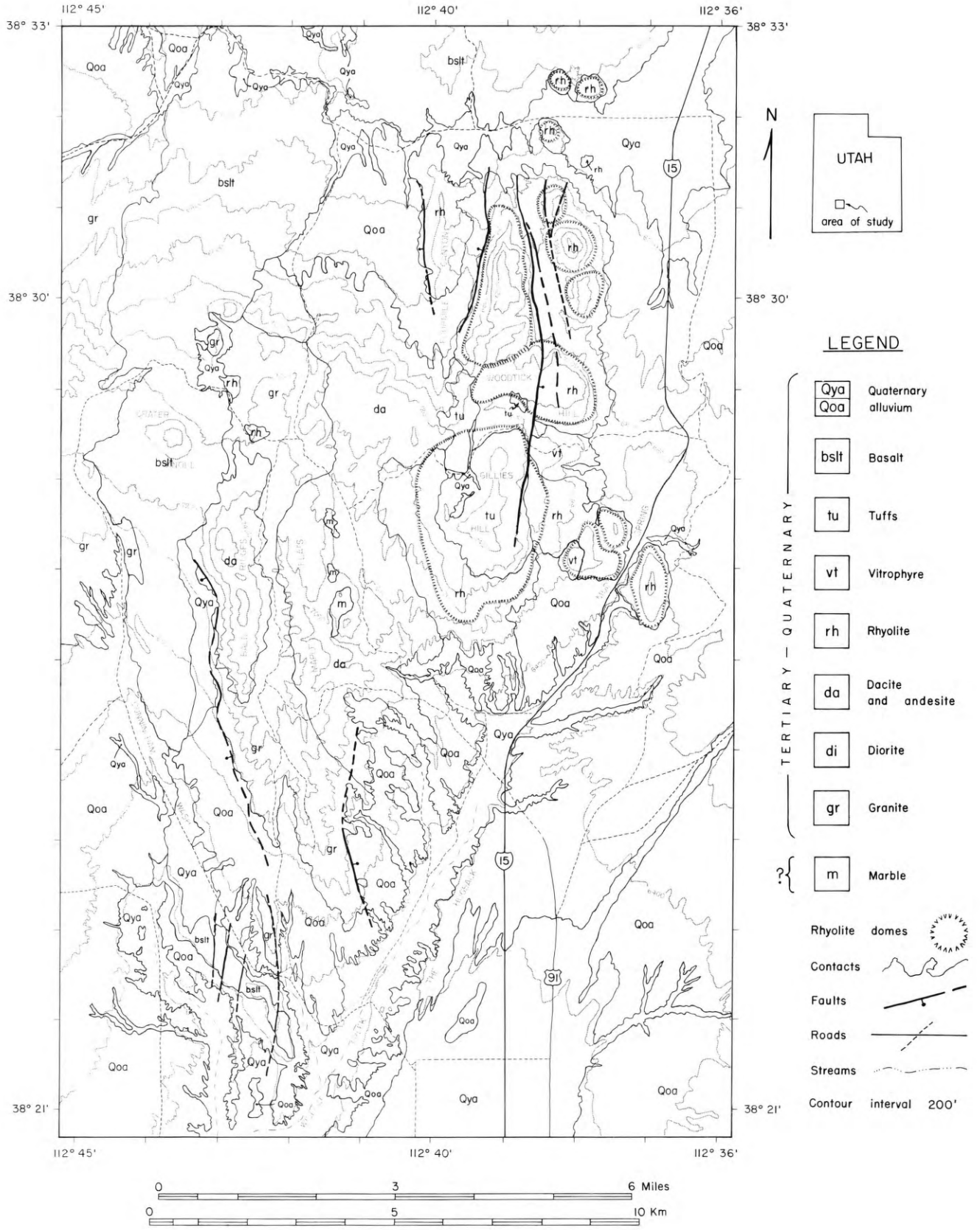

Figure 1. Preliminary geologic map of the Wildcat Creek area.

fore the K-Ar ages cited above must be considered as minimal dates for the pluton.

Silicic alteration of the andesite and dacite in contact with the granite indicates intrusion of the granite into andesitic country rock. This relationship, which suggests the andesite and dacite are older than the granitic material, is corroborated by ages of other nearby intermediate extrusive rocks which range between 17 and 34 m.y. (Stewart and Carlson, 1976).

More recent silicic volcanism has also produced alteration of the dacite and andesite. Rhyolites 25 kilometers to the north have been dated at 0.4 to 2.2 m.y. (Lipman and others, 1977). The rhyolite domes in the Wildcat creek area likely fall within this age range.

Structural relations indicate the basaltic flows and cones are the youngest of the indurated rock units. Within the area the oldest basaltic flows are no more than one million years (Clark, 1977). Ages of morphologically similar basalt flows in the Black Rock Desert, 50 kilometers to the north, have all been found to be less than 1 million years old (Hoover, 1974). However, the inclusion of basalt xenoliths in the Gillies Hill rhyolite and the range of ages given for the rhyolite suggest that there may be an overlapping of ages of rhyolites and basalts.

ACKNOWLEDGEMENTS

Appreciation is given to M. G. Best, L. F. Hintze, and G. R. Nielsen for help in manuscript preparation and reviewing and to Phillips Petroleum Company for financial assistance in support of this project.

REFERENCES

ARMSTRONG, R. L., 1970, Geochronology of Tertiary igneous rocks, eastern Basin and Range Province, western Utah, eastern Nevada, and vicinity: Geochimica Cosmochimica Acta, v. 34, p. 203-232.

CLARK, E., 1977, Late Cenozoic volcanic and tectonic activity along the eastern margin of the Great Basin in the proximity of Cove Fort, Utah: M.S. thesis, Brigham Young University, Provo, Utah.

HINTZE, L.F., 1963, Geologic Map of Utah, Southwest Quarter, Utah Geological & Mineral Survey.

HOOVER, J.D., 1974, Periodic Quaternary volcanism in the Black Rock Desert, Utah: BYU Geology Studies, v. 21, part 1, p.3-72.

LIPMAN, P.W., P.D. Rowley, H.H. Mehnert, S.H. Evans, P.W. Nash, and F.H. Brown, 1977, Pleistocene rhyolite of the Mineral Mountains, Utah: geothermal and archaeological significance: in press.

PARK, G.M., 1968, Geochronology of beryllium deposits, Utah: M.S. thesis, University of Utah, Salt Lake City, Utah.

STEWART, J.H., and J.E. Carlson, 1976, Cenozoic rocks of Nevada: Nevada Bureau of Mines and Geology, Map 52, University of Nevada, Reno, Nevada.

WHELAN, J.A., 1970, Radioactive and isotopic age determinations of Utah rocks: Utah Geological and Mineralogical Survey Bulletin no. 81, p. 25.

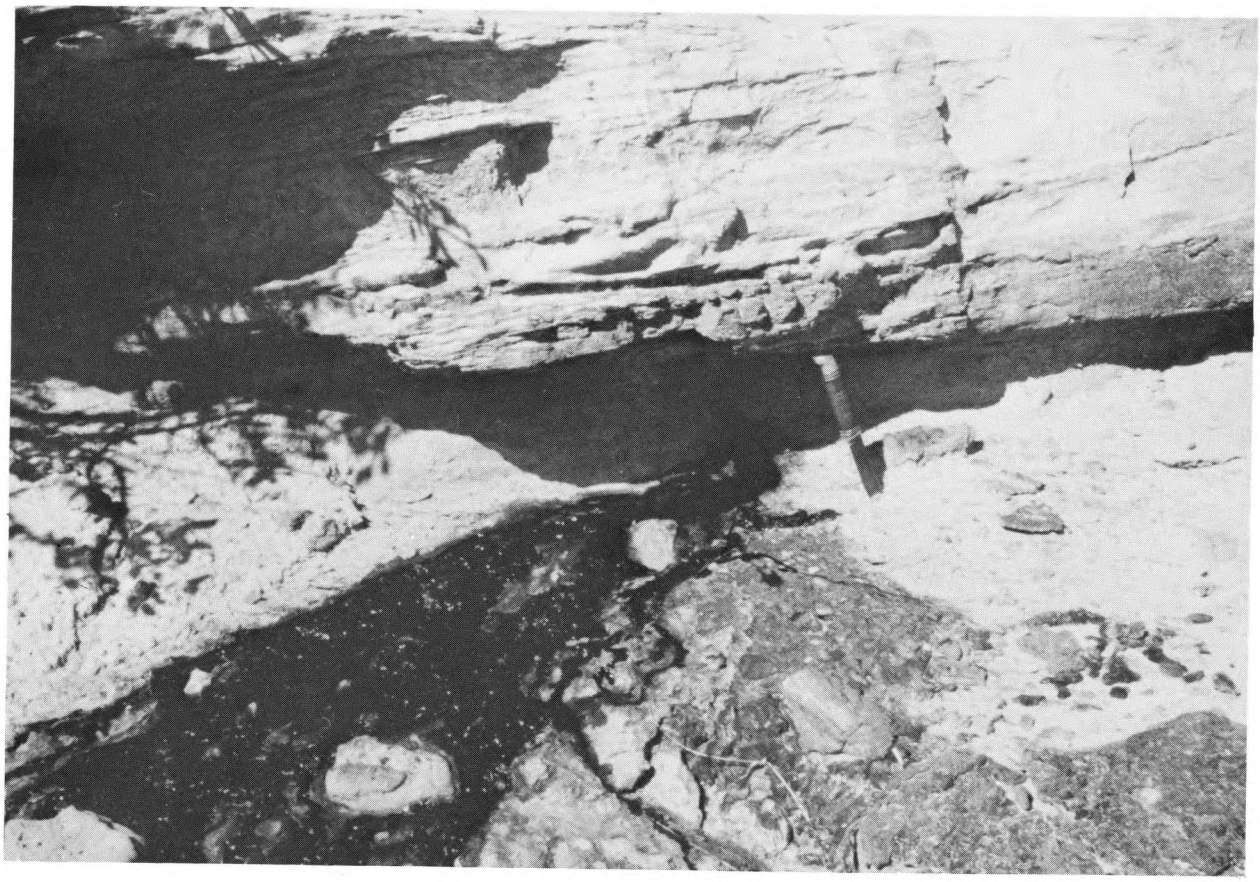

Oil seep in Elaterite Basin, Wayne County, in the northeast part of the giant Tar Sand Triangle oil sand deposit. The seep of oil emerges from a deeply recessed bedding plane in the Permian White Rim Sandstone where it is intersected at near right angles by a zone of closely spaced joints. The joints are parallel to the knife handle.

Seeps of this sort are commonly activated by ground water circulating through the permeable sandstone. During dry periods the seep may cease to flow and become inconspicuous. The outflow often becomes covered with a film of wind-drifted silt and sand and may only become apparent when stepped in by an unwary geologist.

Photo from 35mm. color slide by H. R. Ritzma

GRAVITY STUDY OF THE FUMAROLE BUTTE AREA, JUAB AND MILLARD COUNTIES, UTAH

Timothy B. Smith[1], *Kenneth L. Cook*[2], *and Wayne J. Peeples*[3]

ABSTRACT

A gravity survey was made in 1973 of the Fumarole Butte area, including the Crater Springs KGRA (Baker Hot Springs), located approximately 39 km (22 miles) NW of Delta, Utah. About 500 stations were taken as part of a study of geothermal exploration techniques. The region of investigation includes portions of both Juab and Millard Counties and incorporates parts of the Desert, McDowell and Drum Mountains.

A simple Bouguer gravity anomaly map was computed and two-dimensional geologic models were prepared for two east-west gravity profiles. The analysis of the gravity data, in conjunction with the known geology and the results from other geophysical studies, led to the following interpretations: 1) the indication of two buried intrusive bodies – one a north-northwestward-trending dike lying beneath the Baker Hot Springs and the eastern margin of the Fumarole Butte lava flows and another several miles southwest of Desert Mountain; 2) the delineation of previously unpublished Basin and Range faults and associated grabens; and 3) the existence of a basement flexure with postulated fractures that served as conduits for the upwelling magma to reach the surface at Fumarole Butte.

INTRODUCTION

Location

During the summer and fall of 1973, a gravity survey was conducted in the area over and adjacent to Fumarole Butte, located approximately 39 km (22 miles) northwest of Delta, Utah, in south central Juab County. The total region of investigation encompasses the area from Township 12 South to Township 15 South, and from Range 6 West to Range 10 West, Salt Lake Base Meridian (figures 1 and 2). This region includes portions of both Juab and Millard counties and incorporates parts of the Desert, McDowell, and Drum Mountains.

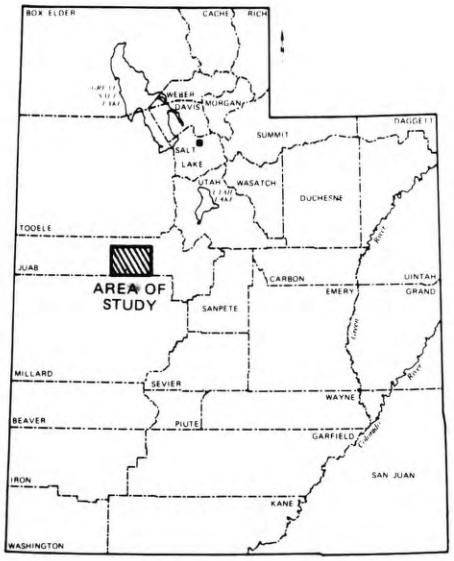

Figure 1. Index Map of Utah showing survey area.

Baker Hot Springs, which lie on the eastern margin of Fumarole Butte, have been designated variously as "Crater Springs" on the Army Map Service Topographic 2-degree Delta sheet, (limited revision 1962) (figure 2), "Abraham Hot Springs" (Milligan and others, 1966), and "Baker Hot Springs" by White and others (1975) and on the Baker Hot Springs, Utah 7 1/2 minute topographic quadrangle map of the U.S. Geological Survey published in 1971. The Known Geothermal Resource Area (KGRA), including the hot springs, has been designated the "Crater Springs KGRA" (Goodwin and others, 1971). In this paper, the springs will be designated "Baker Hot Springs".

Purpose of Investigation

This investigation was designed as one part of a study of geothermal exploration techniques for potential geothermal sites. The Fumarole Butte area (part of which is designated as the Crater Springs Known Geothermal Resource Area - KGRA, (Goodwin and others 1971) appeared to be such a potential geothermal site, and geophysical studies were concentrated there during the summer and fall of 1973. The use of the gravity technique had three objectives: 1) to aid in determining the source of heat at Baker Hot Springs and at the volcanic neck in the interior of Fumarole Butte (figure 2); 2) to locate Basin and Range faults typical in the area which might be acting as geothermal conduits; and 3) to enhance knowledge of the basic geologic structural setting of the region, thereby increasing the effectiveness of the other geophysical techniques.

Previous Investigations

Gilbert (1890), in his Lake Bonneville report, discussed some of the relationships between the volcanics at Fumarole Butte and Lake Bonneville and produced an early record of residual heat at the volcanic neck and hot springs. Erickson (1963), in a regional study of the volcanic rocks in western Juab County, described the geology of Fumarole Butte and the McDowell Mountains. Hogg (1972) documented the petrographic and chemical nature of the middle Tertiary through early Quaternary volcanics, in which the basaltic flows at Fumarole Butte are included. Crittenden and others (1961) described manganese deposits and the geologic setting of the Drum Mountains. Calkins (1970 and 1972) provided some geophysical insight into the geologic setting of Desert Mountain with a magnetic and gravity study, and Rees (1971) presented a more comprehensive geologic picture. Shawe (1972), in a reconnaissance geology and mineral potential study of the Thomas, McDowell, and Desert Mountains, proposed three separate volcanic calderas in the region.

[1] Formerly Graduate Student, University of Utah, Salt Lake City, Utah 84112

[2] Department of Geology and Geophysics, University of Utah, Salt Lake City, Utah 84112

[3] Formerly Department of Geology and Geophysics, University of Utah, Salt Lake City, Utah 84112, now Department of Geological Sciences, Southern Methodist University, Dallas, Texas, 75275.

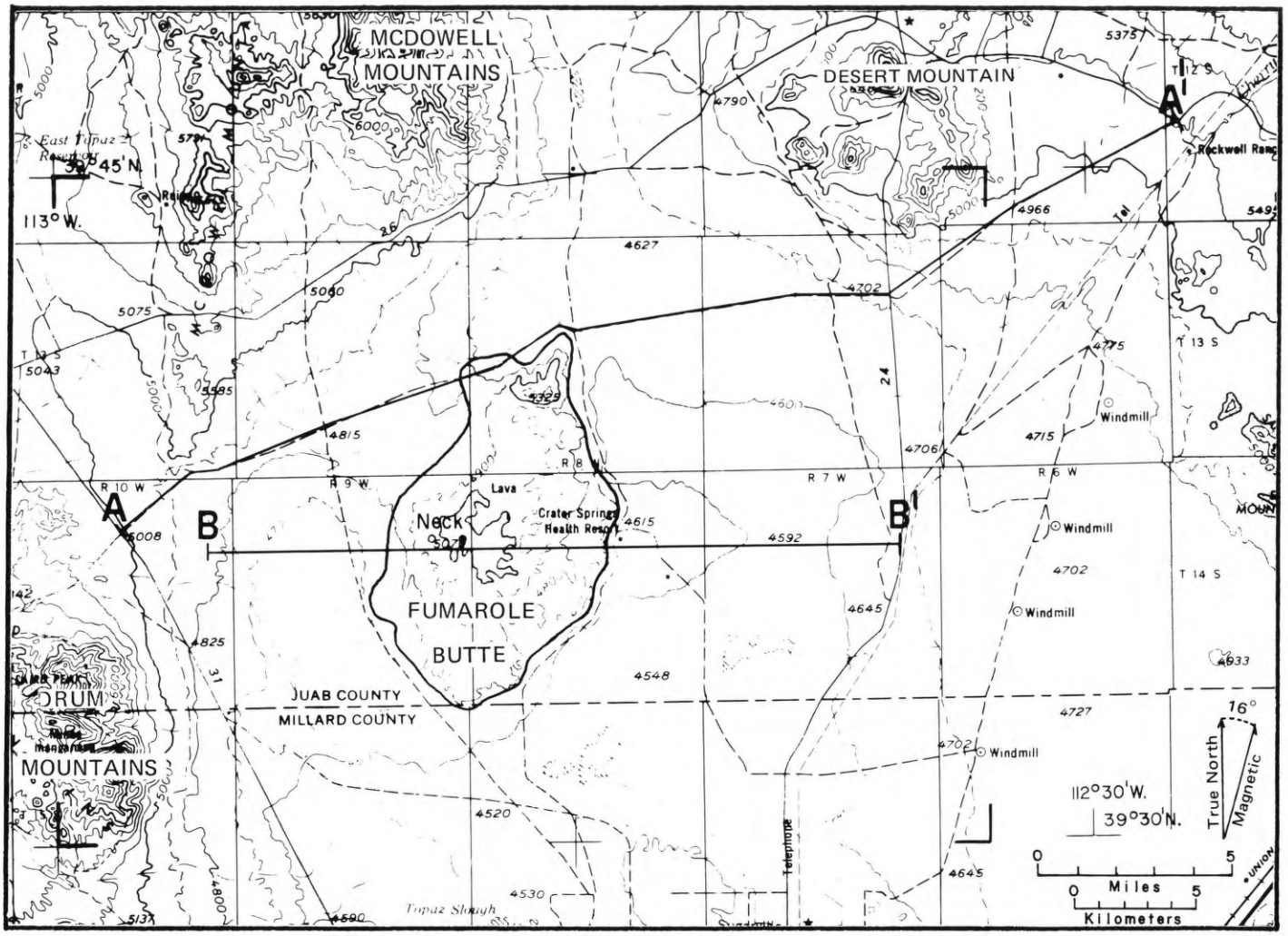

Figure 2. Part of Army Map Service Topographic Base Map, Delta Quadrangle (1962), showing survey area. Corner brackets indicated on this map correspond with corners of maps shown in figures 4 and 5. (The hot springs at "Crater Springs Health Resort", shown on this map, are designated "Baker Hot Springs" throughout this report.

GENERALIZED GEOLOGY

Regional Geology

The area under investigation lies within the Basin and Range province of the western United States. During Precambrian time and much of Paleozoic time, thick layers of marine sediments deposited in the Cordilleran miogeosyncline which encompassed the eastern portion of the Basin and Range province, were converted to the quartzites, shales, and carbonates now observable. Later Mesozoic continental and marine rocks, which may have existed in western Utah, were mostly destroyed by erosional cycles associated with both the Sevier orogeny during the Cretaceous and the later formation of the mountain ranges in the Great Basin during Tertiary time. The Sevier orogeny produced folding and eastward overthrusting of the thick sequences of marine sedimentary rocks, thereby making western Utah a rugged highland for a time. Volcanic activity occurred in three distinct phases. The first phase produced intermediate – composition lavas and agglomerates during the early Tertiary. The second phase produced silicic ash-flow tuffs, as well as the granitic and monzonitic intrusions. The last phase, during the late Tertiary to early Quaternary, produced a bimodal association of basalt and rhyolite. Much of the volcanic episodes was concurrent with the middle Tertiary to present Basin and Range block faulting that created the existing mountains from upthrown blocks and the existing alluvial basins from grabens. Lake Bonneville further modified the geology by depositing lake sediments and by eroding its margins.

Local Geology

The geology in the region of investigation is varied and complex (figure 4). Fumarole Butte, a potential geothermal target area, is comprised of four main rock units which, from bottom to top, are a rhyolite, a conglomerate, a tholeiitic basalt, and a basaltic andesite. The rhyolite,conglomerate, and tholeiitic basalt are exposed in an area of high elevation known as the North Butte at the north end of the lava flows. The rhyolite, which may correlate with the older rhyolite flows in the Thomas Range, contains phenocrysts of sanidine and smoky quartz. The conglomerate is described by Hogg (1972) as:

> "a reddish brown conglomerate 200 feet thick, containing sand, pebble-, and cobble-sized fragments of Paleozoic sediments (mainly white to pink quartzite with minor dark gray limestone), and lesser quantities of pumice, rhyolite, and mafic lava all cemented by calcareous material."

The tholeiitic basalt is somewhat coarser grained than the basaltic andesite flows to the south and is apparently

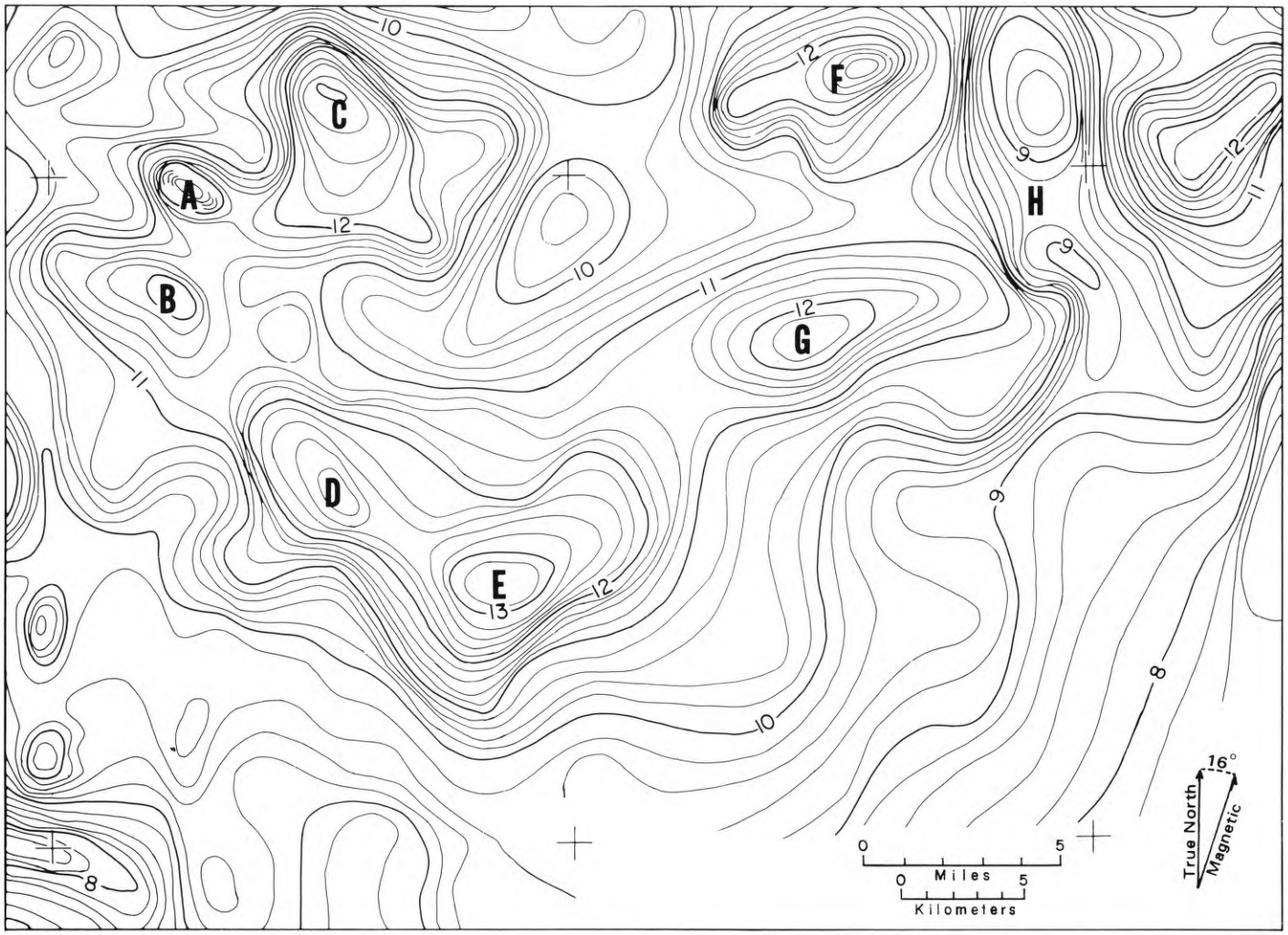

Figure 3. Aeromagnetic map of survey area. Contour interval 20 gammas. (Same area as figure 2). After Shuey, 1974.

older, since the southern basaltic andesites flow around the tholeitic basalt of the North Butte and are less extensively eroded. The southern Fumarole Butte lava is comprised of a number of sequential flows, primarily basaltic andesite in nature. The lava tends to be more scoriaceous in the younger flows of this sequence, at the edges of these flows, and around the volcanic neck in the interior of Fumarole Butte.

Whole-rock K-Ar analysis by the U.S. Geological Survey indicates an age of approximately 900,000 years for the basaltic andesite on the southeastern flank of Fumarole Butte (R.E. Anderson and R.C. Bucknam, 1977, oral communication).

On top of the volcanic neck, warm, moist air is still issuing forth from several cracks in the rock, possibly indicating residual heat. Baker Hot Springs are located east of the volcanic neck at the eastern edge of the lava flow and are comprised of a large number of small springs. The temperature of the water issuing forth from the springs ranges from 71.1° C to 87.2° C (Mundorff, 1970). The chemistry of the springs, including the manganese deposits, was discussed by Callaghan and Thomas (1939). Using the sodium, potassium, and calcium geothermometer techniques of Fournier and Trusdell (1973), Parry (1976) has estimated a temperature of last wallrock equilibrium of the water of Baker Hot Springs to be 155° C.

The Desert Mountain, to the northeast, is composed mainly of igneous rocks including granodiorite, granite, and rhyolitic volcanic rock (Rees, 1971). The granodiorite is the oldest and crops out in a northwest-trending zone through the center of the mountain. The granite appears to be a younger unit intruded under pre-existing granodiorite and may form the core of the mountain. Tertiary volcanics are located on the eastern edge of Desert Mountain.

The McDowell Mountains, to the northwest (figure 4), also known locally as the Keg Mountains, are comprised of a complex system of Teritary extrusive volcanics (Erickson, 1963; Staub, 1975). The rock units include older rhyolite-dacite-quartz latite ignimbrites, andesite-trachyte- latite flows, rhyolite-dacite-quartz latite pyroclastics, rhyolite-dacite-quartz latite flows, and basalt and basaltic andesite flows. For the purposes of this report all of these rock units will be designated Tertiary volcanics.

The Drum Mountains, to the southwest (figure 4), are a westward-tilted block of Cambrian rocks. The section exposes approximately 2800 meters (9,000 feet) of quartzite, some of which may be Precambrian near the base, overlain by some 900 meters (3,000 feet) of carbonate rocks. The rocks strike north

and dip about 30° W. Numerous east- to northeast-trending faults and fractures cut the area. Tertiary volcanic rocks rest on the older Cambrian rocks around the edges of the range. The Detroit mining district produced economic deposits of manganese near the center of the Drum Mountains.

GRAVITY DATA ACQUISITION AND COMPILATION

Surveys

The gravity data utilized in this report originated from three separate surveys and consist of about five hundred stations, a number of which were duplicated between surveys. Approximately half of the stations were established by T.B. Smith during the summer and fall of 1973. The remainder were established as the field projects of two different gravity classes directed by K. L. Cook of the University of Utah. The first survey was conducted in the spring of 1972 and concentrated its efforts on the McDowell Mountains area. The second survey, conducted in the fall of 1973, was concentrated principally near Desert Mountain, but also included two profiles between Desert Mountain and the McDowell Mountains. Thus Smith's survey covers the primary target area of interest, while the additional surveys add information to the fringe areas.

Instruments

During the course of the three surveys, two gravimeters and four altimeters were used. One of the gravimeters was the Worden number 735, which has a scale conversion constant of 1.1246(8) miligals per scale division and a precision capability of 0.01 mgal. The other was the LaCoste & Romberg Model G Geodetic Gravity Meter number 264 with an inherent precision capability of 0.001 mgal. The scale conversion constant ranges from 1.05609 mgal per scale division to 1.05865 mgal per scale division, depending upon the position in the range of scale values in which the reading was taken. The Wallace and Tiernan Company altimeters were either model number 185 or F185 with which altitudes could be estimated to the nearest foot.

Field Techniques

The stations were located and plotted on 7 1/2 minute "blue-line" preliminary topographic quadrangle maps available from the United States Geological Survey. Since most of the stations were located at bench marks, road intersections, or section corners, the horizontal control was excellent. Elevation control was obtained for the stations by several methods. The elevations of stations at bench marks and at road intersections with spot elevations were read directly from the topographic maps. For stations with unknown elevations, altimeters were used in pairs to insure reliable readings.

Since the contour intervals on the topographic maps were as small as 5 to 10 feet, it became apparent in many places that it was more accurate to pick the elevations off the topographic maps at stations where the horizontal control was precise. This technique was utilized in all three surveys, giving elevation accuracy to within a few feet.

All three gravity surveys were tied to the Delta Base Station in the Utah Gravity Base Station Network (Cook and others, 1971). A primary field base station, designated the Fumarole Butte Base Station (figure 4), was established from which to conduct field operations. The observed gravity value for this base was obtained by taking successive gravity readings at the Delta Base Station and the Fumarole Butte Base Station in an ABABA pattern and correcting for instrument drift. The survey conducted in the spring of 1972 similarly established the Keg Mountains Base Station as a primary field base for that survey; and the Keg Mountains Base Station was tied at that time to the Eureka Base Station of the Utah Gravity Base Station Network (Cook and others, 1971).

During the surveys, the gravimeter readings were taken using the standard "looping" technique, in which readings were taken at a gravity base station both before and after a sequence of readings taken at the regular field stations. This technique provides data for making corrections for instrument drift.

Base Station Descriptions

Fumarole Butte Base Station

The Fumarole Butte Base Station, established July 17, 1973, by T.B. Smith, is located .3 meter (1 foot) north of the bench mark stamped 77 HLS, established by the United States Coast and Geodetic Survey in the southwest 1/4 of Section 8, Township 15 South, Range 8 West, Salt Lake Base Meridian, in 1970. This particular bench mark is located approximately 10 m (35 feet) east of and 6 m (20 feet) south of the intersection of the main paved east-west road to the Brush Beryllium mine and the improved gravel

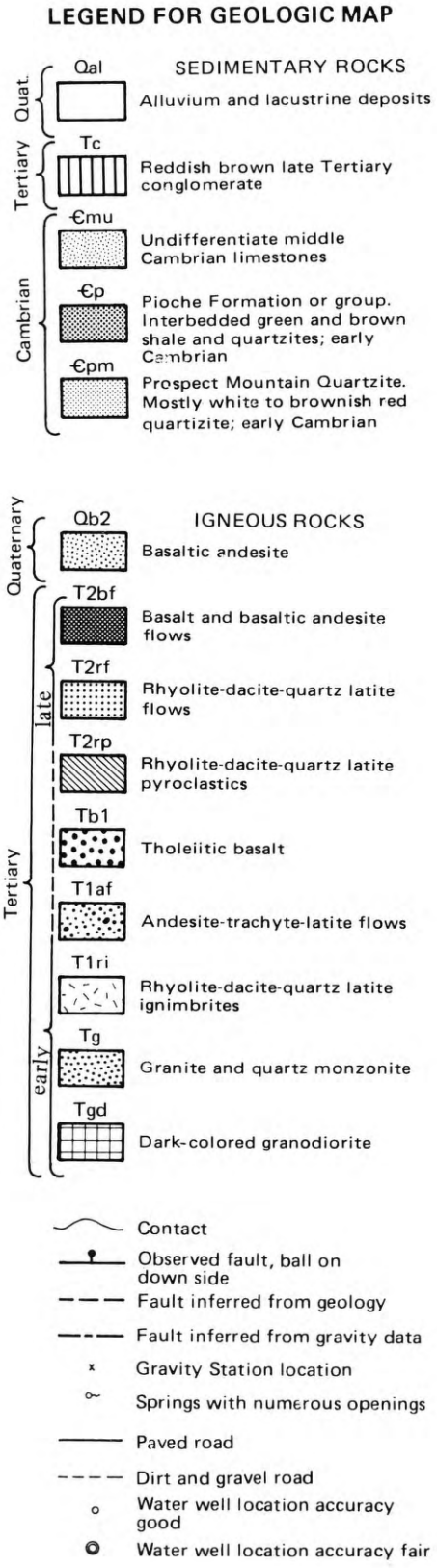

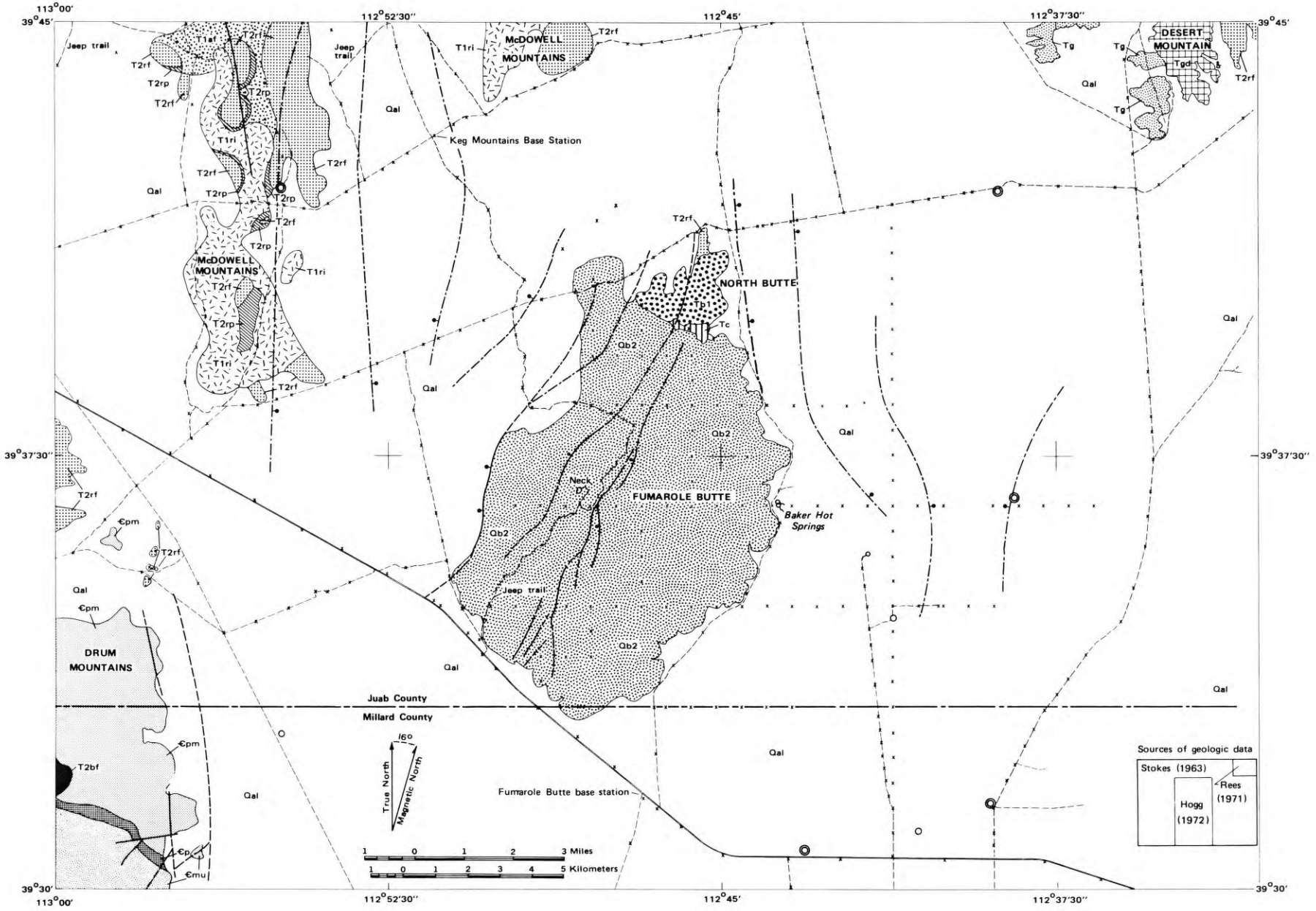

Figure 4. Generalized geologic map of the Fumarole Butte area, Juab and Millard Counties, Utah (from Stokes, 1963).

north-south road from Smelter Knolls, south of the Fumarole Butte lava flows (figure 4 and Fumarole Butte, Utah 7½ minute topographic quadrangle map of the USGS). Readings were taken with the gravimeter placed on a tripod plate, thereby raising the instrument about 2.5 cm (1 inch) above the ground. Pertinent facts:

Station	FB-1
Latitude	39° 31.63' N.
Longitude	112° 47.43' W.
Elevation	4,564 feet
Observed Gravity	979,694.63 mgal
Theoretical Gravity	980,138.54 mgal
Free-air Gravity Anomaly Value	-14.62 mgal
Simple Bouguer Gravity Anomaly Value	-170.07 mgal

The Keg Mountains Base Station

The Keg Mountains Base Station, established April 8, 1972 by K. L. Cook, is located .3 m (1 foot) northwest of the bench mark stamped 43 HSL, established by the United States Coast and Geodetic Survey in Section 4, Township 13 South, Range 9 West, Salt Lake Base Meridian. The bench mark is located approximately 120 m (400 feet) east of the intersection of the east-west road from Jericho and the north-south road west of Fumarole Butte, and is about 1.5 m (5 feet) north of the east-west Jerico road (figure 4 and The Hogback, Utah 7 1/2 minute topographic quadrangle map of the USGS). Readings were taken with the gravimeter placed on a tripod plate, thereby raising the instrument about 2.5 cm (1 inch) above the ground. Pertinent facts:

Station	72501 or Keg Base
Latitude	39° 43.07' N.
Longitude	112° 51.44' W.
Elevation	5,103 feet
Observed Gravity	979,664.69 mgal
Theoretical Gravity	980,155.43 mgal
Free-air Gravity Anomaly Value	-10.75 mgal
Simple Bouguer Gravity Anomaly Value	-184.56 mgal

Data Reduction

The raw gravity field data were compiled for and processed by a computer reduction program. Corrections for instrument drift of the altimeters and gravimeters and for earth tidal effects were made by assuming linear drift with time and performing the necessary computations. The elevations of the gravity stations in the altimeter loops were calculated and the theoretical gravity value computed for each station using the International Gravity Formula (Swick, 1942). Once the horizontal and vertical control of the stations was determined, the free-air and simple Bouguer values were calculated using a density of 2.67 gm/cc. The free-air correction was 0.09406 mgal/ft, and the combined elevation correction was 0.05999 mgal/ft.

Terrain corrections were computed for sample stations throughout the survey area using the United States Coast and Geodetic Survey terrain correction zone charts developed by Hayford and Bowie (Swick, 1942). For calculations carried through zone O, the terrain corrections were sufficiently small (0.1 to 0.4 mgal) to be neglected, and therefore a simple Bouguer gravity anomaly map was compiled.

Error Analysis

The Worden and the LaCoste and Romberg gravity meters have inherent precision capabilities of 0.01 mgal and 0.001 mgal, respectively. The non-validity of the linear interpolation method of correction for instrument drift and earth tidal effects provides another small portion of the accumulative error. The LaCoste and Romberg gravity meter has very small instrument drift (usually less than 0.2 mgal/month): hence the linear approximation of the instrument drift is in error at most 0.005 mgal for 5-hour loops. The Worden gravity meter has slightly more drift due to fluctuation of the quartz spring temperature; but for most cases, the error introduced by the linear approximation of the instrument drift is generally less than 0.05 mgal for 5-hour loops. The maximum earth tidal effect is about 0.3 mgal in a 6-hour interval. When the base station is occupied approximately every 5 hours and the drift removed by linear means, the resultant error is generally less than 0.1 mgal for either the Worden or the LaCoste and Romberg gravity meters. These errors can be reduced by making earth tidal corrections, but this was not done for the present survey. Imprecise horizontal control results in two types of error. Since horizontal control is principally utilized in the latitude correction, which is approximately 1.3 mgal/mile in the latitude of the survey area, 30 m (100 feet) of north-south displacement would contribute a 0.025 mgal error. No direct error would result in an east-west displacement of horizontal control. If the station location was incorrectly plotted an indirect error could be introduced in the vertical control of those stations at which the elevations were estimated from the topographic maps. Many of the stations in this study have known elevations at bench marks and road intersections but the elevations of other stations were dependent on the horizontal location control and the contour interval of the topographic maps from which the elevations were read. Since the contour interval ranged from 1.5 to 6 m (5 to 20 feet), the accuracy of the vertical control ranges from about .3 to 1.5 m (1 to 5 feet). A .3 m (1 foot) vertical variation in the gravimeter height causes a 0.06 mgal variation in the simple Bouguer anomaly value; and a 1.5 m (5 foot) vertical deviation could produce a 0.3 mgal error. The total possible accumulative error in the reduced simple Bouguer gravity anomaly values is then about 0.3 to 0.4 mgal.

Compilation of Gravity Map

To prepare the simple Bouguer gravity anomaly map, the gravity values of the stations occupied by more than one survey or more than one time in any one survey were cross-checked and an appropriate average compiled. Unreasonable values were checked and corrections were made if necessary. The resultant data base was then hand-contoured with a 2-milligal contour interval. At two locations, an intermediate 1-milligal contour was used to define more clearly the character of an anomaly. The gravity data for those stations shown on figure 4, as well as the stations beyond the boundaries of figure 4 that were used in contouring the map, are given in the appendix.

ALLIED DATA SOURCES

Several additional sources of control data influencing gravity model parameters were investigated, including studies of rock densities, water-well logs, and oil-well logs pertinent to the region. The gravity information was compared with a published aeromagnetic map, as well as with resistivity and electromagnetic surveys conducted in the area.

Rock Densities

Representative samples of the common rock types in the surveyed area were collected and analysed using a beam balance; and the results are listed in Table 1 along with the representative densities obtained by Calkins (1970).

The density contrasts between the various geologic units vary considerably. The intrusive rocks in Desert Mountain range in density from 2.60 to 2.85 gm/cc, providing a large range of density values which might be assigned to any suspected intrusive bodies for modeling purposes. The fine-grained basaltic andesites tend to be rather dense at 2.73 gm/cc. The extensive volcanic flows are less dense, with densities ranging from 2.52 to 2.60 gm/cc. The lightest rock, scoria, collected near the volcanic neck at Fumarole Butte, has a density of 1.00 gm/cc. Calkins (1970) computed a density of 1.85 gm/cc for the lake sediment by applying Nettleton's (1949) technique of a gravity density profile across a long linear stream bed

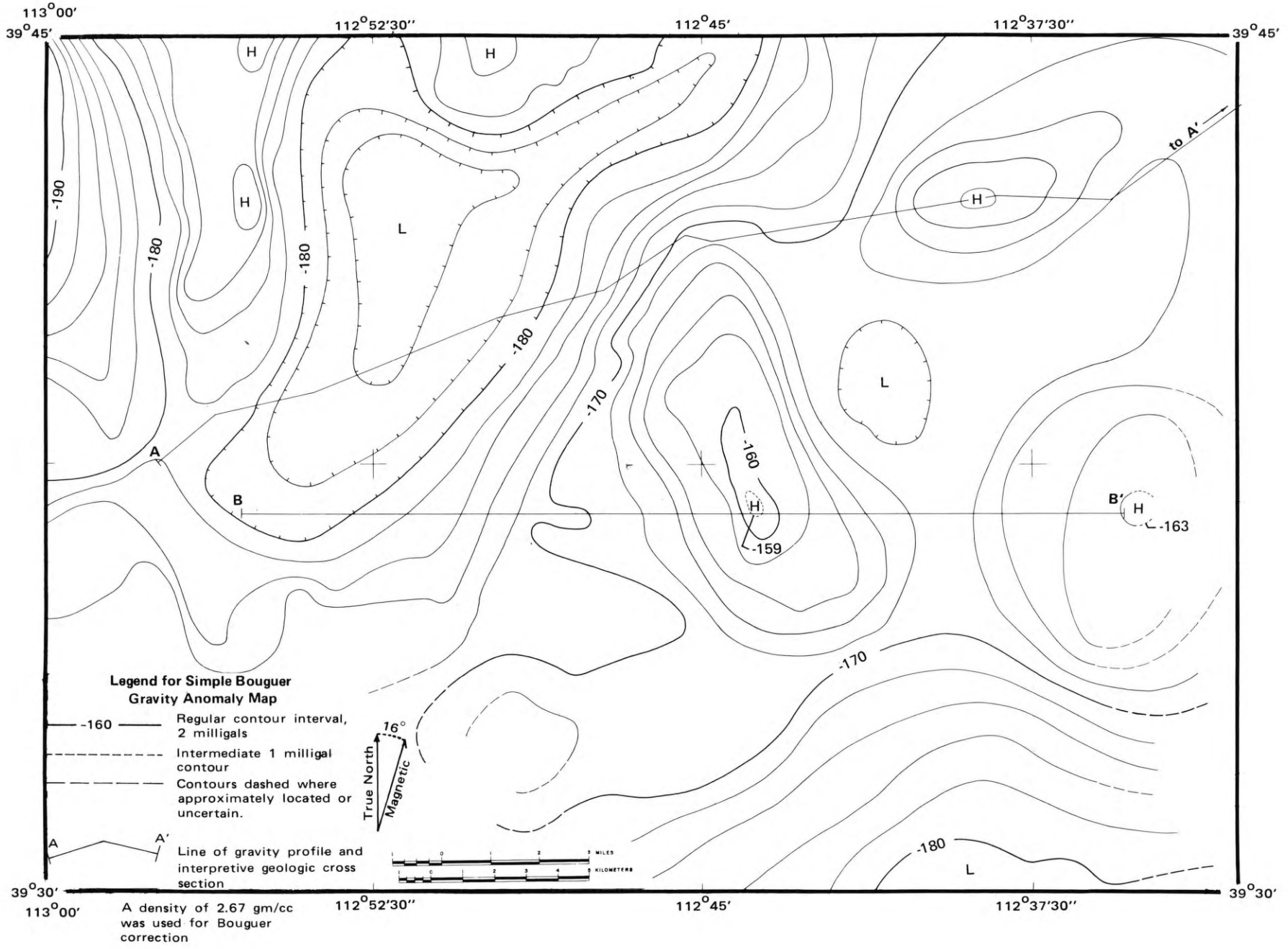

Figure 5. Simple Bouguer Gravity Anomaly Map of the Fumarole Butte Area, Juab and Millard Counties, Utah.

in an alluvial valley. Several other sources of information indicate that there are acidic volcanic flows interbedded with the alluvium so that the average density of the sediments is greater than 1.85 gm/cc. Since a density of 2.20 gm/cc, used as a typical density for Basin and Range sediments, appeared to be a reasonable average for the combined alluvium and volcanic flow material, it was therefore used for modeling purposes. The density of the metamorphic quartzite exposed in the Drum Mountains, the possibility of more basalt at depth, and the increase of rock density with depth due to compaction, makes 2.65 gm/cc appear a reasonable approximation for the unexposed bedrock of the region. A density of 2.80 gm/cc was chosen for the deep basement rock.

Table 1. Rock Densities From Surface Samples

Rock Type	Rock Condition	Density (gm/cc)
Granite	Fresh surface	2.69
Granite	Fresh surface	2.62*
Granite	Moderately weathered	2.60*
Granodiorite	Slightly weathered	2.70*
Granodiorite	Fresh surface	2.76*
Granodiorite	Fresh surface	2.74*
Mafic dike	Fresh surface	2.85*
Mafic dike	Moderately weathered	2.75*
Vesicular basaltic andesite	Slightly weathered	2.52
Vesicular basaltic andesite	Fresh surface	2.57
Fine-grained basaltic andesite	Fresh surface	2.69
Fine-grained basaltic andesite	Fresh surface	2.73
Acidic volcanic flows	Moderately weathered	2.59
Acidic volcanic flows	Fresh	2.60
Acidic volcanic tuff	Moderately weathered	2.52
Scoria	Fresh	1.00

*Data compiled from Calkins (1970)

Water-well Control

All available water-well logs were obtained from the Utah State Water Rights Division for correlation in the gravity modeling. Most of the wells were located at the southern edge of the survey area where there is more agricultural irrigation; however, several are located throughout the region for livestock watering purposes. The well driller's report usually included the location and depth of the well and a crude litholog. The reported well locations occasionally did not correlate with the locations found in the field; hence the notations of "location accuracy good" and "location accuracy fair" on the explanation of the geologic map (figure 4). Well locations accurate to 150 meters (500 feet) were considered good, while wells located less accurately than 300 meters (1,000 feet) were considered fair. The lithologs and depth measurements proved to be helpful in modeling since they gave an indication of the sediment thickness. The lithologs unfortunately were too crude to provide correlatable layers through the region. The well depths ranged from 30 to 280 meters (100 to 900 feet) with most about 180 meters (600 feet) indicating that the unconsolidated sediments are many hundreds of meters thick in this locality. Only two of the available lithologs of wells near the Drum Mountains show wells intersecting basalt flows within the sediments.

The most significant of the well drillers' reports were for two wells located 3 and 5.5 km (2 and 3.5 miles), respectively, southeast of Baker Hot Springs. One of the wells drilled to a depth of 150m (500 feet) had an artesian flow to about 3.5 meters (12 feet) above the ground (Mower and Feltis, 1968) indicating a high meteroic water pressure at depth, and hence a possible source for the spring water. The second well was drilled to a depth of 200 meters (660 feet). Cool, relatively fresh water is produced from both wells; however, both wells also intersect a 22-meter (70 foot) layer of salty water at approximately 4.5 meters (15 feet) below the surface. The salt water probably has its origin in an evaporite layer in the sediments. This layer probably contributes greatly to the extremely low electrical resistivities measured at Fumarole Butte. The thickness of sediments shown by the wells east of the Fumarole Butte lava flows gives evidence for a fault along the eastern edge of the flows, sediments underlying the flows, or a combination. These interpretations are discussed later in connection with the modeling of profile B-B'

Oil-well Control

A wildcat oil well drilled approximately 24 km (15 miles) southeast of Baker Hot Springs in section 24 of Township 16 South and Range 8 West yielded additional information. This well is south of the surveyed area shown in figure 4. The Gronning No. 1, drilled by the Gulf Oil Corporation, has a total depth of over 2,500 meters (8,000 feet) (Mower and Feltis, 1968). Lithologic, spontaneous potential, and resistivity logs are available for the well. The first 600 meters (2,000 feet) of section consists mainly of Tertiary interbedded claystones and sandstones, a few conglomerates, and freshwater sandstones. Several basalt flows were encountered between 750 and 1,100 meters (2,500 and 3,500 feet); three of them were at least 25 meters (80 feet) thick. More claystones, conglomerates, tuffs, and limestones were encountered below the basalts. From 2,000 meters (6,250 feet) to the total depth, a thick section of red beds was encountered. The well did not completely penetrate the red bed sequence. At no point does the well pierce any of the Paleozoic strata observed in the Drum Mountains. It appears that a section of Tertiary rock remains below the strata penetrated.

Since the Fumarole Butte area is much nearer to the periphery of the Sevier Desert basin, the sequence of claystones and sandstones is probably thinner here than at the well. In addition, in the Fumarole Butte area, there are probably more numerous and thicker basalt flows interbedded with the sedimentary rocks,

because the flows are nearer their probable source area. Thus, although the logs of this well provide a good overview of the basin's rock type as a whole, the entire section cannot be extrapolated with complete confidence to the surveyed area. The well does, however, provide evidence of the interrelationships of the sedimentary and volcanic sections.

Aeromagnetic Map

Figure 3, a portion of the Aeromagnetic Map of Utah (Shuey, 1974; see also Zietz and others, 1976), shows a large number of magnetic highs, associated lows, and gradients of interest in the survey area. For convenience, the anomalies will be referred to by letter on the magnetic map. The relative geographic locations of the anomalies are taken from the U. S. Army Map Service base (figure 2). The contour interval for the aeromagnetic map is 20 gammas and the scale is identical to that of figure 2. Anomalies A, B, and C are all magnetic highs whose source can be attributed to the volcanic intrusions in the McDowell Mountains. Anomaly D is a magnetic high located over an area of lake sediments. The source, which has no surface expression, may be inferred as an intrusion, possibly related to the volcanic origin of Fumarole Butte. Anomaly E, overlying Fumarole Butte, could be attributed to the magnetic expression of the intrusion at depth which produced the observed volcanic surficial material. This anomaly, which is offset from the volcanic neck by about 2.4 km (1½ miles) to the southeast, also appears to have a spur which extends part of the magnetic high over the hot springs area, indicating a possible subsidiary magnetic source.

Anomaly F appears to correspond to the granitic intrusive core of Desert Mountain. This correlation was drawn in light of the statement by Calkins (1970) that:

> Although the rock samples tested for magnetic susceptibility tended to indicate the Precambrian rocks to be approximately twice the susceptibility of the granitic rocks, all of the high amplitude anomalies at Desert Mountain (i.e., those exceeding 750 gammas) appear to be associated primarily with the granitic rocks, and, if any correlation exists, the Precambrian rocks are associated with the magnetic lows.

The Precambrian mentioned above was mapped by Rees (1971) as granodiorite. Anomaly G, like anomaly D, is located over an area of lake sediments and does not exhibit any geologic manifestations of the source at the surface; however, we infer that its origin is similar to that of Anomaly F. The magnetic gradient east of the Desert Mountain, designated anomaly H, is a feature that suggests a north-south fault. In all, the erratic magnetic pattern of the aeromagnetic map suggests that this is an area characterized by igneous intrusions. Correlation of the primary magnetic anomaly with the gravity anomalies is discussed later.

Electrical Surveys

Other geophysical techniques have been utilized over and adjacent to Fumarole Butte to give a broader data base. A class in electrical methods of geophysics from the University of Utah, directed by S.H. Ward, conducted resistivity and electromagnetic surveys in the region during the spring of 1973. Resistivity profiles between Baker Hot Springs and the eastern edge of the lava flows at Fumarole Butte confirmed the existence of a very low-resistivity near-surface layer with resistivities in the range of 2 to 5 ohm-meters. Presumably this low-resistivity layer is the salt water zone observed in the water-well logs. A limited resistivity survey was carried out on top of the basaltic andesite flows approximately .8 km (.5 mile) west of Baker Hot Springs to determine the total thickness of the flows. Surface resistivities of less than 10 ohm-meters were measured. A problem with electromagnetic coupling made the results somewhat unreliable. The electromagnetic sounding on the lava flows produced only limited penetration, since the surface resistivities and equipment frequencies made the skin depth less than 30 meters (100 feet) (S.H. Ward, 1973, oral communication).

Johnson (1975) conducted a resistivity and induced polarization survey during the summer of 1973 along the north-south jeep trail across the interior of Fumarole Butte (figure 4) to determine the total thickness of the volcanic flows. Schlumberger sounding data indicated a three-layer geologic model for the area north of the volcanic neck. The first layer, consisting of sediments, is 2.6 meters (8.5 feet) thick and has a low resistivity of 7.4 ohm-meters. The second layer consists of the basalt with a thickness of 100 to 140 meters (320 to 460 feet) and an electrical resistivity of 2200 ohm-meters. The third layer is modeled as a basal half-space with a resistivity of 1 to 3 ohm-meters. This agrees well with the resistivities measured from the 245-meter (800 feet) level to the 2400-meter (7,900 foot) level of the Gronning No. 1 well which averaged from approximately 2 to 5 ohm-meters for almost the entire section. Thus, the basalt layer appears to be 90 to 120 meters (300 to 400 feet) thick and to rest on sediments.

A multispectral 14-frequency electromagnetic survey was conducted on the Lake Bonneville sediments about 4 miles south of the Fumarole Butte flows during the summer of 1973 (Smith, B.D., 1974). Interpretation of the data produced a three-layer model consisting of an upper 5-meter-thick layer with a resistivity of 10 ohm-meters, an intermediate 6-meter-thick layer with a resistivity of 1.7 ohm-meters, and a third layer half-space with a 10 ohm-meter resistivity. The intermediate, highly conductive layer, in all probability, corresponds to the salt-water zone encountered in the well logs previously described. It would appear, however, that this zone thins southward away from the hot springs. With the high conductivities and frequencies used, the effective depth of exploration of the EM system was less than 30 meters (100 feet).

ANALYSIS AND INTERPRETATION OF GRAVITY DATA

Gravity Contour Map

A simple Bouguer gravity anomaly map (figure 5) was prepared from the processed data at the same scale as figure 4, the geology and station location map.

Inspection of the simple Bouguer contour map reveals several interesting gravity features, which are from west to east: a gravity low to the west of the McDowell Mountains, gravity highs associated with the McDowell Mountains, a gravity low between the McDowell Mountains and Fumarole Butte, a northeast-southwest-trending gravity gradient across the north end of Fumarole Butte, an elongate gravity high over the Baker Hot Springs, a gravity high on the road southwest of Desert Mountain, and an inferred gravity high on the eastern edge of the map. A number of the gravity highs show good correlation with the magnetic highs indicated on figure 3. The gravity and magnetic anomalies in the McDowell Mountains and the area southwest of Desert Mountain (magnetic anomaly G) correlate especially well. The center of magnetic anomaly E overlies the gravity spur extending westward from the main large gravity anomaly over the Baker Hot Springs; and the northeastern extension of magnetic anomaly E corresponds with the central portion of the same main large gravity anomaly over the hot springs. It should be noted that the magnetic anomaly D of figure 3 shows no corresponding gravity anomaly.

Although the area of primary interest was the geothermal prospect at Fumarole Butte, a first-order assessment of many of the gravity anomalies shown on

figure 5 was made to obtain an overview of the region and to facilitate the gravity modeling. The 12-mgal gradient west of the McDowell Mountains located in the Basin and Range province where grabens are common and have a character similar to the gravity expression of other grabens, is interpreted as the eastern margin of a deep graben with probable faulting parallel to the western margin of the McDowell Mountains. Using the Bouguer approximation for a slab and assuming a density contrast of 0.5 gm/cc, the 12-mgal anomaly indicates a graben with at least 550 meters (1,800 feet) of valley fill.

The gravity highs over the western part of the McDowell Mountains, like the magnetic anomalies (figure 3), are interpreted as caused by intrusive volcanic rocks in that area. The two gravity maxima located over the main western part of the mountains have an amplitude of approximately 6 mgal. The correlation between the maxima of the gravity and magnetic anomalies A and B suggests related intrusive volcanic bodies at those locations. The gravity high located in the southern edge of the eastern part of the McDowell Mountains emphasizes the higher densities of the volcanic rocks. This gravity feature correlates with the southern part of the associated magnetic high C.

The elongate gravity high at Baker Hot Springs, which has a closure of about 9 mgal and which trends in a north-northwest direction, is about 14 km (9 miles) long by 8 km (5 miles) wide. Due to its elongate nature, this anomaly is interpreted as an intrusive dike. Assuming that the body causing the anomaly is a buried horizontal cylinder and utilizing the appropriate formulas, the depth to the center of the body is estimated as 2000 meters (6,500 feet), the radius of the cylinder is then estimated as 1250 meters (4,000 feet), thereby making the depth to the top of the body about 750 meters (2,500 feet).

The gravity high southwest of Desert Mountain, which has a closure of about 5 mgal and corresponds with the magnetic anomaly G (figure 3), is interpreted to be caused by an intrusive plug. The depth of the body was estimated by assuming a buried vertical cylinder and utilizing the aeromagnetic data (figure 3). Using this procedure, the depth to the top of the plug was estimated to be 550 meters (1,800 feet).

Gravity Profiles

In the analysis and interpretation of the gravity profiles, the Talwani two-dimensional modeling method (Talwani and others, 1959) was used to calculate the theoretical gravitational attraction across a geological model. By modifying the geologic model and recalculating the resultant theoretical gravity curve until the observed gravity curve was matched by the computed theoretical curve, it was possible to define a geologic model for which the gravitational attraction is nearly identical to that recorded in the field. The error produced by the two-dimensional assumption will be negligible, provided that the structure being modeled is several times longer in the direction perpendicular to the line of the profile than it is parallel to the profile.

Two gravity profiles trending approximately east-west were modeled using the Talwani computer modeling program. On figures 2 and 5 they are designated as profile A-A′ on the north and profile B-B′ on the south. Profile A-A′ extends along the road from the Drum Mountains area on the west to a point east of Desert Mountain (figure 2) and beyond the borders of figure 5. The bend points along profile A-A′ are designated by the letter "B" in figure 6. Profile B-B′ is an east-west profile across the central portion of the Fumarole Butte flows and Baker Hot Springs. For both profiles, the observed simple Bouguer gravity values were projected from gravity stations lying within a distance of one mile of the profile, perpendicularly onto the profile line segments, thereby giving points with known gravity values along the profiles.

After multiple iterations of the Talwani computer program, the geologic cross sections shown in Figures 6,7, and 8 were chosen as being the best possible with the available control. In the top diagram of each of these figures, the observed gravity values are connected by a solid line and the computed theoretical values for the structural model are represented by small boxes. It should be noted that 1) the computed gravity values for the models are calculated and plotted at the location of each of the projected stations, and 2) the models are shown with vertical exaggeration.

Profile A-A′

The modeling of profile A-A′ was accomplished by first investigating the broad-scale features and then adding the smaller high-frequency anomalies. Outcrops are exposed at three locations: in the McDowell Mountains, Fumarole Butte, and Desert Mountain. There is almost no regional gravity difference between Fumarole Butte and Desert Mountain. For example, simple Bouguer values of -168.16 and -167.91 mgal were obtained at the north tip of Fumarole Butte and Desert Mountain, respectively. An average simple Bouguer value of about -179.2 mgal was obtained for the south edge of the McDowell Mountains, implying a difference in the regional gravity of about 11 mgal between McDowell Mountains and Fumarole Butte. Examination of figure 5 reveals a northeast-southwest-trending gravity gradient along the western edge of Fumarole Butte approximately 11 mgal in magnitude. It should be noted that the volcanic neck, as the probable source of the lava flows, lies along the eastern margin of the gravity gradient. The inference was thus drawn that a basement flexure causing 11 mgal of total gravity relief exists at depth beneath the gradient. The stress which resulted in the formation of the flexure probably also formed fractures which provided conduits for the magma to reach the surface at Fumarole Butte. This assumed basement feature was then modeled (figure 6) and indicates about 2,500 meters (8,000 feet) of vertical offset with a density contrast of 0.15 gm/cc.

The gravity gradient to the east of Desert Mountain near point A' on figure 6 shows a decreased gravity of an estimated 26 mgal over a distance of 8 km (5 miles). The structure producing the anomaly was interpreted to be a down-faulted graben with a total vertical displacement of about 1,350 meters (4,500 feet). The anomaly could not be accounted for by a single, steeply dipping Basin and Range fault. Instead, several smaller step faults were required to produce the match of the computed and observed gravity curves. The graben modeled in figure 6 supports Calkins' (1970) proposed fault striking north along the east side of Desert Mountain.

The gravity high southwest of Desert Mountain on figure 5 corresponding to magnetic anomaly G in figure 3 was, as previously discussed, interpreted to be a granitic intrusive with its top approximately 550 meters (1,800 feet) from the surface. Using the Talwani gravity modeling technique, a depth of 525 meters (1,700 feet) to the top of the body was indicated (figure 6). The intrusive body is modeled as being approximately 1.6 km (1 mile) wide near the top and broadening to 5 km (3 miles) wide at depth. The exact parameters for this anomaly, however, cannot be reliably obtained from the Talwani two-dimensional method since the structure does not have a great length (along its strike) in proportion to its width, and the solution cannot be unique.

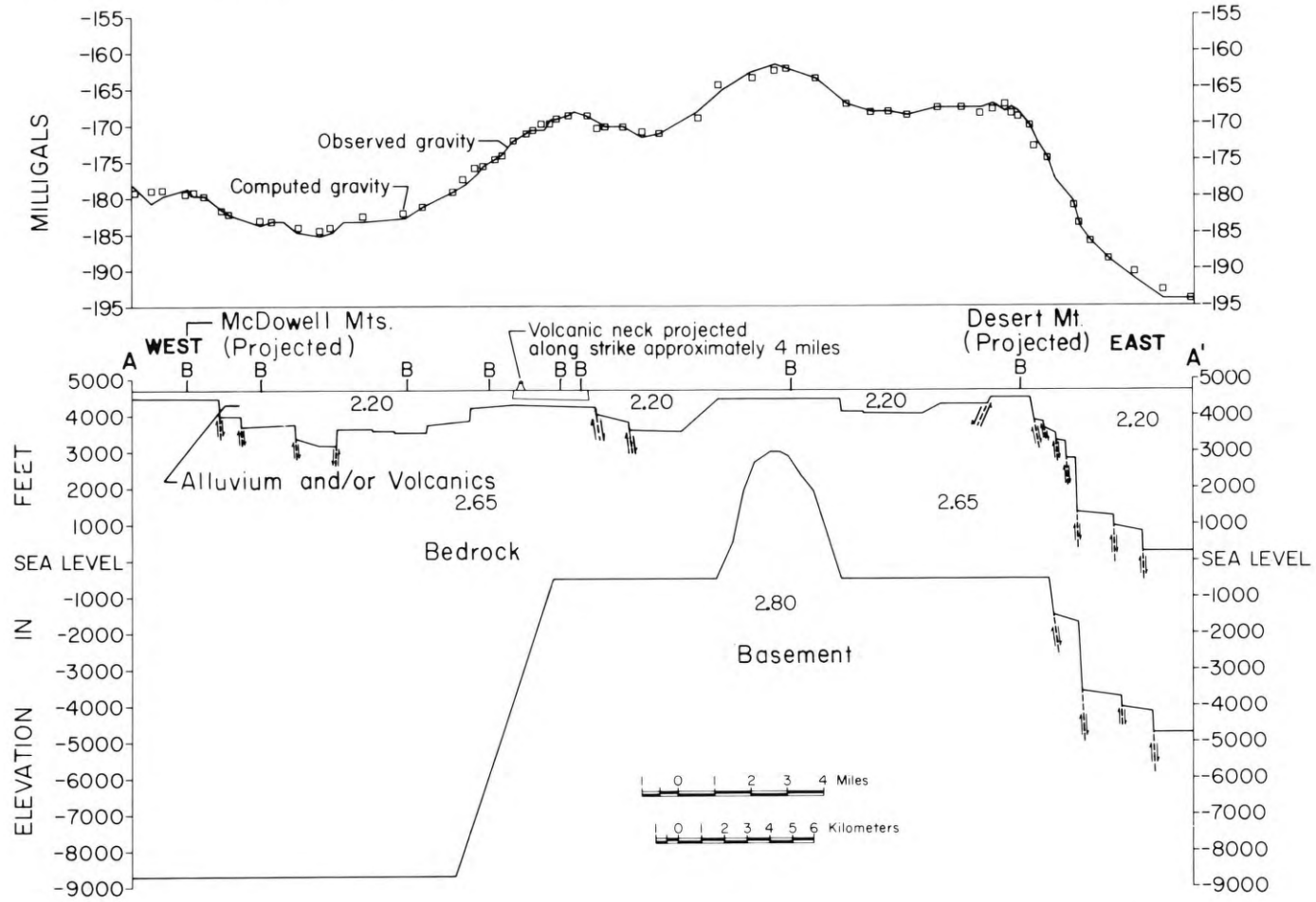

Figure 6. Simple Bouguer gravity anomaly and interpretive geologic cross section along profile A-A'. B indicates a bend point in the profile. Numbers indicate densities in gm/cc.

Analysis of the gravity high at the north end of Fumarole Butte indicated that the basalt thickness was at least 100 meters (300 feet) and, in places, as much as 150 meters (500 feet). Along the profile A-A' shown in figure 6, the basalt is indicated as a horizontal slab 100 meters (300 feet) thick. Both the resistivity survey and the gravity information indicate the possibility of sediments below the basalt flows. The thickness of the underlying sediments is difficult to estimate; for this model, 60 meters (200 feet) was chosen.

Investigation of the smaller high-frequency, near-surface anomalies along profile A-A' implied a number of small faults and grabens in the valley between the McDowell Mountains and Fumerole Butte. Describing them from west to east, the first fault was located along the eastern margin of the McDowell Mountains. It is down-faulted to the east and has a throw of about 150 meters (500 feet). The next fault, located 1 km (0.6 mile) east of the first, is down-faulted again to the east and has a throw of 100 meters (300 feet). The third fault, 2.5 km (1.5 miles) east of the second fault, is down-dropped on the eastern side approximately 125 meters (400 feet). These three faults form the western edges of a deepening valley graben. The fourth fault forms the eastern edge of the deepest portion of the inner graben with a down-faulted western side and a throw of 135 meters (450 feet). Thus, the gravity low extending between Fumarole Butte and the McDowell Mountains is interpreted as a graben filled with sediments and volcanics. The thickness of the valley fill is estimated as 250 to 275 meters (800 to 900 feet) for most of the valley, but may be as deep as 460 meters (1,500 feet) in its deepest parts.

The valley between Fumarole Butte and Desert Mountain is also complex. Two small faults were modeled east of the Fumarole Butte lava flows; however, neither corresponded with the abrupt eastern edge of the flows. The first fault is about 0.3 km (0.2 mile) east of the abrupt margin and has a throw of 60 meters (200 feet). The second is 1.75 km (1.1 miles) east of the Fumarole Butte flows and also has a throw of 60 meters (200 feet). Both of these faults show a deepening of the graben to the east to an estimated depth of 340 meters (1,100 feet). Farther to the east the sediment thickness could not be precisely calculated since it was impossible to isolate the gravitational effect of the intrusion from that produced by variations in the thickness of the sediments. Over the intrusion, the sediment thickness was modeled as 75 meters (250 feet). The sediment thickness between the intrusion and Desert Mountain was estimated as 200 meters (650 feet). East of Desert Mountain is the large fault system previously described.

Profile B-B'

Profile B-B' was modeled using the same techniques. The interpretation of profile B-B' is more difficult because it lacks a station on outcropping bedrock to provide a point at which the computed curve can be matched to the observed data curve. If the match-point cannot be precisely defined, it is difficult to delin-

eate the correct proportion of the total observed gravity curve due to low density anomalies from that due to high density anomalies. To circumvent this problem on profile B-B', two models were constructed. Model 1 (figure 7) attributes all of the gravity relief of the Bouguer anomaly to high-density intrusions with the exception of the downward basement flexure at the west end of the profile. Model 2 of profile B-B' (figure 8) estimates the depths of the grabens and the size of the intrusions in a more intuitive manner and probably represents a more realistic geologic explanation.

The basement flexure discussed in profile A-A' is also shown in both models of profile B-B'. The vertical relief of the basement flexure at the location crossed by profile B-B', an estimated 2,100 to 2,400 meters (7,000 to 8,000 feet), appears to be slightly less than at the northern profile. The top of the flexure shows good horizontal position correlations with the location of the volcanic neck. Thus, as noted previously in the discussion of profile A-A', the model suggests that fracturing of the deep basement at the time of the formation of this flexure may have provided a conduit by which the magma could reach the surface.

Model 1 of profile B-B' (figure 7) shows no classical grabens and attributes the anomalies to high density contrasts. The Fumerole Butte basalt flows are represented by a 90-meter (300 foot) thick layer with a density of 2.65 gm/cc. The sediments are shown as a layer 180 meters (600 feet) thick in most areas and with at least 60 meters (200 feet) of thickness under the basalt flows. The elongate gravity high extending north from Baker Hot Springs is modeled as being caused by a huge dike intrusion having a density of 2.96 gm/cc. The top of this intrusion is inferred to be 250 meters (800 feet) below the surface. The rise in the observed gravity curve at the east end of the profile is interpreted as an intrusion of higher density material into the overlying rocks. It is indeterminable whether the intrusive material is typical of basement rock type.

Model 2 of profile B-B' (figure 8) incorporates both grabens and intrusions in the geologic cross section. The Fumarole Butte basalt flows were modeled exactly as in Model 1. With the inclusion of grabens, the relief of the gravity anomaly due to the intrusive dike at Baker Hot Springs was reduced, thereby producing a more realistic geologic model. The dike is estimated to be about 1.6 km (1 mile) wide near its top, which is at an estimated 250 meters (800 feet) below the surface. There is an indication of a graben east of the dike with a depth of 370 meters (1,200 feet). In this model, the increase in the observed gravity values at the east end of profile B-B' is attributed to a thinning of the sediments rather than a structural high in the basement. The sediment thickness under the basalt is estimated as 280 meters (900 feet) whereas the sediment thickness west of Fumarole Butte is projected to be 370 meters (1,200 feet). The source of the feeder for the dike is uncertain, but may be associated with the main feeder of the volcanic neck at depth.

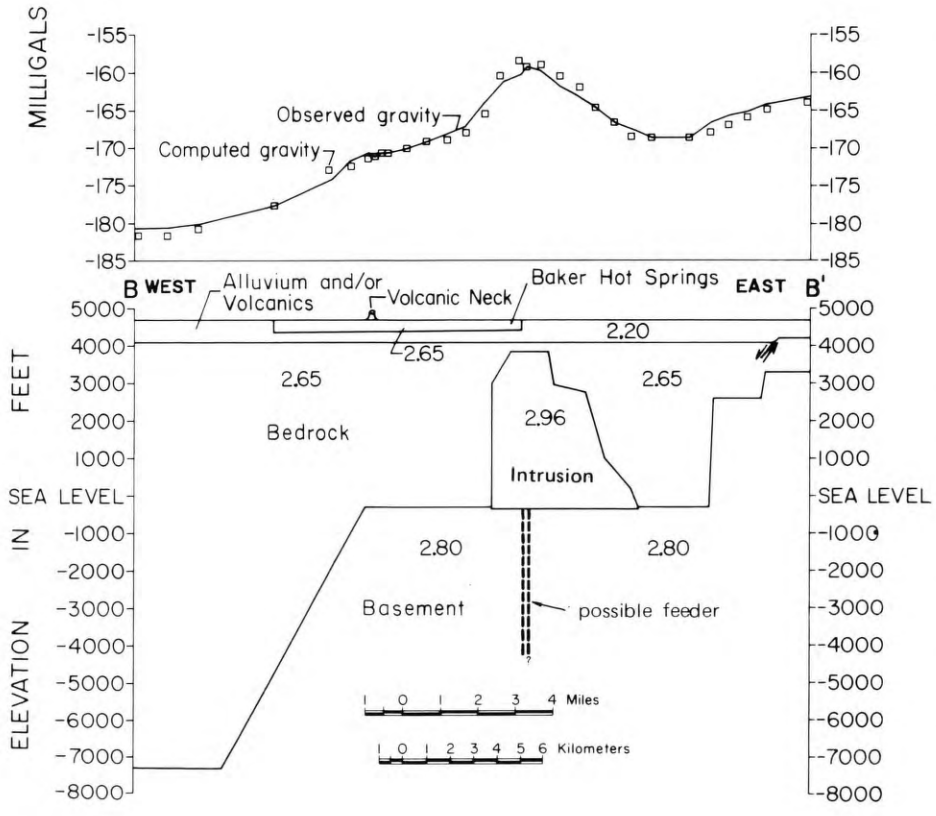

Figure 7. Simple Bouguer gravity anomaly and interpretive geologic cross section along profile B-B' (Model 1). Numbers indicate densities in gm/cc.

SUMMARY AND CONCLUSIONS

In this gravity investigation, the following three main objectives were accomplished: 1) To determine the possible source of heat at Baker Hot Springs and at the volcanic neck in the interior of Fumarole Butte; 2) to locate faults typical of the Basin and Range province which might be acting as geothermal conduits in the area; and 3) to enhance the general knowledge of the basic geologic structural setting of the region.

The gravity data indicate a possible intrusive dike under the Baker Hot Springs area which may be interpreted as the source of the heat transferred to the water of the numerous hot springs. The size and depth of the intrusion were estimated to be 8 km (5 miles) long by 2 km (1.3 miles) wide by 1 km (0.6 mile) high with a depth to the top of 0.65 km (0.4 mile) (figure 8). Perhaps just as importantly, no gravity high was found associated with the volcanic neck. This observation, along with the aeromagnetic high noted, tends to indicate that, if there is magma chamber associated with the volcanic neck, it must be too deep, too small, and/or lacking in density contrast to produce a gravity anomaly. Thus, the heat source for the moist, warm air escaping from the top of the volcanic neck could be due to either the proposed buried intrusion beneath the Baker Hot Springs or hydrothermal fluids rising along fractures associated with the inferred basement flexure.

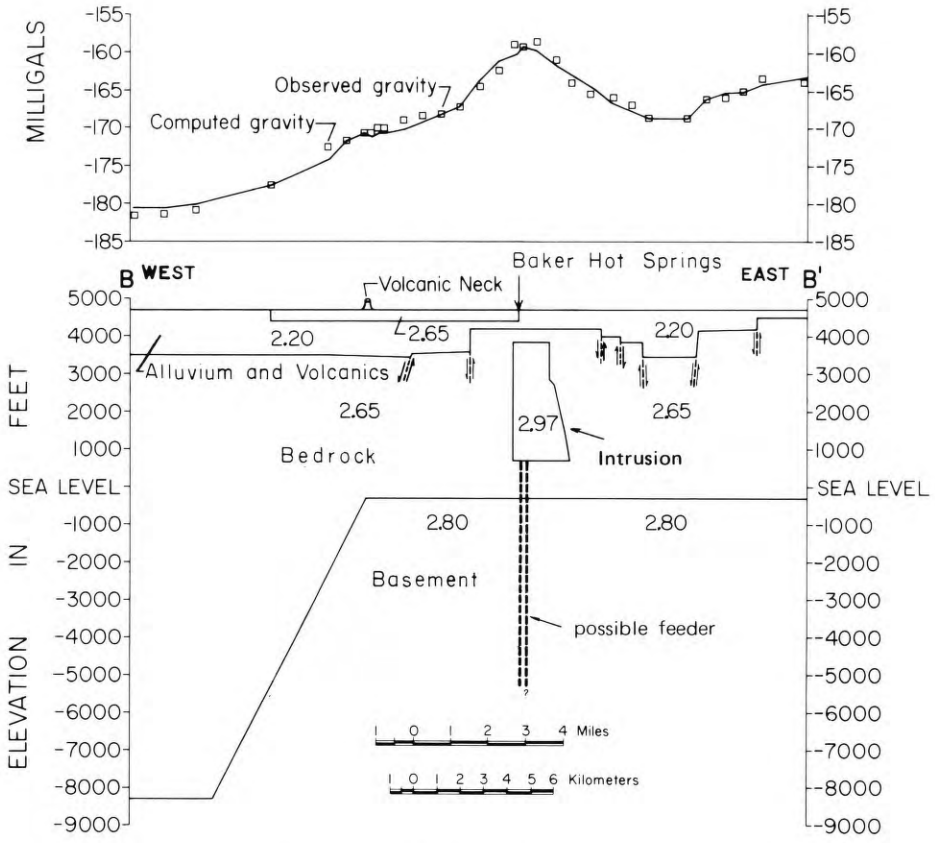

Figure 8. Simple Bouguer gravity anomaly and interpretive geologic cross section along profile B-B' (Model 2). Numbers indicate densities in gm/cc.

The gravity investigation also attempted to determine if there is a fault acting as a geothermal conduit along which the hot water is circulated to the Baker Hot Springs vicinity. The gravity data indicate two north-south trending faults located east of the flows which may have influence on the hydrogeology of the springs. The first of the faults is shown on Profile A-A' (figure 6) and figure 4 about 0.4 km (0.25 mile) east of the flows near the northeastern margin of Fumarole Butte, and may continue southward through the Baker Hot Springs. The gravity data, however, do not indicate any throw or density contrast across the possible fault at the springs. The second fault, also shown on profile A-A' (figure 6) and on figure 4, strikes south to southeast and lies about 1.6 to 3.2 km (1 to 2 miles) east of the basalt flows.

The study also suggested the existence of a large basement flexure, near the western margin of Fumarole Butte, with postulated fractures that served as conduits for the upwelling magma to reach the surface at Fumarole Butte. Several magnetic anomalies over suspected structural features show corresponding gravity anomalies. Especially interesting is the gravity high which is located southwest of Desert Mountain and modeled as an intrusive plug. A number of typical Basin and Range faults were interpreted along with associated graben basins. The most prominent of the indicated faults were the fault east of Desert Mountain and the faults lying both to the west and to the east of the McDowell Mountains. The most clearly defined graben was located in the valley between the McDowell Mountains and Fumarole Butte.

ACKNOWLEDGMENTS

Appreciation is expressed to J.A. Whelan for his advice on the geology of the survey area. Financial support for this study was provided by the University Research Fund (Grant No. 1892) of the University of Utah. The senior author was provided financial aid through 1) a Teaching Assistantship in the Department of Geology and Geophysics, University of Utah, and a Society of Exploration Geophysicists Scholarship during the academic year 1972-73 and 2) a grant-in-aid from the Geophysics Special Awards Fund of the Department of Geology and Geophysics, University of Utah during the Spring Quarter of the academic year 1973-74.

REFERENCES

CALKINS, W.G., 1970, Magnetic and gravity study of Desert Mountain, Juab County, Utah: M.S. thesis, University of Utah, 64 p.

CALKINS, W.G., 1972, Magnetic and gravity study of Desert Mountain, Juab County, Utah: Utah Geological and Mineralogical Survey Bulletin 95, 21 p.

CALLAGHAN, E., and H. E. Thomas, 1939, Manganese in a thermal spring in west central Utah: Economic Geology, v. 34, 8, p. 905-920.

COOK, K.L., T.H. Nilsen, and J.F. Lambert, 1971, Gravity base station network in Utah - 1967: Utah Geological and Mineralogical Survey Bulletin 92, 57 p.

CRITTENDEN, M.D., Jr., J.A. Straczek, and R.J. Roberts, 1961, Manganese deposits in the Drum Mountains, Juab and Millard Counties, Utah: U.S. Geological Survey Bulletin 1082H, p. 492-543.

ERICKSON, M.P., 1963, Volcanic geology of western Juab County, Utah: in Utah Geological Society Guidebook to the Geology of Utah, no. 17, Beryllium and uranium mineralization in western Juab County, Utah, ed. B.J. Sharp and N.C. Williams, p. 23-35.

FOURNIER, R.O., and A.H. Truesdell, 1973, An empirical Na-K-Ca geothermometer for natural waters; Geochemica et Cosmochemica, Acta, v 37, p. 1255.

GILBERT, G.K., 1890, Lake Bonneville: U.S. Geological Survey Monograph 1.

GOODWIN, L.H., L.B. Haighley, R.L. Rioux, D.E. White, L.J.P. Muffler, and R.G. Wayland, 1971. Classification of public lands valuable for geothermal resources: U.S. Geological Survey Circular 647, 18 p.

HOGG, N.C., 1972, Shoshonitic lava in west central Utah: Brigham Young University Geology Studies, v. 19, part 2, p. 133-184.

JOHNSON, E.H., 1975, Resistivity and induced polarization survey of a basalt flow in a geothermal environment, western Utah: unpublished M.S. thesis, University of Utah, 69 p.

MILLIGAN, J.H., R.E. Marsell, and J.M. Bagley, 1966, Mineralized springs in Utah and their effect on manageable water supplies: Utah Water Research Laboratory Report No. WG23-6, Utah State University in cooperation with Utah Water and Power Board, 50 p.

MOWER, R.W. and R.D. Feltis, 1968, Groundwater hydrology of the Sevier District, Utah: U.S. Geological Survey Water Supply Paper 1854.

MUNDORFF, J.C., 1970, Major thermal springs of Utah: Utah Geological and Mineralogical Survey, Water Resources Bulletin 13.

NETTLETON, L.L., 1949, Geophysical prospecting for oil: McGraw Hill Book Company, New York.

PARRY, W.T., N.L. Benson, and C.D. Miller, 1976, Geochemistry and hydrothermal alteration at selected Utah hot springs: National Science Foundation Report, contract GI-43741, Department of Geology and Geophysics, University of Utah, 131 p.

REES, D.C., 1971, Geology and diatremes of Desert Mountain, Utah: unpublished M.S. thesis, University of Utah.

SHAWE, D.R., 1972, Reconnaissance geology and mineral potential of Thomas, Keg, and Desert Calderas, central Juab County, Utah: U.S. Geological Survey Professional Paper 800-B, p. B67-B77.

SHUEY, R.T., 1974, Aeromagnetic map of Utah: Department of Geology and Geophysics, University of Utah and Utah Geological and Mineralogical Survey.

SMITH, B.D., 1974, Interpretation of electromagnetic field measurements: unpublished Ph.D. thesis, University of Utah, 244 p.

SMITH, T.B., 1974, Gravity study of the Fummerole Butte area, Juab and Millard counties, Utah: unpublished M.S. thesis, University of Utah, 58 p.

State of Utah, Reports of well drillers: Utah Water Rights Division, Utah State Capitol Bldg., Salt Lake City, Utah.

STAUB, A. M., 1975, Geology of the Picture Rock Hills Quadrangle, Southwestern Keg Mountains, Juab County, Utah, unpublished M.S. thesis, University of Utah, 87 p.

STOKES, W.L., 1963 Geologic map of Utah: Utah Geological and Mineralogical Survey.

SWICK, C. H., 1942, Pendulum gravity measurements and isostatic reductions: U.S. Coast and Geodetic Survey Special Publication 232, 86 p.

TALWANI, Manik, J. L. Worzel, and Mark Landisman, 1959, Rapid gravity computations for two-dimensional bodies with application to the Mendocino Submarine Fracture Zone: Journal Geophysical Research, v. 64, p. 49-59.

WHITE, D. F., and D. L. Williams, editors, 1975, Assessment of geothermal resources in the United States–1975, U. S. Geological Survey Circular 726, compilation of 8 papers, 155 p.

ZIETZ, Isidore, Ralph Shuey, and J. R. Kirby, Jr., 1976, Aeromagnetic map of Utah: U. S. Geological Survey Map GP-907.

APPENDIX
Station Gravity Values

Listed are the station number, its latitude and longitude in degrees and minutes, its elevation in feet, and its free-air and simple Bouguer gravity anomaly values in milligals. Stations obtained from three different surveys are listed. The prefix FB- in the station number denotes those stations occupied in the field by T. B. Smith. The prefixes F1- and F2- designate those stations occupied by the University of Utah gravity class of 1973-1974. The prefix 72- denotes those stations occupied by the University of Utah gravity class of 1971-1972. The word "KEG" refers to the Keg Mountains Base Station. The question mark following the simple Bouguer anomaly value at several stations indicates that the accuracy of the value is questionable, and therefore that value was not used in compiling the simple Bouguer gravity anomaly map (figure 5).

STATION NUMBER	LATITUDE DEG MIN	LONGITUDE DEG MIN	ELEV (FEET)	FREE AIR	SIMPLE BOUGUER
FB 1	39 31.63	112 46.79	4564.	-14.62	-170.07
FB 2	39 32.08	112 47.43	4577.	-12.97	-168.86
FB 3	39 32.59	112 48.28	4592.	-11.08	-167.49
FB 4	39 33.15	112 49.13	4616.	-9.80	-167.02
FB 5	39 33.75	112 49.92	4631.	-11.17	-168.90
FB 6	39 34.41	112 50.70	4660.	-13.62	-172.34
FB 7	39 34.98	112 51.46	4677.	-14.17	-173.47
FB 8	39 35.45	112 52.52	4709.	-15.19	-175.58
FB 9	39 35.70	112 51.15	4707.	-14.77	-175.09
FB 10	39 35.87	112 53.55	4745.	-16.85	-178.46
FB 11	39 36.22	112 54.44	4778.	-17.75	-180.49
FB 12	39 36.70	112 55.52	4816.	-16.44	-180.48
FB 13	39 37.13	112 56.50	4875.	-13.72	-179.77
FB 14	39 37.52	112 57.42	4932.	-9.84	-177.82
FB 15	39 37.93	112 58.47	4964.	-13.02	-182.09
FB 16	39 38.41	112 59.50	5026.	-15.04	-186.23
FB 17	39 30.79	112 47.04	4564.	-16.41	-171.86
FB 18	39 31.41	112 46.39	4564.	-15.42	-170.87
FB 19	39 31.10	112 45.86	4560.	-16.77	-172.09
FB 20	39 30.59	112 44.98	4560.	-18.98	-174.29
FB 21	39 30.53	112 43.53	4562.	-20.22	-175.60
FB 22	39 30.53	112 42.34	4561.	-21.96	-177.31
FB 23	39 30.53	112 41.18	4571.	-23.33	-179.01
FB 24	39 31.40	112 41.18	4571.	-21.16	-176.85
FB 25	39 32.28	112 41.18	4573.	-19.46	-175.21
FB 26	39 33.15	112 41.18	4576.	-17.22	-173.08
FB 27	39 33.91	112 41.61	4576.	-15.44	-171.30
FB 28	39 34.46	112 41.18	4576.	-12.64	-168.49
FB 29	39 34.90	112 41.18	4578.	-10.80	-166.73
FB 30	39 35.76	112 41.18	4577.	-10.64	-166.53
FB 31	39 35.92	112 41.92	4582.	-9.31	-165.37
FB 32	39 32.34	112 46.47	4572.	-12.75	-168.48
FB 33	39 33.17	112 46.49	4575.	-12.37	-168.20
FB 34	39 33.86	112 46.09	4587.	-13.66	-169.90
FB 35	39 34.45	112 45.50	4579.	-13.96	-169.92
FB 36	39 35.11	112 44.48	4583.	-9.52	-165.62
FB 37	39 35.94	112 43.92	4597.	-4.67	-161.24
FB 38	39 36.65	112 43.85	4623.	-1.43	-158.89
FB 39	39 36.91	112 43.68	4616.	-2.02	-159.24
FB 40	39 37.39	112 43.45	4599.	-5.07	-161.71
FB 41	39 38.07	112 43.80	4596.	-4.58	-161.12
FB 42	39 38.67	112 44.11	4586.	-3.99	-160.19
FB 43	39 39.28	112 44.40	4594.	-3.83	-160.30
FB 44	39 40.00	112 44.60	4586.	-6.67	-162.87
FB 45	39 40.74	112 44.66	4597.	-8.20	-164.77
FB 46	39 41.42	112 44.82	4608.	-11.03	-167.98
FB 47	39 30.51	112 40.02	4576.	-24.82	-180.67
FB 48	39 30.53	112 38.91	4587.	-24.87	-181.10
FB 49	39 31.42	112 38.91	4592.	-22.76	-179.16
FB 50	39 32.17	112 38.43	4596.	-21.18	-177.72
FB 51	39 30.76	112 38.92	4588.	-24.33	-180.60

STATION NUMBER	LATITUDE DEG	MIN	LONGITUDE DEG	MIN	ELEV (FEET)	FREE AIR	SIMPLE BOUGUER
FB 52	39	36.97	112	58.15	5013.	-5.73	-176.47
FB 53	39	37.42	112	58.58	5015.	-9.32	-180.13
FB 54	39	36.38	112	58.87	5107.	-.32	-174.26
FB 55	39	35.80	112	59.60	5246.	4.29	-174.39
FB 56	39	35.48	112	58.00	5060.	-1.42	-173.76
FB 57	39	35.56	112	57.87	5114.	1.15	-173.03
FB 58	39	35.76	112	57.08	4927.	-8.92	-176.73
FB 59	39	35.28	112	56.77	4876.	-10.63	-176.71
FB 60	39	34.42	112	56.20	4790.	-12.35	-175.50
FB 61	39	35.13	112	53.85	4741.	-13.26	-174.74
FB 63	39	36.84	112	48.05	5093.	3.86	-169.61
FB 64	39	36.69	112	48.16	5068.	2.20	-170.41
FB 65	39	36.51	112	48.33	5063.	1.63	-170.81
FB 66	39	36.44	112	48.65	4998.	.36	-169.87
FB 67	39	36.22	112	48.81	4960.	-.80	-169.74
FB 68	39	35.96	112	49.03	4912.	-3.52	-170.82
FB 69	39	35.76	112	49.38	4896.	-4.47	-171.22
FB 70	39	35.60	112	49.54	4810.	-7.51	-171.34
FB 71	39	35.43	112	49.87	4750.	-9.96	-171.74
FB 72	39	29.98	112	47.40	4561.	-16.82	-172.17
FB 73	39	29.16	112	47.77	4562.	-16.93	-172.31
FB 74	39	35.20	112	50.05	4740.	-10.12	-171.56
FB 75	39	34.95	112	50.20	4712.	-11.89	-172.38
FB 76	39	34.73	112	50.28	4698.	-12.32	-172.33
FB 77	39	34.36	112	50.37	4662.	-13.13	-171.92
FB 78	39	34.08	112	50.34	4645.	-12.65	-170.86
FB 79	39	35.56	112	52.09	4696.	-15.13	-175.08
FB 80	39	35.30	112	53.35	4714.	-15.64	-176.20
FB 81	39	41.48	112	44.06	4595.	-12.87	-169.38
FB 82	39	41.58	112	43.28	4588.	-14.31	-170.58
FB 83	39	41.72	112	42.25	4601.	-14.42	-171.13
FB 84	39	41.82	112	41.47	4604.	-12.21	-169.03
FB 85	39	41.91	112	40.69	4608.	-9.63	-166.57
FB 86	39	41.99	112	40.02	4618.	-6.47	-163.76
FB 87	39	42.07	112	39.35	4624.	-4.69	-162.19
FB 88	39	42.13	112	38.78	4637.	-3.84	-161.78
FB 89	39	37.10	112	47.66	5027.	1.88	-169.34
FB 90	39	37.41	112	47.35	4992.	1.15	-168.88
FB 91	39	37.74	112	47.11	4916.	-1.37	-168.81
FB 92	39	38.03	112	46.98	4897.	-1.04	-167.83
FB 93	39	38.26	112	47.46	4880.	-3.20	-169.41
FB 94	39	38.45	112	48.29	4832.	-8.93	-173.51
FB 95	39	38.34	112	49.26	4820.	-10.97	-175.14
FB 96	39	38.71	112	49.47	4795.	-15.47	-178.78
FB 97	39	39.23	112	49.41	4782.	-17.05	-179.92
FB 98	39	39.60	112	49.61	4790.	-17.69	-180.83
FB 99	39	40.07	112	49.70	4794.	-19.09	-182.38
FB100	39	38.35	112	55.89	4880.	-12.37	-178.58
FB101	39	39.30	112	52.13	4816.	-21.12	-185.16
FB102	39	38.30	112	51.92	4813.	-18.55	-182.49
FB103	39	37.70	112	51.74	4764.	-19.27	-181.53

STATION NUMBER	LATITUDE DEG	MIN	LONGITUDE DEG	MIN	ELEV (FEET)	FREE AIR	SIMPLE BOUGUER
FB104	39	37.11	112	51.57	4745.	-17.13	-178.75
FB105	39	36.51	112	51.40	4724.	-16.53	-177.43
FB106	39	36.02	112	51.27	4712.	-15.81	-176.30
FB107	39	35.42	112	51.10	4697.	-15.18	-175.16
FB108	39	34.86	112	50.79	4678.	-2.37	-161.70 ?
FB109	39	34.34	112	50.39	4661.	-14.40	-173.15 ?
FB110	39	35.14	112	54.12	4736.	-13.06	-174.37
FB111	39	34.86	112	54.76	4747.	-10.77	-172.45
FB112	39	34.63	112	55.48	4762.	-13.13	-175.32
FB114	39	42.20	112	45.00	4603.	-17.14	-173.91
FB115	39	43.07	112	51.44	5103.	-10.75	-184.56
FB116	39	30.02	112	43.47	4564.	-21.62	-177.07
FB117	39	30.51	112	37.77	4605.	-24.16	-181.00
FB118	39	30.21	112	36.54	4629.	-23.43	-181.10
FB119	39	30.08	112	36.05	4637.	-22.50	-180.44
FB120	39	30.97	112	41.18	4576.	-21.91	-177.77
FB121	39	31.84	112	41.18	4574.	-19.71	-175.51
FB122	39	32.28	112	41.18	4575.	-19.02	-174.84
FB123	39	32.71	112	41.18	4574.	-18.30	-174.09
FB124	39	33.15	112	41.18	4574.	-17.46	-173.25
FB125	39	33.59	112	41.18	4575.	-16.18	-172.00
FB126	39	34.02	112	41.18	4577.	-14.38	-170.27
FB127	39	34.46	112	41.18	4578.	-12.38	-168.30
FB128	39	34.90	112	41.18	4579.	-10.67	-166.64
FB129	39	35.32	112	41.18	4582.	-9.52	-165.59
FB130	39	35.76	112	41.18	4583.	-9.34	-165.43
FB131	39	36.20	112	41.17	4583.	-9.49	-165.59
FB132	39	36.63	112	41.18	4585.	-10.15	-166.31
FB133	39	37.07	112	41.18	4587.	-11.21	-167.44
FB134	39	37.51	112	41.17	4582.	-12.27	-168.34
FB135	39	37.95	112	41.16	4579.	-13.92	-169.89
FB136	39	38.38	112	41.16	4584.	-14.92	-171.05
FB137	39	38.82	112	41.16	4583.	-15.38	-171.48
FB138	39	39.25	112	41.17	4584.	-15.11	-171.24
FB139	39	39.69	112	41.17	4584.	-14.54	-170.67
FB140	39	40.12	112	41.16	4590.	-13.37	-169.70
FB141	39	40.56	112	41.16	4592.	-12.65	-169.06
FB142	39	40.99	112	41.17	4595.	-11.40	-167.90
FB143	39	41.42	112	41.17	4598.	-11.03	-167.64
FB144	39	41.85	112	41.17	4606.	-11.28	-168.16
FB145	39	33.58	112	49.06	4704.	-8.60	-168.82
FB146	39	34.02	112	49.06	4727.	-8.89	-169.89
FB147	39	36.63	112	42.85	4577.	-5.50	-161.39
FB148	39	36.63	112	42.29	4576.	-7.05	-162.91
FB149	39	36.63	112	41.74	4582.	-8.46	-164.53
FB150	39	36.63	112	40.61	4580.	-11.45	-167.44
FB151	39	36.62	112	40.04	4580.	-12.55	-168.54
FB152	39	36.62	112	38.92	4586.	-12.05	-168.25
FB153	39	36.62	112	38.35	4589.	-9.85	-166.15
FB154	39	36.62	112	37.79	4596.	-8.58	-165.12
FB155	39	36.63	112	37.22	4603.	-8.28	-165.05

STATION NUMBER	LATITUDE DEG MIN	LONGITUDE DEG MIN	ELEV (FEET)	FREE AIR	SIMPLE BOUGUER
FB156	39 36.63	112 36.67	4613.	-6.92	-164.04
FB157	39 34.02	112 48.49	4744.	-8.51	-170.09
FB158	39 34.02	112 47.93	4790.	-7.28	-170.43
FB159	39 36.63	112 43.41	4600.	-2.86	-159.53
FB160	39 36.63	112 43.97	4701.	.36	-159.75
FB161	39 36.63	112 44.53	4751.	1.12	-160.70
FB162	39 36.64	112 45.10	4810.	.18	-163.65
FB163	39 36.64	112 45.66	4932.	1.29	-166.69
FB164	39 36.64	112 46.22	4960.	1.02	-167.92
FB165	39 36.64	112 46.78	5042.	2.72	-169.01
FB166	39 36.20	112 46.79	5030.	2.32	-169.00
FB167	39 35.76	112 46.79	5000.	.60	-169.70
FB168	39 35.33	112 46.79	4863.	-4.55	-170.19
FB169	39 34.90	112 46.79	4778.	-7.68	-170.41
FB170	39 34.90	112 47.36	4842.	-5.36	-170.28
FB171	39 34.89	112 47.93	4895.	-4.02	-170.75
FB172	39 34.45	112 47.93	4839.	-5.03	-169.85
FB173	39 34.90	112 51.30	4670.	-14.40	-173.46
FB174	39 34.90	112 50.74	4684.	-14.04	-173.58
FB175	39 34.90	112 50.18	4710.	-11.71	-172.13
FB176	39 34.90	112 49.62	4824.	-7.18	-171.49
FB177	39 34.90	112 49.06	4807.	-6.95	-170.67
FB178	39 34.90	112 48.49	4847.	-5.53	-170.62
FB179	39 34.90	112 46.23	4757.	-8.63	-170.66
FB180	39 34.90	112 45.66	4720.	-9.48	-170.25
FB181	39 34.90	112 45.10	4625.	-11.43	-168.96
FB182	39 34.90	112 44.54	4580.	-10.71	-166.70
FB183	39 34.90	112 43.98	4572.	-9.40	-165.12
FB184	39 34.90	112 43.41	4567.	-8.84	-164.39
FB185	39 34.90	112 42.85	4567.	-8.44	-163.99
FB186	39 34.90	112 42.29	4566.	-8.83	-164.34
FB187	39 34.90	112 41.74	4578.	-9.38	-165.30
FB188	39 34.90	112 40.60	4578.	-12.17	-168.09
FB189	39 34.90	112 40.04	4581.	-13.24	-169.27
FB190	39 34.89	112 39.48	4586.	-13.43	-169.63
FB191	39 34.89	112 38.91	4591.	-12.98	-169.34
FB192	39 40.55	112 47.89	4765.	-15.70	-178.00
FB193	39 40.12	112 47.89	4754.	-15.02	-176.94
FB194	39 39.68	112 47.90	4774.	-12.30	-174.90
FB195	39 39.25	112 47.89	4812.	-10.56	-174.46
FB196	39 39.25	112 47.34	4828.	-6.74	-171.18
FB197	39 39.25	112 46.79	4855.	-4.19	-169.55
FB198	39 39.68	112 46.79	4840.	-3.21	-168.06
FB199	39 40.12	112 46.79	4830.	-6.59	-171.10
FB200	39 39.25	112 46.23	4848.	-.18	-165.30
FB201	39 39.25	112 45.67	4803.	.95	-162.64
FB202	39 38.82	112 45.67	4852.	3.57	-161.68
FB203	39 38.38	112 45.67	4863.	3.66	-161.97
FB204	39 37.95	112 45.67	4882.	2.58	-163.70
FB205	39 37.51	112 45.66	4890.	2.76	-163.80
FB206	39 37.07	112 45.67	4912.	1.76	-165.54
FB207	39 38.38	112 46.23	4899.	3.23	-163.63
FB208	39 38.38	112 46.79	4879.	-.40	-166.58
FB209	39 38.38	112 47.35	4870.	-3.54	-169.42
FB210	39 38.37	112 43.37	4577.	-5.65	-161.54
FB211	39 38.36	112 42.73	4579.	-10.64	-166.60
FB212	39 38.37	112 42.19	4592.	-12.66	-169.07
FB213	39 38.41	112 41.79	4580.	-13.97	-169.97
FB214	39 38.38	112 43.97	4589.	-4.34	-160.64
FB215	39 38.38	112 44.54	4675.	-1.64	-160.87
FB216	39 38.38	112 45.10	4822.	3.13	-161.11
FB217	39 36.34	112 43.70	4602.	-2.68	-159.43
FB218	39 29.15	112 47.77	4562.	-16.54	-171.92
FB219	39 28.32	112 48.14	4563.	-14.66	-170.08
FB220	39 27.44	112 48.49	4567.	-13.17	-168.72
FB221	39 36.64	112 47.94	5070.	2.49	-170.19
FB222	39 36.64	112 47.36	5135.	4.99	-169.91
FB223	39 36.64	112 48.50	5053.	1.75	-170.35
FB224	39 36.64	112 49.06	5007.	-.87	-171.41
FB225	39 36.64	112 49.62	4935.	-5.64	-173.73
FB226	39 38.38	112 47.94	4828.	-7.40	-171.84
FB227	39 32.48	112 38.23	4603.	-19.75	-176.53
FB228	39 32.79	112 38.02	4599.	-18.93	-175.57
FB229	39 33.09	112 37.79	4599.	-17.42	-174.06
FB230	39 33.36	112 37.50	4599.	-15.60	-172.24
FB231	39 33.63	112 37.25	4603.	-13.37	-170.15
FB232	39 34.06	112 36.86	4604.	-9.81	-166.63
FB233	39 33.15	112 46.24	4571.	-12.80	-168.49
FB234	39 33.15	112 45.68	4564.	-12.85	-168.30
FB235	39 33.15	112 45.12	4564.	-13.30	-168.75
FB236	39 33.15	112 44.56	4563.	-13.50	-168.92
FB237	39 33.15	112 43.99	4563.	-13.52	-168.93
FB238	39 33.15	112 43.42	4562.	-14.02	-169.40
F1001	39 42.13	112 35.71	4704.	-7.49	-167.71
F1 2	39 44.13	112 32.05	4936.	.72	-167.40
F1 3	39 47.48	112 32.76	5170.	-.25	-176.34
F1004	39 47.50	112 32.54	5173.	-2.07	-178.27
F1005	39 47.50	112 32.18	5172.	-4.36	-180.53
F1006	39 47.52	112 31.83	5179.	-5.16	-181.56
F1007	39 47.49	112 31.49	5179.	-7.95	-184.34
F1008	39 47.45	112 31.14	5177.	-10.10	-186.43
F1 9	39 47.34	112 30.79	5151.	-12.82	-188.25
F1 10	39 47.20	112 30.34	5147.	-14.69	-189.99
F1 11	39 47.13	112 30.03	5144.	-16.05	-191.25
F1 12	39 46.99	112 29.51	5154.	-17.70	-193.24
F1 13	39 46.92	112 29.11	5174.	-17.88	-194.10
F1 14	39 46.79	112 28.81	5187.	-18.34	-195.01
F1 15	39 46.63	112 28.50	5175.	-18.84	-195.10
F1 16	39 46.52	112 28.25	5176.	-19.34	-195.64
F1 17	39 46.35	112 27.93	5174.	-18.82	-195.04
F1 18	39 46.15	112 27.58	5160.	-18.99	-194.74
F1 19	39 46.03	112 27.31	5183.	-17.77	-194.30

STATION NUMBER	LATITUDE DEG MIN	LONGITUDE DEG MIN	ELEV (FEET)	FREE AIR	SIMPLE BOUGUER
F1 20	39 47.48	112 33.14	5182.	2.51	-173.99
F1 21	39 47.47	112 33.48	5230.	4.87	-173.26
F1 22	39 47.31	112 33.74	5245.	5.49	-173.16
F1 23	39 47.38	112 33.98	5223.	4.75	-173.14
F1 24	39 47.48	112 34.21	5195.	3.38	-173.57
F1 25	39 47.58	112 34.46	5163.	1.12	-174.74
F1 26	39 47.73	112 34.71	5127.	-.29	-174.91
F1 27	39 47.88	112 34.94	5098.	-1.56	-175.20
F1 28	39 48.11	112 35.31	5057.	-3.19	-175.43
F1 29	39 48.21	112 35.61	5018.	-2.94	-173.85
F1 30	39 48.34	112 35.94	4976.	-3.62	-173.10
F1 31	39 48.41	112 36.25	4953.	-4.92	-173.62
F1 32	39 48.40	112 36.66	4932.	-5.35	-173.33
F1 33	39 48.30	112 37.00	4928.	-5.35	-173.20
F1 34	39 48.24	112 37.40	4921.	-6.43	-174.04
F1 35	39 48.09	112 37.75	4904.	-7.04	-174.07
F1 36	39 47.95	112 38.07	4888.	-7.02	-173.51
F1 37	39 47.83	112 38.35	4882.	-6.73	-173.02
F1 38	39 47.68	112 38.72	4860.	-7.38	-172.91
F1 39	39 47.55	112 39.01	4845.	-7.42	-172.44
F1 40	39 47.44	112 39.28	4828.	-7.54	-171.98
F1 41	39 47.30	112 39.61	4815.	-7.49	-171.49
F1 42	39 47.09	112 40.01	4803.	-7.78	-171.37
F1 43	39 46.94	112 40.29	4794.	-8.18	-171.46
F1 44	39 46.81	112 40.58	4813.	-8.33	-172.26
F1 45	39 46.68	112 40.84	4804.	-9.33	-172.96
F1 46	39 46.24	112 41.16	4777.	-8.78	-171.48
F1 47	39 46.10	112 41.40	4760.	-10.13	-172.25
F1 48	39 45.93	112 41.78	4749.	-11.26	-173.00
F1 49	39 45.79	112 42.06	4743.	-11.84	-173.40
F1 50	39 45.64	112 42.29	4703.	-13.67	-173.85
F1 51	39 45.38	112 42.68	4664.	-16.12	-174.98
F1 52	39 45.19	112 42.94	4656.	-17.70	-176.29
F1 53	39 45.05	112 43.22	4640.	-20.23	-178.26
F1 54	39 45.02	112 43.55	4631.	-22.48	-180.21
F1 55	39 44.91	112 44.57	4599.	-25.14	-181.78
F1 56	39 44.77	112 45.70	4712.	-20.41	-180.90
F1 57	39 44.98	112 43.87	4602.	-24.56	-181.32
F1 58	39 44.95	112 44.19	4596.	-24.95	-181.49
F1 59	39 44.85	112 44.98	4630.	-23.39	-181.09
F1 60	39 44.80	112 45.47	4678.	-21.91	-181.24
F1 61	39 44.68	112 46.33	4798.	-16.04	-179.46
F1 62	39 44.63	112 46.77	4868.	-12.94	-178.75
F1 63	39 44.65	112 47.09	4917.	-11.54	-179.01
F1 64	39 44.64	112 47.77	5046.	-5.75	-177.62
F1 65	39 44.36	112 48.00	5072.	-5.34	-178.09
F1 66	39 44.21	112 48.28	5106.	-3.76	-177.67
F1 67	39 44.02	112 48.71	5095.	-5.09	-178.62
F1 68	39 43.88	112 49.18	5126.	-2.74	-177.33
F1 69	39 43.73	112 49.60	5130.	-3.00	-177.73
F1 70	39 43.68	112 49.83	5125.	-3.27	-177.84
F1 71	39 43.43	112 50.28	5144.	-3.84	-179.05
F1 72	39 43.37	112 50.74	5125.	-6.60	-181.15
F1 73	39 43.24	112 51.03	5108.	-8.27	-182.25
F1 74	39 43.06	112 51.48	5103.	-11.29	-185.10
F1 75	39 42.74	112 52.07	5079.	-12.57	-185.56
F1 76	39 42.58	112 52.38	5065.	-13.20	-185.72
F1 77	39 37.48	112 52.61	5061.	-5.92	-178.29 ?
F1 78	39 42.27	112 53.03	5056.	-12.32	-184.52
F1 79	39 42.07	112 53.44	5039.	-11.41	-183.04
F1 80	39 41.87	112 53.85	5050.	-9.24	-181.24
F1 81	39 41.80	112 54.40	5117.	-4.42	-178.69
F1 82	39 41.84	112 54.85	5135.	-.93	-175.83
F1 83	39 41.86	112 55.18	5160.	4.55	-171.20
F1 84	39 41.90	112 55.57	5199.	5.15	-171.93
F1 85	39 41.92	112 56.75	5105.	-1.22	-175.10
F1 86	39 30.53	112 41.20	4572.	-23.36	-179.08
F1 87	39 30.97	112 41.17	4576.	-22.00	-177.87
F1 88	39 31.40	112 41.17	4574.	-20.81	-176.62
F1 89	39 31.62	112 41.27	4575.	-20.11	-175.94
F1 90	39 31.98	112 41.34	4576.	-19.48	-175.34
F1 91	39 32.10	112 41.37	4573.	-19.18	-174.93
F1 93	39 32.54	112 41.44	4575.	-18.10	-173.92
F1 92	39 32.32	112 41.40	4575.	-18.60	-174.41
F1 94	39 32.76	112 41.47	4573.	-17.77	-173.54
F1 95	39 32.97	112 41.50	4573.	-17.27	-173.03
F1 96	39 33.52	112 41.57	4573.	-16.10	-171.85
F1 97	39 33.94	112 41.60	4581.	-13.98	-170.00
F1 98	39 34.25	112 41.67	4578.	-12.33	-168.25
F1 99	39 34.52	112 41.70	4578.	-10.95	-166.87
F1100	39 34.94	112 41.77	4575.	-9.26	-165.10
F1101	39 35.23	112 41.79	4581.	-7.86	-163.90
F1102	39 35.56	112 41.85	4578.	-7.63	-163.55
F1103	39 34.67	112 41.17	4578.	-11.33	-167.26
F1104	39 34.90	112 41.16	4579.	-10.53	-166.49
F1105	39 34.91	112 40.60	4573.	-12.28	-168.04
F1106	39 34.91	112 40.15	4576.	-13.19	-169.06
F1107	39 35.34	112 41.16	4581.	-9.59	-165.61
F1108	39 35.76	112 41.16	4582.	-9.31	-165.38
F1109	39 36.21	112 41.17	4586.	-9.19	-165.37
F1110	39 36.63	112 41.17	4584.	-10.06	-166.19
F1111	39 40.04	112 38.92	4587.	-38.23	-194.46 ?
F1112	39 40.47	112 38.92	4590.	-37.42	-193.76 ?
F1113	39 40.91	112 38.92	4592.	-36.79	-193.19 ?
F1114	39 31.88	112 38.63	4597.	-21.71	-178.28
F1115	39 32.17	112 38.44	4596.	-21.15	-177.69
F2 01	39 42.12	112 35.71	4704.	-7.70	-167.92
F2 2	39 44.13	112 32.05	4936.	.08	-168.04
F2 3	39 44.23	112 31.77	4941.	-1.90	-170.20
F2 4	39 44.33	112 31.55	4944.	-3.77	-172.18
F2 5	39 44.42	112 31.30	4951.	-5.85	-174.48
F2 6	39 44.52	112 31.02	4956.	-8.54	-177.33

STATION NUMBER	LATITUDE DEG MIN	LONGITUDE DEG MIN	ELEV (FEET)	FREE AIR	SIMPLE BOUGUER
FC 7	39 44.67	112 30.62	4966.	-11.37	-180.52
FC 8	39 44.79	112 30.35	4972.	-14.83	-184.17
FC 9	39 44.92	112 30.01	4988.	-16.03	-185.92
FC 10	39 46.01	112 27.24	5193.	-17.36	-194.23
FC 11	39 46.03	112 27.31	5183.	-17.74	-194.27
FC 12	39 45.69	112 26.00	5111.	-19.78	-193.85
FC 13	39 45.35	112 28.89	5042.	-19.18	-190.92
FC 14	39 45.11	112 29.51	5014.	-17.70	-188.48
FC 15	39 44.03	112 32.22	4926.	.44	-167.34
FC 16	39 43.91	112 32.40	4918.	-.42	-167.93
FC 17	39 43.75	112 32.65	4898.	-.39	-167.21
FC 18	39 43.58	112 32.91	4880.	-1.29	-167.50
FC 19	39 43.33	112 33.30	4850.	-2.29	-167.48
FC 20	39 42.97	112 33.89	4812.	-3.50	-167.40
FC 21	39 42.52	112 34.62	4753.	-6.57	-168.45
FC 22	39 42.19	112 35.19	4716.	-7.65	-168.27
FC 23	39 42.92	112 35.77	4739.	-5.36	-166.77
FC 24	39 43.16	112 35.81	4774.	-2.58	-165.19
FC 25	39 43.69	112 35.87	4839.	-1.37	-166.18
FC 26	39 44.36	112 35.94	4953.	1.61	-167.09
FC 27	39 41.10	112 35.63	4657.	-10.12	-169.74
FC 28	39 41.62	112 35.67	4683.	-8.50	-168.00
FC 29	39 42.15	112 36.55	4678.	-7.72	-167.05
FC 30	39 42.17	112 37.45	4659.	-5.04	-163.74
FC 31	39 42.20	112 38.32	4648.	-3.76	-162.07
FC 32	39 42.13	112 38.78	4638.	-3.80	-161.77
FC 33	39 42.05	112 39.55	4622.	-5.01	-162.44
FC 34	39 41.96	112 40.34	4612.	-7.82	-164.91
FC 35	39 41.86	112 41.17	4606.	-11.35	-168.22
FC 36	39 41.72	112 42.26	4601.	-14.46	-171.17
FC 37	39 41.65	112 42.88	4596.	-14.77	-171.32
FC 38	39 41.57	112 43.43	4591.	-13.88	-170.25
FC 39	39 41.52	112 43.87	4588.	-13.66	-169.93
FC 40	39 41.48	112 44.18	4595.	-13.02	-169.53
FC 41	39 41.43	112 44.51	4601.	-12.06	-168.76
FC 42	39 41.43	112 44.82	4608.	-11.17	-168.11
FC 43	39 41.48	112 45.12	4611.	-11.37	-168.41
FC 44	39 41.53	112 45.39	4619.	-11.60	-168.92
FC 45	39 41.38	112 45.54	4629.	-11.57	-169.23
FC 46	39 41.32	112 45.76	4635.	-12.64	-170.50
FC 47	39 41.20	112 46.00	4646.	-12.37	-170.61
FC 48	39 41.07	112 46.29	4656.	-12.60	-171.19
FC 49	39 40.94	112 46.53	4670.	-13.11	-172.15
FC 50	39 40.80	112 46.81	4689.	-14.23	-173.93
FC 51	39 40.67	112 47.00	4706.	-14.23	-174.52
FC 52	39 40.57	112 47.24	4719.	-14.73	-175.46
FC 53	39 40.52	112 47.54	4742.	-14.99	-176.50
FC 54	39 40.43	112 47.84	4761.	-15.80	-177.96
FC 55	39 40.35	112 48.27	4720.	-18.50	-179.26
FC 56	39 40.22	112 49.04	4762.	-18.90	-181.11
FC 57	39 40.06	112 49.70	4794.	-19.23	-182.52
FC 58	39 39.85	112 50.34	4810.	-18.63	-182.45
FC 59	39 39.69	112 50.88	4811.	-18.99	-182.86
FC 60	39 39.54	112 51.33	4815.	-19.23	-183.22
FC 61	39 39.43	112 51.71	4817.	-20.26	-184.34
FC 62	39 39.29	112 52.12	4816.	-21.03	-185.06
FC 63	39 39.10	112 52.73	4824.	-20.11	-184.40
FC 64	39 38.96	112 53.18	4832.	-18.61	-183.19
FC 65	39 38.86	112 53.49	4837.	-18.41	-183.17
FC 66	39 38.73	112 53.91	4844.	-18.44	-183.43
FC 67	39 38.55	112 54.66	4854.	-16.79	-182.11
FC 68	39 38.48	112 55.00	4856.	-16.12	-181.52
FC 69	39 38.38	112 55.39	4867.	-13.61	-179.40
FC 70	39 38.37	112 55.78	4876.	-13.38	-179.46
FC 71	39 38.36	112 56.10	4881.	-12.32	-178.56
FC 72	39 38.06	112 56.55	4858.	-13.88	-179.35
FC 73	39 37.81	112 56.93	4885.	-13.89	-180.28
FC 74	39 37.52	112 57.43	4932.	-9.81	-177.80
FC 75	39 41.86	112 44.93	4604.	-14.38	-171.19
FC 76	39 42.20	112 45.00	4603.	-17.17	-173.95
FC 77	39 42.76	112 45.09	4598.	-21.57	-178.18
FC 78	39 43.51	112 45.04	4596.	-23.98	-180.52
FC 79	39 44.22	112 44.78	4600.	-24.53	-181.21
FC 80	39 44.91	112 44.57	4599.	-25.09	-181.73
FC 81	39 45.05	112 43.23	4640.	-20.21	-178.25
FC 82	39 44.64	112 43.05	4631.	-19.52	-177.26
FC 83	39 44.21	112 42.93	4621.	-19.22	-176.62
FC 84	39 43.79	112 42.82	4620.	-17.89	-175.25
FC 85	39 43.36	112 42.70	4617.	-16.96	-174.20
FC 86	39 42.83	112 42.56	4611.	-16.43	-173.47
FC 87	39 42.40	112 42.45	4607.	-15.90	-172.83
FC 88	39 42.06	112 42.35	4604.	-15.04	-171.85
FC 89	39 40.67	112 35.59	4652.	-10.72	-169.16
FC 90	39 40.45	112 35.57	4648.	-10.99	-169.31
FC 91	39 40.10	112 35.54	4644.	-11.44	-169.61
FC 92	39 39.69	112 35.50	4639.	-11.25	-169.27
FC 93	39 38.95	112 35.45	4638.	-8.66	-166.63
FC 94	39 38.53	112 35.42	4642.	-6.53	-164.62
FC 95	39 38.19	112 35.38	4648.	-5.09	-163.39
FC 96	39 37.91	112 35.37	4648.	-4.46	-162.78
FC 97	39 37.43	112 35.33	4650.	-4.42	-162.80
FC 98	39 36.87	112 35.40	4647.	-4.71	-162.97
FC 99	39 36.44	112 35.45	4645.	-4.69	-162.88
FC100	39 35.94	112 35.53	4636.	-4.65	-162.54
FC101	39 35.20	112 35.80	4627.	-4.62	-162.20
FC102	39 34.63	112 36.06	4618.	-5.22	-162.50
FC103	39 34.05	112 36.87	4604.	-9.84	-166.65
FC104	39 32.17	112 38.44	4596.	-21.10	-177.64
KEG	39 43.08	112 51.42	5103.	-10.75	-184.56
72502	39 43.43	112 50.28	5144.	-3.93	-179.13
72503	39 43.89	112 49.17	5126.	-1.44	-176.03
72504	39 44.22	112 48.29	5106.	-6.80	-180.71

STATION NUMBER	LATITUDE DEG MIN	LONGITUDE DEG MIN	ELEV (FEET)	FREE AIR	SIMPLE BOUGUER
72505	39 44.65	112 47.77	5046.	-5.84	-177.71
72506	39 44.63	112 46.77	4868.	-13.09	-178.90
72507	39 44.77	112 45.70	4712.	-19.52	-180.01
72508	39 45.23	112 44.70	4599.	-25.51	-182.15
72509	34 44.01	124 46.30	4600.	-24.79	-181.47
72510	39 43.52	112 45.05	4596.	-24.03	-180.57
72511	39 42.77	112 45.07	4598.	-21.57	-178.18
72512	39 42.12	112 45.45	4603.	-17.05	-173.83
72513	39 41.39	112 45.55	4629.	-11.50	-169.17
72514	39 40.79	112 46.81	4689.	-14.09	-173.80
72515	39 40.53	112 47.54	4742.	-14.93	-176.44
72516	39 40.47	112 47.84	4761.	-15.74	-177.90
72517	39 42.32	112 50.94	4995.	-17.86	-187.10
72518	39 41.72	112 50.22	4905.	-20.70	-186.24
72519	39 40.94	112 49.99	4855.	-21.80	-185.47
72520	39 40.07	112 49.70	4794.	-19.22	-182.51
72521	39 39.30	112 49.44	4780.	-17.79	-180.60
72522	39 39.69	112 50.87	4811.	-19.24	-183.10
72523	39 39.29	112 52.14	4816.	-21.07	-185.10
72524	39 38.97	112 53.18	4830.	-19.01	-183.43
72525	39 38.56	112 54.64	4872.	-22.14	-185.52
72526	39 38.37	112 55.78	4876.	-13.32	-179.39
72527	39 38.35	112 56.10	4881.	-12.23	-178.48
72528	39 37.53	112 57.42	4932.	-9.80	-177.78
72529	39 37.94	112 58.49	4964.	-13.11	-182.18
72530	39 38.41	112 59.51	5026.	-15.01	-186.20
72531	39 38.23	112 56.97	4885.	-12.52	-178.90
72532	39 38.77	112 57.06	4890.	-12.12	-178.67
72533	39 39.37	112 56.82	4945.	-10.63	-179.06
72534	39 39.90	112 56.59	5023.	-4.89	-175.97
72535	39 40.54	112 56.81	5051.	-1.76	-173.80
72536	39 40.56	112 49.42	4805.	-17.96	-181.85
72537	39 41.09	112 48.58	4760.	-18.09	-180.42
72538	39 41.59	112 47.79	4735.	-17.35	-178.64
72539	39 41.85	112 47.36	4721.	-17.10	-177.90
72542	39 41.87	112 55.87	5168.	2.70	-173.33
72544	39 41.85	112 57.01	5078.	-5.45	-178.41
72558	39 40.12	112 54.93	5015.	-4.94	-175.75
72559	39 40.21	112 55.26	5030.	-5.35	-176.67
72560	39 39.42	112 55.44	4990.	-7.17	-177.13
72561	39 38.80	112 55.78	4938.	-10.71	-178.90
72562	39 44.11	112 50.97	5290.	2.53	-177.65
72572	39 45.04	112 43.22	4638.	-20.29	-178.25
72573	39 45.62	112 42.28	4703.	-13.36	-173.55
72574	39 44.09	112 41.45	4763.	-6.74	-168.97
72575	39 44.65	112 40.84	4805.	-5.91	-169.55
72576	39 47.08	112 40.04	4803.	-7.46	-171.05
72002	39 43.80	112 51.98	5220.	-9.76	-187.06
72003	39 44.63	112 52.32	5348.	5.18	-177.75
72024	39 44.96	112 57.05	5475.	23.80	-162.65
72025	39 44.56	112 56.91	5479.	24.55	-162.06
72026	39 43.58	112 56.91	5333.	19.90	-161.77
72027	39 43.06	112 57.07	5223.	12.53	-165.37
72028	39 42.11	112 57.06	5096.	7.95	-165.85
72029	39 41.90	112 56.74	5105.	11.32	-162.56
72030	39 41.84	112 54.84	5135.	11.77	-163.13
72031	39 41.88	112 53.85	5050.	3.67	-168.34
72032	39 42.28	112 53.04	5056.	.18	-172.02
72035	39 44.61	112 52.48	5318.	12.73	-168.40
72036	39 43.94	112 53.79	5318.	11.59	-169.55
72037	39 43.59	112 53.53	5249.	-3.08	-181.86
72039	39 41.64	112 57.78	5026.	-10.36	-181.54
72040	39 41.37	112 58.87	4973.	-16.97	-186.35
72041	39 41.20	112 59.89	4971.	-20.76	-190.07
72042	39 41.87	113 .27	4994.	-18.07	-188.16
72043	39 44.25	112 59.95	4994.	-19.38	-191.24
72044	39 44.06	112 58.60	5217.	-3.85	-181.34
72077	39 42.72	112 52.65	5297.	1.85	-178.57
72078	39 43.12	112 55.04	5484.	10.53	-176.26
72080	39 44.88	112 53.75	5543.	10.33	-173.47
72111	39 44.51	112 51.85	5367.	3.67	-179.13

STRATIGRAPHY OF THE COAL-BEARING BLACKHAWK FORMATION ON NORTH HORN MOUNTAIN, WASATCH PLATEAU, UTAH

By Jan L. Johnson[1]

ABSTRACT

Coal-bearing rocks of the Cretaceous Blackhawk Formation crop out along the eastern margin of the Wasatch Plateau in central Utah. On North Horn Mountain the Blackhawk Formation ranges from 215 to 290 meters in thickness and consists of interbedded sandstone, shale, siltstone, carbonaceous shale, coal, and limestone. The lower half of the formation, which contains the economically important coal beds, was deposited predominantly in a shallow water, wave-modified delta system. The upper half of the unit was deposited in fluvial environments of meandering streams and floodplains. The source for the clastic sediments of the Blackhawk Formation was to the west.

Potentially minable coal exists in the Hiawatha and Blind Canyon beds and possibly in the Bear Canyon bed. The thickest beds were measured in the southeastern part of the study area, with 5.3 meters of the Blind Canyon bed found in one measured section. These coals are high quality and have lateral continuity, but the thickness varies and scattered wants and splits are to be found. Coal reserves on North Horn Mountain are large and should become an important source of supply for local and regional markets.

INTRODUCTION

Location and Accessibility

North Horn Mountain, on the eastern edge of the Wasatch Plateau in central Utah (figure 1), is approximately 50 kilometers south of the city of Price, Utah, and directly west of the small towns of Castle Dale and Orangeville (figure 2). The general area may be reached via Utah State Highway 10 which extends in a southerly direction from Price to Castle Dale. Utah State Highway 29 joins State highway 10 a few miles north of Castle Dale, and, after passing through Orangeville, traverses Straight Canyon on the north side of North Horn Mountain to Joes Valley Reservoir.

Physical Features

North Horn Mountain is bounded on the west side by Joes Valley, a north-south trending graben, and on the east by Castle Valley. Straight Canyon and Rock Canyon form its northern and southern boundaries.

The relief between Castle Dale and Orangeville and The Cap at the top of the mountain (figure 2) is 1,170 meters, and the cliffs are approximately 500 meters high along Castle Valley. The major coal-bearing strata are found one third of the distance from the base to the top of the cliffs, near the base of the Blackhawk Formation.

GEOLOGY

The coal-bearing strata are found in nearly flat-lying Cretaceous fluvial and shallow marine sediments in the Wasatch Plateau. Figure 3 is a geologic map of the study area showing the locations of eight stratigraphic sections measured for this report (see Appendix A).

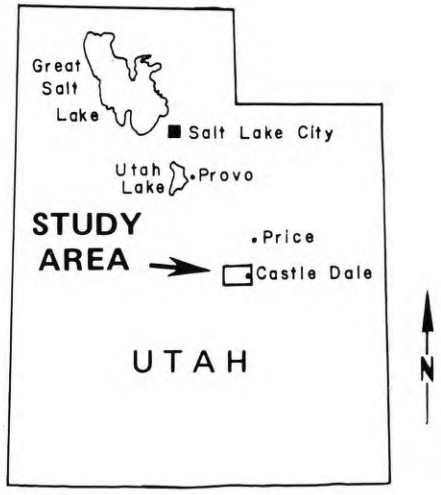

Figure 1. Index Map

STRATIGRAPHY

The generalized Cretaceous stratigraphy for the Wasatch Plateau area is shown on figure 4. The units exposed range from the Masuk Shale Member of the upper Cretaceous Mancos Shale at the base of North Horn Mountain to the early Tertiary Flagstaff Formation at the top of the mountain. Except for the more comprehensive explanation and description of the Blackhawk Formation, a short discussion of each unit follows, from older to younger.

Mancos Shale

The Mancos Shale is predominantly marine shale with two major sandstone members that range from shallow marine to deltaic plain type deposits. It is divided into five members, which in ascending order are: Tununk Shale, Ferron Sandstone, Blue Gate Shale, Emery Sandstone, and Masuk Shale. The upper Mancos is the open water equivalent of the fluviatile, deltaic, and barrier beach-lagoon facies found in the Mesaverde Group.

Mesaverde Group

The Mancos Shale is overlain by the Mesaverde Group, which, from older to younger, includes the Star Point Sandstone, the Blackhawk Formation, the Castlegate Sandstone and the Price River Formation.

Star Point Sandstone

The Star Point sandstone, in its type locality, consists of three prominent sandstones separated by shales or partings of thin-bedded sandstone. These three sandstones are designated, in ascending order, the Panther, Storrs, and Spring Canyon Tongues by Clark (1928). Spieker (1931, p. 21-27) states that the Star Point sandstones were regressive, prograding beach near-shore deposits.

[1] 823 Saranac , Mesa, Arizona, 85208

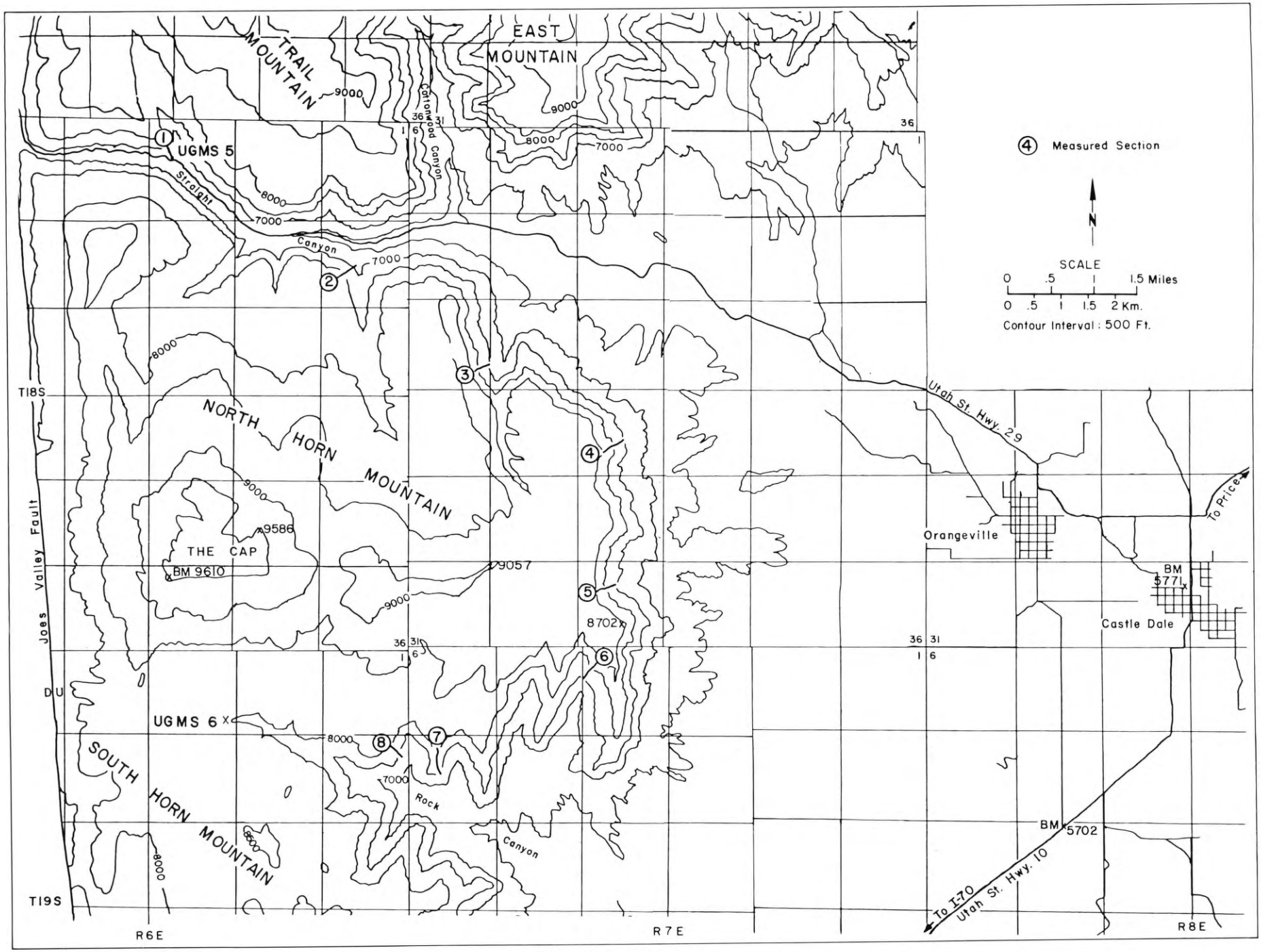

Figure 2. Location Map

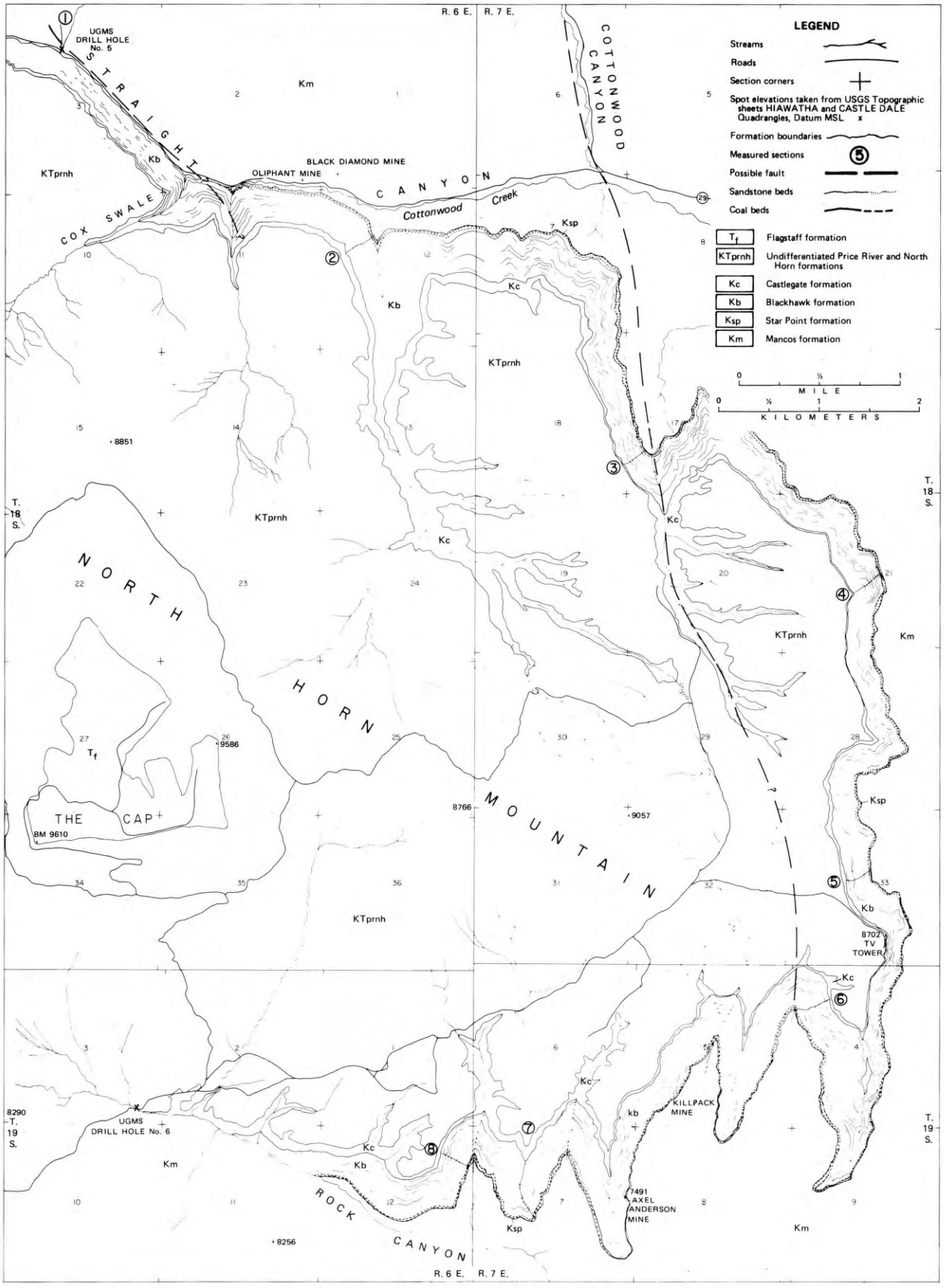

Figure 3. Geologic map of Trail Mountain.

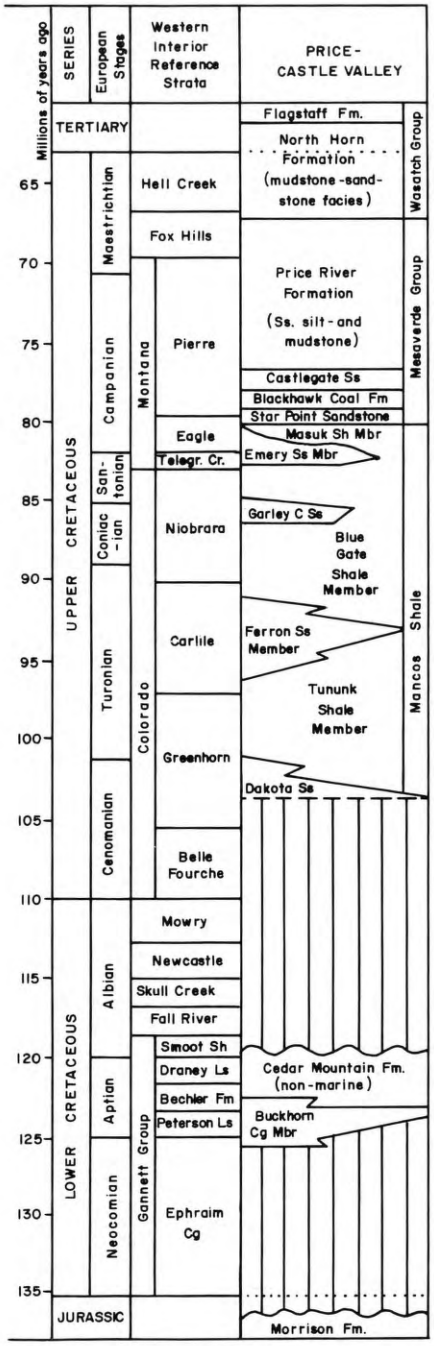

Figure 4. Generalized Cretaceous stratigraphy, after Hintze, (1973, p. 70)

Howard (1966,1975) indicates that parts of the Star Point are of deltaic origin. In the study area near measured section 3, (figure 2) a few thin discontinuous coal beds are found in the upper part of the Spring Canyon Sandstone. This sandstone is bleached white below the overlying Hiawatha coal bed of the Blackhawk Formation where the iron was leached from the sandy sediments beneath the swamp in which the coal was formed (Young, 1966, p. 13). The bleached sandstone makes an excellent marker bed and guide for the Hiawatha coal bed.

Blackhawk Formation

The Blackhawk Formation is Upper Cretaceous of Montanan (Campanian) age. Peterson and Ryder (1975) and Maxfield (1976) indicate that the Blackhawk Formation is time stratigraphically equivalent to the Masuk Shale Member of the Mancos Shale in the Henry Mountains. In the study area the Masuk Shale underlies the Star Point Sandstone. Young (1955, 1966) demonstrates that the Blackhawk Formation intertongues with the Mancos Shale in the Book Cliffs. He also indicates that the wesward equivalent of the Blackhawk is the upper part of the Indianola Group. A diagram from Armstrong (1968) shown in McGookey and others (1972, p. 192) illustrates the Blackhawk Formation to be equivalent to the South Flat Formation (a conglomerate) of the Gunnison Plateau. Hintze (1973) also follows this correlation.

Spieker and Reeside (1925) named the Blackhawk Formation and designated the type section near what was then the Blackhawk mine (later called the King No. 1 mine) near Hiawatha, Utah. The formation included the coal-bearing rocks of the Book Cliffs and the Wasatch Plateau that are below the Castlegate Sandstone Member of the Price River Formation. Young (1955) redefined the lower boundary of the Blackhawk to include the upper standstone of the Star Point Formation and designated six members in the Book Cliffs. In this study, the usage of Spieker and Reeside is followed; the base of the Blackhawk Formation is considered the lowermost coal or associated swamp facies above the Star Point Formation.

The Blackhawk Formation consists of interbedded and interfingering shale, sandstone, siltstone, limestone, and coal. Each member is associated with a prominent littoral sandstone; in ascending order these are: Spring Canyon, Aberdeen, Kenilworth, Sunnyside, Grassy, and Desert Members. At the western end of the Book Cliffs and in the eastern part of the Wasatch Plateau, only the lower two of these members are present. Seven complete stratigraphic sections and one partial section of the Blackhawk Formation were measured in the study area. The lithologic descriptions are included as Appendix A.

Thin section studies show the sands in the Blackhawk to be fine to medium grained, subrounded to angular, and well to moderately sorted. They range from almost pure quartz sands to sands containing considerable amounts of carbonate material both as detrital grains and in the interstices between grains. There is a widespread occurrence of clastic ankerite (or dolomite), found in varying amounts in both the channel sandstones and the more laterally continuous sandstones. In some sandstone samples the carbonate grains appear to have been the nuclei for ankeritization or dolomitization of the matrix and quartz grains. Some lenticular sandstone bodies grade laterally and vertically into interbedded shale, siltstone, and sandstone, and finally into shale.

Normally the siltstones are similar in character to the sandstones but are finer grained, especially where they are associated with sandstone bodies. Where the siltstones are found interbedded with shales, they tend to have a higher clay content and to resemble the shales in color and outward appearance.

Shales range from claystone to highly silty and sandy shales. They fall naturally into two categories; (1) the brown to black carbonaceous varieties and (2) the gray, calcareous varieties. The carbonaceous shales occur in interbedded sequences with the gray shales, siltstones, and sandstones. The carbonaceous shales are also found associated with coal beds as underclays and, locally, are found above them. The shales range from brown to black to bony coals (coals with high sediment content). The gray calcareous shales also are commonly in interbedded sandstone-siltstone-shale sequences with some minor carbonaceous shale interbeds.

Most carbonate rocks are found interbedded with shales and silty shales. They occur in thin beds not easily recognized in the field. Typically, they contain varying amounts of clastic material or appear to be shales that have been diagenetically replaced by carbonate. The carbonates are typically gray to tan, dense, and fine-grained to microcrystalline, with no evident fossils other than plant debris.

Throughout the area the coals of the Blackhawk Formation vary greatly in quality and thickness. The thickest minable coals are found in the lowermost part of the formation and have rather consistantly high percentages of vitrain and resin with varying amounts of durain and fusain. Coal beds found higher in the section show more lateral variation, are thinner, and generally of lower quality; they also tend to have higher amounts of durain and fusain, (may have some resin) and a higher silt and clay content. Coals are commonly weathered (oxidized) at least 1 meter in from the outcrop surface

and have a slightly dull luster. They exhibit apparent cleating, but this may be a weathering phenomenon.

The correlation between the measured sections described in Appendix A is shown on the fence diagram in figure 5: the locations of the sections are shown on figures 2 and 3. The base of the Castlegate Sandstone is the datum for the columns. Measured section 6 has been shifted west for ease in drafting. Measured section 4 is omitted because it is not complete. The geologic map (figure 3) shows the lateral distribution of the sandstone and major coal units.

The Blackhawk Formation is characterized by both vertical and lateral facies changes. Measured section 6 (figure 6) was chosen as representative of the vertical variation in lithology. (Figure 7 shows the traverse of measured section 6 up the side of Wash Canyon.) There is a distinct difference in the overall abundance and thickness of different rock types in the lower half of the Blackhawk Formation (unit 2 through unit 42) and in the upper half of the formation (unit 43 through unit 62).

The lower part is characterized by the following: (1) thin sandstone units, many of which are laterally discontinuous and lenticular; (2) a high proportion of carbonaceous shale and coal with thick and laterally continuous coal beds, especially near the base of the formation; (3) the presence of thin limestone beds (that are absent in the upper part of the formation); and (4) a high proportion of siltstone and sandstone beds in the shale units between the prominent sandstone units.

Lateral facies changes in the formation were investigated by tracing segments of measured section 6 laterally. The coal of unit 3, which has been designated the Hiawatha bed, varies in thickness with a maximum of about 3 or 4 meters in the vicinity of the Killpack and Axel Anderson mines (figure 3). In some areas lenticular sandstone bodies create partial or complete wants in the underlying coal. Figure 5 shows an example of this type of want in the Bear Canyon coal bed between measured section 7 and UGMS drill hole 6. Unit 30, a fine grained, thin- to medium-bedded sandstone with small-scale cross-bedding, ripples, minor convolute bedding, and minor shale interbeds, grades to the south into a massive sandstone with prominent cross-bedding and convolute bedding. This massive sandstone replaces the underlying coal beds. Several of the lenticular sandstone bodies examined have angular to round shale clasts in their lower part.

Coal beds are commonly located within gray shale-siltstone-sandstone sequences or above sandstone units, with rarely more than a couple of meters of gray and carbonaceous shale between sandstone and coal. The Hiawatha bed in many places has a dusky yellowish brown underclay containing bands and fragments of coal and occasional resin inclusions. This underclay is normally less than 0.5 meter thick. Many of the better developed coals have the same type of underclay. In many places coal beds are overlain by sandstone. The overlying sandstone may be lenticular and laterally discontinuous, or massive, relatively continuous, and more sheetlike. Numerous carbonaceous shale units are so coaly that they could be labelled bone coal. They, too, are mostly found in gray shale-siltstone-sandstone sequences or under sandstone ledges, as are the coal beds of the area.

In contrast, the upper part of the Blackhawk Formation typically has thicker, more laterally continuous massive sandstone units, a higher proportion of shale in the inter-sandstone units, much less carbonaceous shale, and only minor coal beds which rarely exceed 0.3 meter in thickness. The massive sandstones appear to be composed of multiple lenticular sand bodies (unit 55 of measured section 6). These are medium to thick bedded and the lenses appear almost to be interwoven. In a few places some of these sandstones are as thick as 20 to 25 meters, as in Straight Canyon north and west of measured section 2. Some of the sandstones in the upper part of the formation have minor shale or silty interbeds that follow cross-bedding planes. The carbonaceous shale and coal beds in the upper part of the Blackhawk are more commonly found associated with sandstones rather than the interbedded sequences. Most are found just below a massive sandstone ledge. No ankerite or dolomite was found in two thin sections cut from samples collected in the upper part of the formation.

By far the most common sedimentary structures in the Blackhawk Formation sandstones are cross bedding and convolute bedding (figure 8 a & b). Figure 8a, taken of a sandstone in the main gully of the wash in Rock Canyon in which section 6 was measured, shows unimodal crossbedding in one of the lower more continuous sandstones of the upper part of the formation. Many of the sets seen in the photograph are trough crossbeds, found throughout the formation and the most common. Bimodal crossbedding is less common in the upper formation. Convolute bedding (figure 8b) is common in many massive and thick-bedded sandstone units throughout the Blackhawk. 8b shows unit 75 of measured section 7. This type of soft sediment deformation ranges from very slightly disturbed beds to beds even more highly contorted than those shown in figure 8b.

Individual channels traced from ridge to ridge in Rock Canyon contain primary features which indicate the direction of water movement (figure 7).

Logs are imbedded in some of the sandstone units and can be seen at road level in Straight Canyon. Some of these logs are in growth position. Many are found in the upper part of the section and few in the lower part.

Sedimentary structures in shales are less obvious because they are usually covered by a thick slopewash. Some of the gray shales in the upper part of the formation contain shredded bits of plant debris. This was also noted in the lower part of the formation but mainly near carbonaceous shales or coals. Mottling or burrowing might be present in the shales, but no positive observation could be made.

Castlegate Sandstone

Originally considered a member of the Price River Formation by Spieker and Reeside (1925) and Clark (1928), the Castlegate Sandstone which overlies the Blackhawk Formation was designated a formation by Fisher, Erdman, and Reeside (1960). Van de Graaff (1972) summarizes previous work on the Castlegate and the distribution of the facies of the formation. In the study area, rocks in the formation range from fine- to course-grained, and moderately to well-sorted sandstones. There are some quartzite and chert pebble conglomerates and siltstone and shale interbeds. These rocks are interpreted to be a fluvial facies deposited by coalescing braided streams flowing predominantly eastward. The Castlegate Sandstone in the study area is estimated to range from 60 to 90 meters in thickness. It is the top cliff-forming unit of the eastern edge of the Wasatch Plateau and can be a major obstacle to gaining access to the Blackhawk Formation from the top of the plateau. Its type locality is in Price River Canyon, just west of the Utah Power and Light Company's coal-washing and power-generating installations near the narrow, steep-walled section of the canyon known as the Castle Gate.

Younger sedimentary units present on North Horn Mountain are the Cretaceous Price River Formation, the Cretaceous-Tertiary North Horn Formation

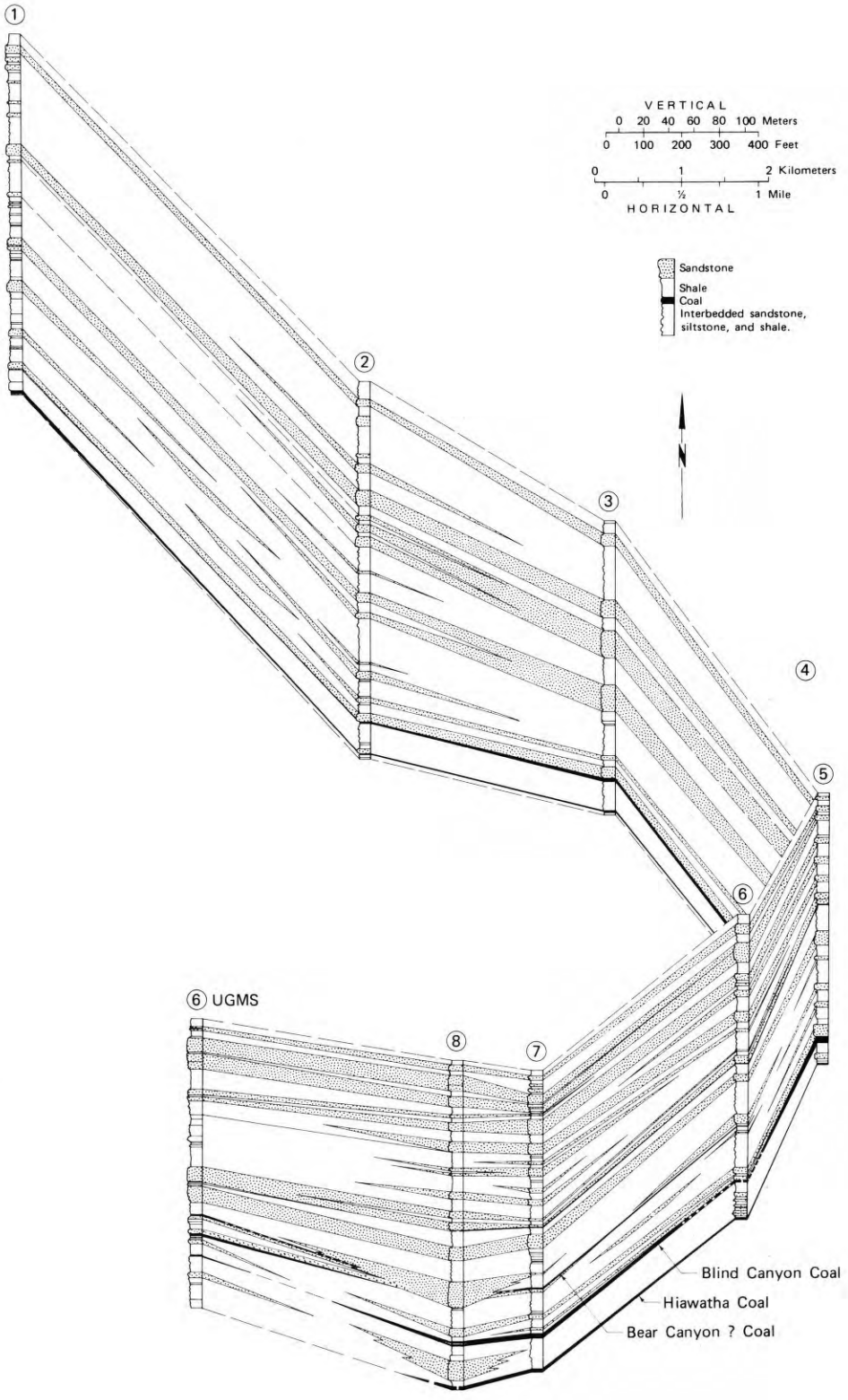

Figure 5. Fence diagram.

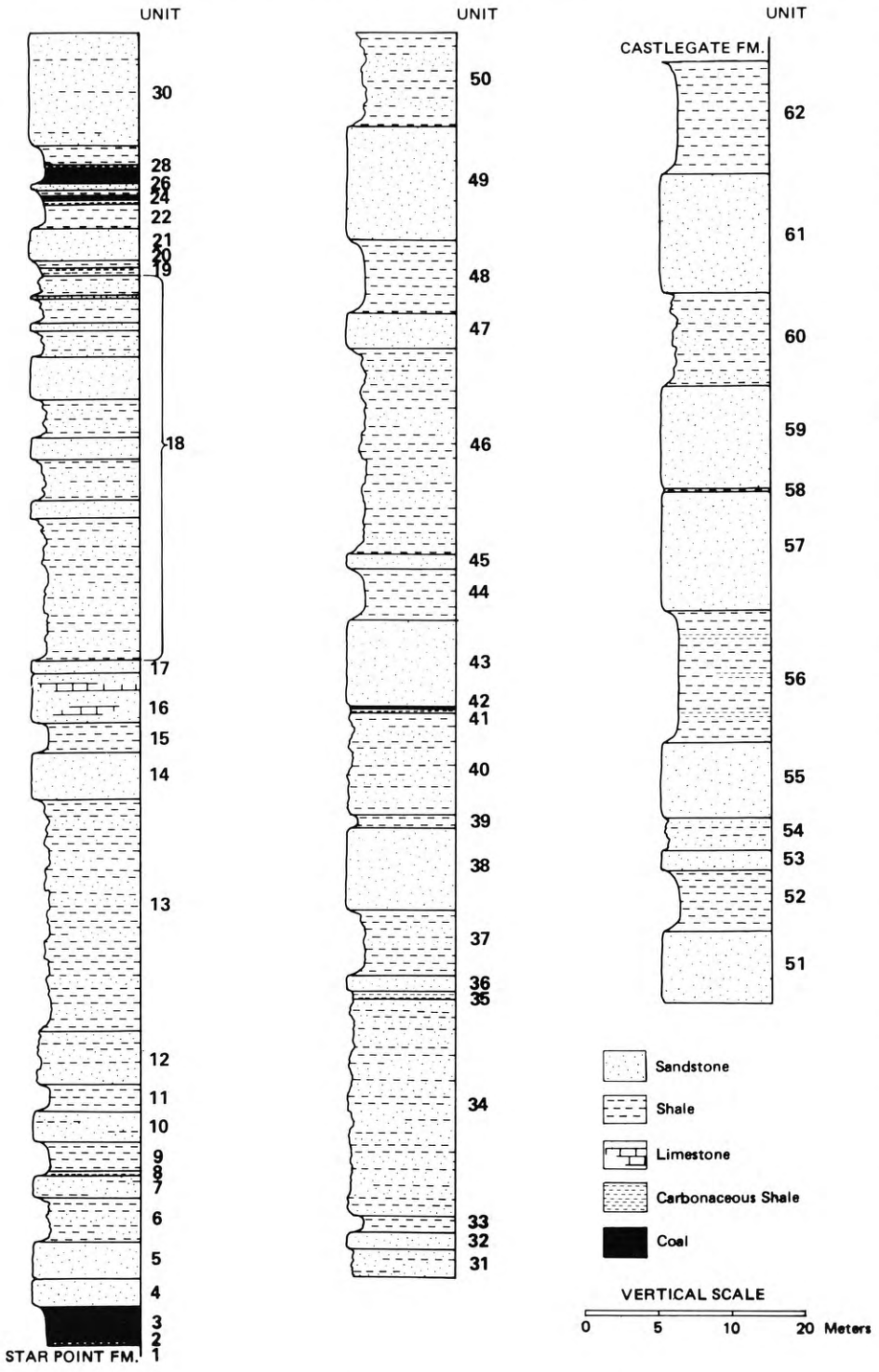

Figure 6. Measured stratigraphic section 6

and the Tertiary Flagstafff Limestone. These formations are discussed in detail by Spieker (1931 and 1946).

STRUCTURE

The strata along the eastern edge of the Wasatch Plateau dip to the west, away from the San Rafael Swell, an early Tertiary northeasterly-trending upwarp, which lies to the east of Castle Valley. In general the dips are very gentle in the Wasatch Plateau, although Spieker (1931, p. 53) found that in a few places they attain inclinations of 19 to 20 degrees.

Spieker (1931) constructed structural contours on top of the Spring Canyon sandstone member of the Star Point Formation. He mapped a broad, westward plunging syncline with an east-trending axis roughly paralleling Straight Canyon and a 490-meter structural relief from the northwest to the southeastern parts of North Horn Mountain. Dips rarely exceed 5 to 6 degrees, and are commonly less.

Spieker (1931, pl. 31 and 32) found no faults on North Horn Mountain with the exception of the north-trending Joes Valley fault on the western edge of the study area. Although no offset is visible, the relatively straight alignment of Cottonwood Canyon between Trail Mountain and East Mountain (see the very northern part of figure 2) and the washes in which sections 3 and 6 were measured suggest control by a prominent fracture or joint (figure 3). Another possible fault extends through the northwest-trending section of Straight Canyon and passes just to the west of UGMS drill hole 5 and measured section 1. These possible faults are compatible with the orientation of the other mapped faults in the region and may have enough offset to cause problems in future mining.

ENVIRONMENTS OF DEPOSITION OF THE BLACKHAWK FORMATION

Spieker (1931) envisioned a broad, flat, low flood plain with streams meandering back and forth between low swampy areas as the environment in which the sediments of the Blackhawk Formation accumulated. He suggests that these streams may have emptied into lagoons of brackish water into which the marine water of the Mancos Sea occasionally transgressed from the east (p. 37). Young (1955, 1966), who worked mostly in the Book Cliffs, reevaluated this interpretation and proposed a model of barrier beaches with lagoonal and paludal deposits forming behind them. As these beaches prograded seaward, swamp and other sediments were deposited over them. Repeated intervals of subsidence caused repeated westward transgressions of the sea.

At the very western end of the Book Cliffs, which is in about the same relative position to the Mancos Sea paleoshoreline (McGookey and others, 1972, p. 218) as the study area, Young (1955, p. 283) indicated that both environments were present. Parker (1976) studied fossil plants of the Blackhawk Formation in Salina Canyon, near the southern end of the Wasatch Plateau, and in Straight Canyon and concluded that the contained flora was indicative of flood plain, levee, and point-bar environments.

Figure 7. Oblique photograph showing traverse of stratigraphic section 6 in Rock Canyon. Arrows point to channel fillings (ch)

The upper sandstone unit of the underlying Star Point Formation is a regressive littoral sandstone of the barrier beach and bar facies. The locally irregular contact at the base of the Blackhawk Formation is due to runnels and surge channels in the beach and bar sands of the underlying Spring Canyon Member of the Star Point.

Above the Star Point sandstone lie either gray and black shales or the Hiawatha coal bed of the Blackhawk Formation. The shales are of the lagoonal and interdistributary bay facies. In most places the shales are thin, and the swamps from which the overlying coal formed must have migrated seaward closely behind the bar and beach sands. Carbonaceous, coaly shales are representative of swamp conditions. The coals may be overlain by interdistributary facies or distributary channels and levee and crevasse facies rocks.

Sand bodies, which locally displace coal beds, have lens-shaped cross sections and are elongate distributary channels. Unit 30 of measured section 6 is a levee deposit as indicated by grain size and bedding features. It grades laterally from a massive distributary channel sandstone into the shale-dominated interdistributary sediments. Other examples of distributary channels are units 21, 26, and 36 of measured section 6 (figure 6).

The thin limestone units in the lower Blackhawk may be interdistributary bay and lagoon deposits, or possibly lacustrine deposits. The detrital, rounded to subangular ankerite or dolomite contained in them indicates a nearby source. The carbonates are found in varying amounts in distributary channel, levee and crevasse, delta front, and interdistributary bay and lagoon facies rocks in the lower part of the Blackhawk Formation. A few of these may be marine, but no fossil evidence was found to substantiate or negate this possibility. The highly calcareous gray shales and silty shales are interdistributary bay and lagoon deposits, upper deltaic plain deposits, and possibly lacustrine deposits formed in levee flank depressions. The sediments show cyclical deposition in the lower part of the formation, beginning with a sandstone and grading upward into a predominantly shale unit.

Near the middle of the Blackhawk Formation there is a lithologic change which reflects a change in the dominant depositional environment. The lower half of the formation was deposited in a wave modified, shallow water delta in the Mancos Sea, the upper part of the formation in a fluvial environment, with sediment-laden streams meandering across a broad, low profile flood plain.

In the upper part of the Blackhawk Formation is a series of massive, fine- to medium-grained, calcareous, cross-bedded sandstones with convolute bedding. A number of these sandstones are continuous laterally, although they thicken and thin and locally appear to be composed of multiple compound lenses, as in unit 55 of measured section 6 (figure 6). These sand bodies are interpreted as being predominently coalescing river channel deposits.

The interbedded shale units are flood plain deposits. Minor coal beds developed in low boggy swampy areas on the flood plain. Most coal beds in the upper Blackhawk lie above the shales and other fine sediments of the flood plain facies, and below the massive sandstones and thinner bedded and interbedded sandstones of the channel and levee facies. Fossil plants studied by Parker (1976) confirm a fluvial environment for these rocks.

The high calcite content in some of these rocks may be due to diagenetic processes whereby calcite is deposited as matrix and cement. The corroded edges of quartz grains seen in thin section indicates replacement by calcite.

The source for the sediments of the Blackhawk Formation as indicated by the geometries and distribution of lithologic types in the study area was to the west. Deposition of coarser sediments (the thick sandstone units) may have been the result of uplift of the source area. Shifting distributary patterns were important in creating the variety of facies present in the lower part of the Blackhawk Formation, while the changes in the supply of sediment and base level were more important in the upper part of the formation.

COAL BEDS

In the study area three potentially minable coal beds, the Hiawatha, Blind Canyon, and Bear Canyon (Spieker, 1931) have been identified and are shown

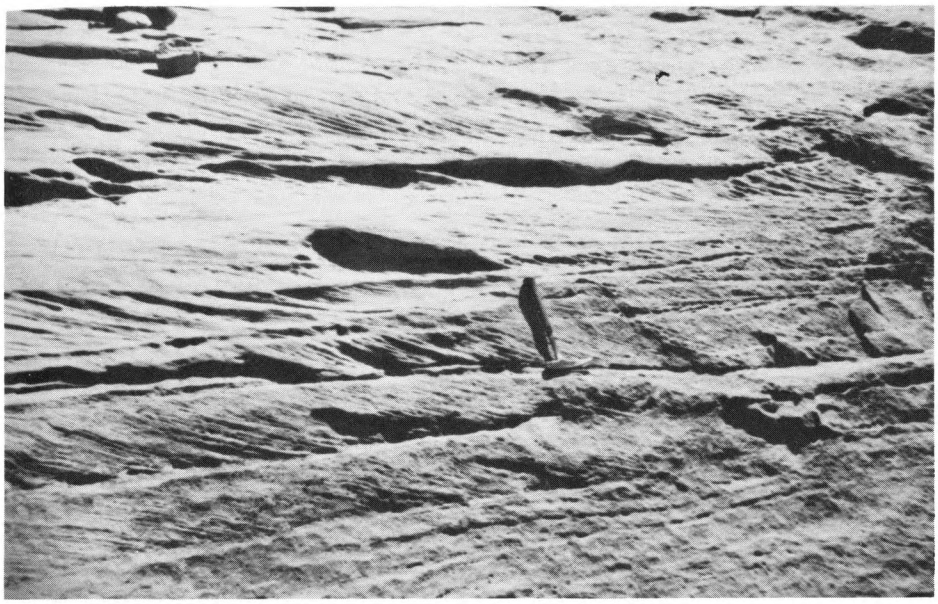

Figure 8. Cross-bedding in upper Blackhawk Formation sandstones.

a. Unimodal bedding

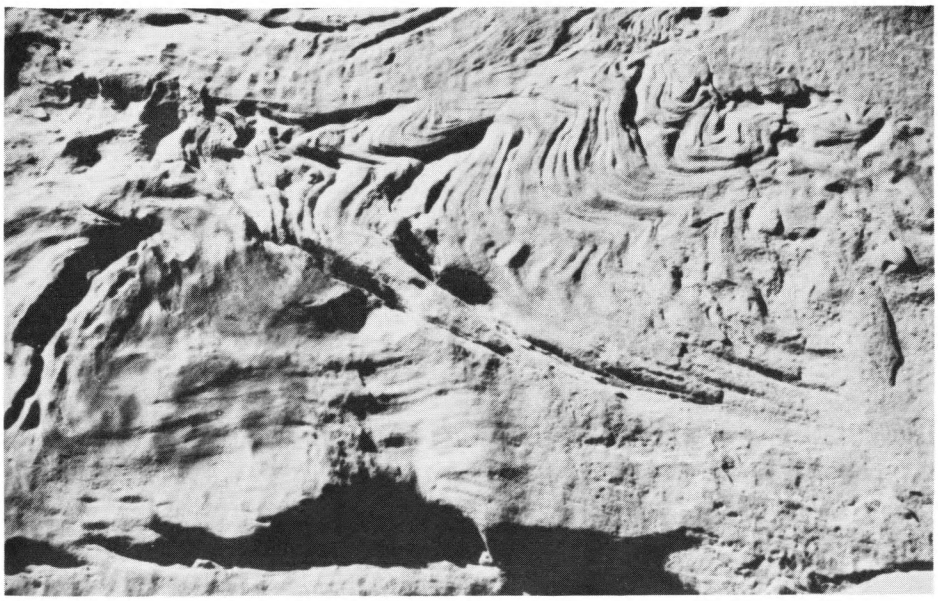

b. Convolute bedding

in figure 5. The thickness of these beds varies throughout the area; they are locally found to be greatly reduced in thickness or lacking completely. The Hiawatha and Blind Canyon coals have the best economic potential. The Bear Canyon bed is submarginal to marginal, although drilling may prove it to be thick enough in some areas to merit exploitation.

Two abandoned mines in Straight Canyon, west and north of measured section 2 (figure 3) are the Black Diamond, operated from 1898 until the 1950's, and the Oliphant operated from 1906 until the 1950's. Both operated in the Hiawatha bed, which here is about 1.5 to 1.7 meters thick. Two other abandoned mines in the wash directly west of Rock Canyon Wash in which measured section 6 is found are the Axel Anderson mine, operated from 1906 to 1932 in the Hiawatha bed, which here is 4 meters thick, and the Killpack mine for which no records were found. The Hiawatha bed is 2.5 meters thick near the Killpack mine.

Some of the thicker coal beds are found in the southeastern part of the study area. The Blind Canyon bed was found to be 5.3 meters thick in section 5. The Hiawatha bed is consistantly greater than 2.5 meters thick between measured sections 5 and 7, where lenticular sandstone bodies have created wants. In places the major coal beds are split. Near the head of the wash in section 8 the Blind Canyon bed is 3 to 4 meters thick with a 0.6-meter split in the upper part of the bed. The geometry could not be ascertained, but the split appears to be a lenticular, elongate sandy body.

ACKNOWLEDGMENTS

The John S. Berge fund provided a grant for field and laboratory expenses. Dr. H. H. Doelling of the Utah Geological and Mineral Survey aided in the selection of the study area and provided data from two holes drilled by UGMS during the summer of 1975. My special thanks go to my thesis advisor, Dr. Harold J. Bissell.

REFERENCES

Armstrong, R. L., 1968, Sevier orogenic belt in Nevada and Utah: Geological Society of America Bulletin, v. 79 no. 4 p. 429-458

Clark, F. R. 1928, Economic Geology of the Castlegate, Sunnyside, and Wellington quadrangles, Carbon County, Utah: U.S. Geological Survey Bulletin 793

Fisher, D. A., C. E. Erdman, and J. B. Reeside Jr., 1960, Cretaceous and Tertiary formations of the Book Cliffs, Carbon, Emery and Grand Counties, Utah and Garfield and Mesa Counties, Colorado: U. S. Geological Survey Professional Paper 332, 80 p.

Hintze, Lehi F., 1973, Geologic history of Utah: Brigham Young University Geology Studies, v. 20, pt. 3

Howard, J. D., 1966, Sedimentation of the Panther Sandstone Tongue: Utah Geological and Mineral Survey Bulletin 80, p. 23-34

——— 1975, Field Trip leader, Geological Society of America Convention Coal Geology Trip. Wasatch Plateau, Book Cliffs Coal Fields, Utah.

Maxfield, E. Blair, 1976, Foraminifera from the Mancos Shale of east central Utah: Brigham Young University Geology Studies, v. 23 pt. 3, p. 67-162.

McGookey, D. P., J. D. Haun, Lyle A. Hale, H. G. Godell, D. G. McCubbin, Robert J. Weimer, and George R. Wulf, 1972, The Cretaceous System, *in* Geologic atlas of the Rocky Mountain region, U.S.A., Rocky Mountain Association Geologists, Denver, Colorado.

Parker, Lee R. 1976, The Paleoecology of the fluvial coal-forming swamps and associated floodplain environments in the Blackhawk Formation (Upper Cretaceous) of central Utah; Brigham Young University Geology Studies, v. 22, pt. 3, p. 99-116

Peterson, Fred, and Robert T. Ryder, 1975, Cretaceous rocks in the Henry Mountains region and their relation to neighboring regions: Four Corners Geological Society Guidebook, 8th Field Conference, Canyonlands.

Spieker, E. M. 1931, The Wasatch Plateau coal field, Utah: U.S. Geological Survey Bulletin 819

——— 1946, Late Mesozoic and early Cenozoic history of central Utah: U.S. Geological Survey Professional Paper 205-D 43 p.

Spieker, E. M. and J. B. Reeside, Jr., 1925, Cretaceous and Tertiary formations of the Wasatch Plateau, Utah: Geological Society of America Bulletin v. 36, p. 435-454

Van de Graaff, F. R., 1972, Fluvial-deltaic facies of the Castlegate Sandstone (Cretaceous) east-central Utah: Journal of Sedimentary Petrology, v. 42, no. 3, p. 558-571.

Young, Robert G., 1955, Sedimentary facies and intertonguing in the Upper Cretaceous of the Book Cliffs, Utah-Colorado: Geological Society of America Bulletin v. 66, p. 177-202.

——— 1966, Stratigraphy of coal-bearing rocks of the Book Cliffs, Utah-Colorado: Utah Geological and Mineralogical Survey Bulletin 80, p. 7-22.

APPENDIX A

Unit		Meters
	Measured section no. 1: partial section of Blackhawk Formation measured from the top of UGMS Drill Hole 5 in Straight Canyon NW 1/4 section 3, T. 18 S., R. 6 E.	
	Castlegate Sandstone	
	Blackhawk Formation	
28.	Shale, medium gray, weathers light gray, highly calcareous, mostly covered slope	8.7
27.	Sandstone, light olive gray, weathers grayish orange, fine to medium-grained, calcareous, cross-bedded, convolute bedding, massive, iron oxide flecks, ledge former	6.4
26.	Sandstone, light olive gray, weathers grayish orange, fine to medium-grained, calcareous, medium to thick-bedded, cross-bedded, convolute bedding, iron oxide flecks, interbedded with medium gray shale, calcareous, weathers light gray, ledge former and siltstone	2.7
25.	Sandstone, light olive gray, weathers grayish orange, fine to medium-grained, calcareous, iron oxide flecks, cross-bedded, convolute bedding, massive, ledge former	3.7
24.	Shale, very light gray to white for lower .6 M medium gray for rest, weathers very pale orange with popcornlike surface, highly calcareous, slope former	3.4
23.	Sandstone, light olive gray, weathers grayish orange, fine to medium-grained, calcareous, cross-bedded, convolute bedding, massive, top .3 M bleached white in places	4.1
22.	Shale, medium gray, weathers light gray; calcareous, possibly some interbedded siltstone and carbonaceous shale; covered slope	8.5
21.	Sandstone, light olive gray, weathers grayish orange, fine to medium-grained, calcareous, iron oxide flecks, cross-bedded, ledge former	1.2
20.	Shale, medium gray, weathers light gray, highly calcareous, interbedded with siltstone and sandstone, weathers grayish orange, fine-grained, calcareous, and some shale, dark gray to black, coaly fragments, vitrain bands, shales weathered with popcornlike surface in places, slope former	14.6
19.	Shale, dusky yellowish brown, silty, carbonaceous, fissile, slope former	.3
18.	Sandstone, light olive gray; weathers grayish orange, fine to medium-grained, calcareous, iron oxide flecks, cross-bedded, thick-bedded to massive, lenticular, ledge former	1.8
17.	Shale, medium gray, weathers light gray, calcareous, very poorly exposed, slope former	7.6
16.	Sandstone, light olive gray, weathers grayish orange, fine to medium-grained, calcareous, highly cross-bedded, convolute bedding, shale interbeds between some of the cross beds, ledge former	2.7
15.	Shale, medium gray, weathers light gray, calcareous, interbedded with siltstone and sandstone, light olive gray?, weathers grayish orange, fine-grained, calcareous, thin- to medium-bedded, slope former	30.3
14.	Sandstone, light olive gray, weathers grayish orange, fine to medium-grained, calcareous, iron oxide flecks, cross-bedded, friable, massive, top .1 to .3 M bleached white, ledge former	8.5
13.	Shale, medium gray, weathers light gray, calcareous, slope former	3.8
12.	Sandstone, light olive gray, weathers grayish orange, fine to medium-grained, calcareous, iron oxide flecks, cross-bedded, massive, ledge former	1.8
11.	Sandstone, light olive gray, weathers grayish orange, fine-grained, calcareous, thick to medium-bedded with thin shale, black, carbonaceous interbeds, interbedded with shale, medium gray, weathers light gray, calcareous, slope former	23.5
10.	Sandstone, light olive gray, weathers grayish orange, fine to medium-grained, calcareous, numerous iron oxide specks, highly cross-bedded, massive, lenticular bodies within unit, ledge former	3.7
9.	Shale, medium gray, weathers light gray, calcareous, interbedded with siltstone and sandstone, light olive gray, weathers grayish orange, very fine- to fine-grained, calcareous, thin-bedded, thin beds of shale, black, carbonaceous were noted; poorly exposed, slope former	4.6
8.	Sandstone, light olive gray, weathers grayish orange, fine-grained, calcareous, abundant iron oxide, cross-bedded, ledge former	.7
7.	Covered slope	1.2
6.	Sandstone, white, weathers white to grayish orange, fine-grained, subrounded to well-rounded, calcareous	.7
5.	Covered slope	1.5
4.	Sandstone, light olive gray, weathers dark yellowish orange, very fine-grained, calcareous, irregular slope former	1.5
3.	Shale, medium dark gray, weathers medium gray, calcareous, very thin bands of carbonaceous shale, coaly fragments, slope former	4.8
2.	Sandstone, medium to light gray, weathered or bleached light gray to white, slope former	.2
1.	Sandstone, light olive gray, weathers grayish orange, highly calcareous, cross-bedded, medium- to thick-bedded, lenticular bodies within unit, interbedded with shale, medium gray, weathers light gray, calcareous, carbonaceous streaks, ledge former	3.7
	Total	147.8

	Measured section No. 2: Section of Blackhawk Formation measured in the SW 1/4 section 12, T. 18 S., R. 6 E	
	Castlegate Sandstone	
	Blackhawk Formation	
53.	Covered slope	13.8
52.	Sandstone, light olive gray, weathers grayish orange, fine to medium-grained, calcareous, massive, cross-bedded, convolute bedding, ledge former	5.4
51.	Covered slope	7.8

Unit		Meters
50.	Sandstone, light olive gray, weathers grayish orange, fine to medium-grained, calcareous, massive, cross-bedded, convolute bedding, ledge former	7.6
49.	Covered slope	22.1
48.	Sandstone, light olive gray, weathers grayish orange, fine to medium-grained, calcareous, massive, cross-bedded, convolute bedding, ledge former	2.1
47.	Shale, medium gray, weathers light gray, calcareous, interbedded in about equal proportion with sandstone, light olive gray, weathers grayish orange, fine-grained, calcareous, thin- to thick-bedded, cross-bedded, wavy bedding, irregular slope former	4.5
46.	Sandstone, light olive gray, weathers grayish orange, fine- to medium-grained, calcareous, massive, cross-bedded, convolute bedding, ledge former	6.7
45.	Shale, medium gray, weathers light gray, calcareous, with some interbeds of siltstone and sandstone, light olive gray, weathers grayish orange, fine-grained, calcareous, thin- to thick-bedded, slope former	13.8
44.	Sandstone, light olive gray, weathers grayish orange, fine to medium-grained, calcareous, massive, cross-bedded, convolute bedding, ledge former	12.2
43.	Shale, medium gray, weathers light gray, calcareous, slope former	7.3
42.	Sandstone, light olive gray, weathers grayish orange, fine to medium-grained, calcareous, massive, cross-bedded, convolute bedding, ledge former	3.6
41.	Shale, medium gray, weathers light gray, calcareous slope former	3.1
40.	Sandstone, light olive gray, weathers grayish orange, fine to medium-grained, calcareous, massive, cross-bedded, convolute bedding, ledge former	6.4
39.	Sandstone light olive gray, weathers grayish orange, fine-grained calcareous, thin to medium-bedded, cross-bedded, interbedded with siltstone, and shale, medium gray, weathers light gray, calcareous, ledge former	3.0
38.	Sandstone, light olive gray, weathers grayish orange, fine to medium-grained, calcareous, massive, cross-bedded, convolute bedding, ledge former	7.6
37.	Shale, medium gray, weathers light gray, calcareous, interbedded with siltstone and sandstone, light olive gray, weathers grayish orange, fine-grained, calcareous, thin to thick-bedded, irregular slope former	19.9
36.	Sandstone, light olive gray, weathers grayish orange, fine-grained, calcareous, thin to medium-bedded, cross-bedded, wavy bedding, intermittant ledge former	1.5
35.	Shale, medium gray, weathers light gray, calcareous, interbedded with siltstone and sandstone, light olive gray, weathers grayish orange, fine-grained, calcareous, thin to medium-bedded, cross-bedded, wavy bedding, irregular slope former	14.9
34.	Sandstone, light olive gray, weathers grayish orange, fine to medium-grained, calcareous, thin- to medium-bedded, cross-bedded, wavy bedding, irregular slope former	7.0
33.	Sandstone, light olive gray, weathers grayish orange, fine-grained calcareous, medium to thick-bedded, interbedded with siltstone, and shale, medium gray, weathers light gray, calcareous, ledge former	8.2
32.	Sandstone, light olive gray, weathers grayish orange, fine to medium-grained, calcareous, massive, cross-bedded, convolute bedding, ledge former	4.6
31.	Shale, medium gray, weathers light gray, calcareous, interbedded with siltstone and sandstone, light olive gray, weathers grayish orange, fine-grained, calcareous, thin to thick-bedded, cross-bedded, wavy bedding, irregular, slope former	34.7
30.	Sandstone, light olive gray, weathers grayish orange, fine to medium-grained, calcareous, massive, cross-bedded, ledge former	1.2
29.	Shale, medium gray, weathers light gray, calcareous, slope former	5.4
28.	Sandstone, light olive gray, fine to medium-grained, calcareous, weathers grayish orange massive, cross-bedded, convolute bedding, ledge former	6.4
27.	Shale, medium gray, weathers light gray, calcareous, slope former	1.1
26.	Coal, mostly vitrain weathered dull, minor resin, minor durain, cleated?	0.7
25.	Shale, black, carbonaceous, fissile	0.1
24.	Shale, medium gray, weathers light gray, calcareous, interbedded with siltstone and sandstone, light olive gray, weathers grayish orange, fine-grained, calcareous, thin to thick-bedded, cross-bedded, wavy bedding, irregular, slope former	11.8
23.	Coal, durain with vitrain bands and vitrain resin, cleated (?)	0.5
22.	Shale, dark gray, carbonaceous, slope former	0.1
21.	Sandstone, light olive gray, weathers grayish orange, fine to medium-grained, calcareous, massive, cross-bedded, convolute bedding, ledge former	4.7
20	Shale, medium gray, carbonaceous; coaly fragments; carbonized plant fossils; fissile	0.1
19.	Shale, light olive gray, weathers grayish orange, slightly silty, calcareous, thin-bedded, wavy bedding, carbonized plant imprints	0.6
18.	Shale, black, highly carbonaceous, fissile	0.6
17.	Sandstone, light olive gray, weathers grayish orange, fine-grained, calcareous, thin to medium-bedded, cross-bedded, wavy bedding, interbedded	

Unit		Meters
	with siltstone, and shale, medium gray, weathers light gray, calcareous, irregular slope former	6.7
16.	Sandstone, light olive gray, weathers grayish orange, fine to medium-grained, calcareous, iron oxide flecks, massive, cross-bedded, convolute bedding, ledge former	6.7
15.	Coal, vitrain weathered dull, resin, cleated?	1.2
14.	Shale, medium gray, weathers light gray, calcareous, with interbedded siltstone and sandstone, light olive gray, weathers grayish orange, fine-grained, calcareous, thin to thick-bedded, cross-bedded, wavy bedding, irregular slope former	15.4
13.	Coal, mostly vitrain weathered dull, resin, cleated?	1.5
12.	Shale, black, carbonaceous, coaly fragments, fissile	0.6
11.	Shale, medium gray, weathers light gray, calcareous, with sandy lenses, slope former	2.8
10.	Sandstone, light olive gray, weathers grayish orange, fine to medium-grained, calcareous, massive, cross-bedded, convolute bedding, ledge former	3.8
9.	Coal, vitrain, weathered dull, resin, cleated? minor splits of shale near top	0.4
8.	Shale, medium to dark gray, calcareous, slope former	0.1
7.	Sandstone, light olive gray, weathers grayish orange, fine-grained, calcareous, thin to medium-bedded, wavy bedding, cross-bedded, ledge former	0.2
6.	Shale, medium gray, weathers light gray, calcareous, slope former	0.9
5.	Sandstone, light olive gray, weathers grayish orange, fine-grained, calcareous, thin to medium-bedded, cross-bedded, wavy bedding, ledge former	1.3
4.	Shale, medium gray, weathers light gray, calcareous, slope former	0.2
3.	Coal, durain and vitrain, resin, cleated?, woody fragments	0.3
2.	Shale, medium gray, weathers light gray, calcareous, slope former	0.9
1.	Star Point Sandstone Not Measured	
	Total	289.3

Measured Section No. 3 Section of Blackhawk Formation measured in the SW 1/4 section 18, T. 18 S., R. 7 E.

Castlegate Sandstone

Blackhawk Formation

Unit		Meters
23.	Shale, medium gray, with light yellow iron oxide staining, calcareous, vitrain bands, coaly fragments	2.1
22.	Shale, medium gray, weathers light gray, calcareous, with interbeds of sandstone, light olive gray, weathers grayish orange, calcareous, slope former	7.6
21.	Sandstone, light olive gray, weathers grayish orange, fine to medium-grained, calcareous, cross-bedded, convolute bedding, massive, ledge former	9.8
20.	Shale, medium gray, weathers light gray, calcareous, interbedded with siltstone and sandstone, light olive gray, weather grayish orange, fine to medium-grained, calcareous, some cross-bedding, sandstones are not continuous and are probably lenticular, slope and irregular slope former	42.6
19.	Sandstone, light olive gray, weathers grayish orange, fine to medium-grained, calcareous, cross-bedded, convolute bedding, massive, ledge former	13.7
18.	Sandstone, light olive gray, weathers grayish orange, fine to medium-grained, calcareous, medium to thick-bedded with up to .3 M thick interbeds of shale, medium gray, calcareous minor coal and shale, black, carbonaceous, ledge former	10.3
17.	Sandstone, light olive gray, weathers grayish orange, fine to medium-grained, calcareous, cross-bedded, convolute bedding, longitudinal ripples on bottom surface of sandstone, ledge symmetrical, wave length about 30 to 45 centimeters, ledge former	21.3
16.	Sandstone, light olive gray, weathers grayish orange, fine-grained, calcareous, thin to medium-bedded, cross-bedded, wavy bedding, interbedded with shale, medium gray, weathers light gray, calcareous, slope former	16.6
15.	Shale, medium gray, weathers light gray, calcareous, slope former	4.6
14.	Sandstone, light olive gray, weathers grayish orange, fine to medium-grained, calcareous, cross-bedded, massive, grades laterally in places to thinner bedded sandstone with shale interbeds, where this occurs the transition happens over a distance of 20 to 40 meters, ledge former	21.2
13.	Sandstone, light olive gray, weathers grayish orange, fine-grained, calcareous, wavy bedding, cross-bedded, interbedded with siltstone, and shale, medium gray, weathers light gray, calcareous, .3 M shale, black, carbonaceous, vitrain bands and inclusions, irregular slope former	7.6
12.	Sandstone, light olive gray, weathers grayish orange, fine to medium-grained, calcareous, bimodal cross-bedding, convolute bedding, ledge former	2.6
11.	Shale, black, carbonaceous, coaly, resin inclusions, fissile	0.3
10.	Shale, medium gray, weathers light gray, calcareous, interbedded with siltstone and sandstone, light olive gray, weathers grayish orange, fine-grained, calcareous, thin to medium-bedded, wavy bedding, cross-bedded, irregular slope former	19.8
9.	Sandstone, light olive gray, weathers grayish orange, fine to medium-grained, calcareous, cross-bedded, thin to thick-bedded, lenticular, with interbeds of siltstone and shale, medium gray, calcareous, irregular slope former	4.3
8.	Sandstone, light olive gray, weathers grayish orange, fine-grained, calcareous, cross-bedded, medium-bedded, ripple marks, minor shale interbeds	3.3
7.	Shale, medium gray, weathers light gray, calcareous, slope former	5.8
6.	Sandstone, light olive gray, weathers grayish orange, fine to medium-grained, calcareous, cross-bedded, convolute bedding, massive becoming thin-bedded at the top, ledge former	8.5

Unit		Meters
5.	Partially covered slope; shale, medium gray, weathers light gray, calcareous, interbedded with siltstone and sandstone, light olive gray, weathers grayish orange, fine-grained, cross-bedded, thin to thick-bedded, .9 M sandstone .9 M above base of unit, .6 M sandstone 4 M above base, .9 M sandstone 8.8 M above base, 1.2 M sandstone 19.8 M above base, irregular slope former	26.0
4.	Coal, vitrain weathered dull, resin, cleated, slope former	1.0
3.	Shale, dusky yellowish brown, carbonaceous, coaly fragments fissile, slope former	0.3
2.	Shale, medium gray, weathers light gray, calcareous, slope former	1.8
1.	Star Point Sandstone, 2 or 3 minor discontinuous coal beds were noted across the wash near the top of the Star Point. Not Measured	
	Total	231.3

Measured section No. 4: Section of the Blackhawk Formation measured in the SW 1/4 section 21, T. 18 S., R. 7 E.

Castlegate Sandstone

Blackhawk Formation

29.	Shale, medium gray, weathers light gray, calcareous, slope former	11.0
28.	Sandstone, light olive gray, weathers grayish orange, fine to medium-grained, calcareous, iron oxide flecks, cross-bedded, convolute bedding, massive, lenticular, intermittent ledge former	3.1
27.	Shale, medium gray, weathers light gray, calcareous, slope former	9.1
26.	Sandstone light olive gray, weathers grayish orange, fine to medium-grained, calcareous, cross-bedded, convolute bedding, thin to thick-bedded, ledge former	9.8
25.	Sandstone, light olive gray, weathers grayish orange, fine-grained, calcareous, cross-bedded, wavy bedding, thin to thick-bedded; interbedded with siltstone, and shale, medium gray, weathers light gray, calcareous, irregular slope former	11.4
24.	Sandstone, light olive gray, weathers grayish orange, fine-grained, calcareous, iron oxide flecks, cross-bedded, convolute bedding, massive to medium-bedded, minor shale interbeds, becomes finer grained and thinner bedded and contains more shale toward top of unit, ledge former	6.7
23.	Shale, medium gray, weathers light gray, calcareous, slope former	16.2
22.	Sandstone, light olive gray, weathers grayish orange, fine to medium-grained, calcareous, iron oxide flecks, cross-bedded, convolute bedding massive, ledge former	14.7
21	Mostly covered slope; shale, medium gray, weathers light gray calcareous, with interbeds of siltstone and sandstone, light olive gray, weathers grayish orange, fine-grained, calcareous, wavy bedding, cross-bedded, thin-to thick-bedded, 2.4 M sandstone, thin-bedded, highly convolute 12.2 M above base of unit, slope former	21.1
20.	Sandstone, light olive gray, weathers grayish orange, fine to medium-grained, calcareous, iron oxide flecks, cross-bedded, convolute bedding, massive, ledge former	7.6
19.	Shale, medium gray, weathers light gray, calcareous; interbedded with siltstone and sandstone, light olive gray, weathers grayish orange, calcareous, wavy bedding, cross-bedded, thin-to thick-bedded, slope former, 1.5 M sandstone, weathers dark moderate red, fine-to medium-grained 6.5 M above base of unit	22.8
18.	Sandstone, light olive gray, weathers grayish orange, fine-to medium-grained, calcareous, highly cross-bedded, thick-bedded to massive, appears lenticular, ledge former	5.5
17.	Sandstone, light olive gray, weathers grayish orange, fine-grained, calcareous, cross-bedded, thin to thick-bedded; interbedded with siltstone, and shale, medium gray, weathers light gray, calcareous, irregular slope former	11.3
16.	Sandstone, light olive gray, weathers grayish orange, fine-grained, calcareous, cross-bedded, highly convolute bedding, thin to thick-bedded, ledge former	3.5
15.	Shale, medium gray, weathers light gray, calcareous; interbedded with siltstone, and sandstone, light olive gray, weathers grayish orange, calcareous, cross-bedded, wavy bedding, thin to thick-bedded, slope former	9.1
14.	Sandstone, light olive gray, weathers grayish orange, fine to medium-grained, calcareous, iron oxide flecks, cross-bedded, convolute bedding, massive, lenticular, ledge former	1.6
13	Shale, medium gray, weathers light gray, calcareous, interbedded with siltstone and sandstone, light olive gray, weathers moderate reddish brown, fine-grained, calcareous, cross-bedded, convolute bedding, thin to thick-bedded, irregular slope former, .3 M sandstone 7.3 M above base of unit, .6 M sandstone 10.5 M above base, .9 M sandstone 15.9 M above base, .5 M sandstone 19.5 M above base, .6 M sandstone 21.2 M above base	25.1
12.	Sandstone, light olive gray, weathers moderate reddish brown to grayish orange, fine-grained, calcareous, cross-bedded, highly convolute bedding, thin to thick-bedded, lenticular, minor shale interbeds, ledge former	2.3
11.	Shale, medium gray, weathers light gray, calcareous slope former	2.3
10.	Sandstone, light olive gray, weathers grayish orange to moderate reddish brown, fine- to medium-grained, calcareous, laminated, cross-bedded, convolute bedding, medium-bedded to massive; minor shale interbeds, base covered and irregular, ledge former	5.5
9.	Shale, medium gray, weathers light gray, calcareous, slope former	3.3
8.	Sandstone, light olive gray, weathers moderate reddish brown, fine-grained, calcareous, wavy bedding, cross-bedded, thin to medium-bedded, with interbeds of shale, medium gray, weathers light gray, calcareous, ledge former	1.5
7.	Shale, medium gray, weathers light gray, calcareous, interbedded with siltstone and sandstone, light olive gray, weathers grayish orange, fine-grained, calcareous, wavy bedding, cross-bedded,	

Unit		Meters
	thin to medium-bedded; and minor shale, black, carbonaceous, fissile, slope former	22.0
6.	Coal, vitrain and durain, weathered dull, minor resin, cleated?	0.3
5.	Sandstone, light olive gray, weathers same, fine to medium-grained, calcareous, wavy bedding, cross-bedded, thin to medium-bedded; with some shale interbeds, irregular ledge former	3.5
4.	Shale, medium gray, weathers light gray, calcareous, slope former	0.2
3.	Shale, black, carbonaceous, vitrain bands, coaly fragments, wood fragments, crumbly, slope former	0.3
2.	Shale, dark to medium gray, weathers light gray, calcareous, slightly carbonaceous, slope former	1.5
1.	Star Point Sandstone. Not Measured	
	Total	232.3

Measured Section No. 5. Section of the Blackhawk Formation measured in the NW 1/4 section 33, T. 18 S., R. 7 E

Castlegate Sandstone, base covered and irregular

Blackhawk Formation

Unit		Meters
36.	Shale, light to medium gray, weathers light gray, calcareous, fissile, slope former	3.7
35.	Sandstone, light olive gray, weathers grayish orange, medium to fine-grained, calcareous, highly cross-bedded, massive, ledge former	1.8
34.	Shale, medium to light gray, weathers light gray, calcareous, slope former	4.9
33.	Sandstone, light olive gray, weathers grayish orange, medium-grained, calcareous, highly cross-bedded, massive, ledge former	4.9
32.	Shale, medium gray, weathers light gray, calcareous, slope former	2.4
31.	Sandstone, light olive gray, weathers grayish orange, fine-to medium-grained, calcareous, cross-bedded, massive to medium-bedded, ledge former	4.6
30.	Covered slope	11.6
29.	Sandstone, light olive gray, weathers grayish orange, fine-grained, convolute bedding, easily eroded, irregular slope former	1.5
28.	Sandstone, light olive gray, weathers grayish orange, fine to medium-grained, calcareous, cross-bedded, massive, ledge former	4.9
27.	Covered slope	10.7
26.	Sandstone, light olive gray, weathers grayish orange, fine to medium-grained, calcareous, highly cross-bedded, base highly irregular and difficult to define, ledge former	6.0
25.	Covered slope	8.6
24.	Sandstone, light olive gray, weathers grayish orange, calcareous, cross-bedded, massive, ledge former	5.1
23.	Sandstone, light olive gray, weathers grayish orange, fine-grained, calcareous, medium-bedded; interbedded with siltstone and shale, medium gray, weathers light gray, calcareous, irregular slope former	8.6
22.	Sandstone, light olive gray, weathers grayish orange, fine to medium-grained, calcareous, highly cross-bedded, convolute bedding, massive, lenticular, channels? ledge former	4.5
21.	Shale, medium gray, weathers light gray, calcareous; interbedded with siltstone and sandstone, weathers grayish orange, fine-grained, calcareous, slope former	4.3
20.	Sandstone, light olive gray, weathers grayish orange, fine-grained, calcareous, cross-bedded, convolute bedding, ledge former	0.7
19.	Coal, vitrain, weathered dull, resin, cleated?	0.1
18.	Shale, medium gray, weathers light gray, calcareous, with interbedded sandstone, weathers grayish orange, fine-grained, calcareous, cross-bedded, medium-bedded, slope former	20.2
17.	Sandstone, light olive gray, weathers grayish orange, fine-grained, calcareous, cross-bedded, medium-bedded; interbedded with siltstone, and shale, medium gray, weathers light gray, calcareous, forms stair-step slope	11.3
16.	Shale, medium gray, weathers light gray, calcareous; interbedded with siltstone and sandstone, weathers grayish orange, fine-grained, calcareous, very poorly exposed and highly weathered, slope former	8.2
15.	Sandstone, light olive gray, weathers grayish orange, fine to medium-grained, calcareous, medium-bedded, ledge former	2.8
14.	Shale, light to medium gray, weathers light gray, calcareous, weathers readily; interbedded with siltstone and sandstone, weathers grayish orange, very fine-grained, poorly exposed, irregular slope former, .1 M coal 15.8 M above base of unit	18.9
13.	Sandstone, light olive gray, weathers grayish orange, fine to medium-grained, calcareous, cross-bedded, convolute bedding, massive ledge former	4.9
12.	Covered slope	9.1
11.	Sandstone, light olive gray, weathers grayish orange, fine to medium-grained, calcareous, cross-bedded, ledge former	4.3
10.	Sandstone, light olive gray, weathers grayish orange, fine-grained, calcareous, thin-bedded; interbedded with shale, siltstone and carbonaceous shale, mostly slope former	8.7
9.	Covered slope	4.3
8.	Sandstone, light olive gray, weathers grayish orange, fine to medium-grained, calcareous cross-bedded, massive to thin-bedded, some interbeds of shale, forms ledges and slope	9.1
7.	Coal, vitrain, weathered dull, resin, cleated? slope former	5.3
6.	Covered slope	7.6
5.	Sandstone, light olive gray, weathers grayish orange, fine-grained, calcareous, small scale cross-bedding, massive- to medium-bedded, ledge former	4.1

Unit		METERS
4	Coal, vitrain?, dulled by weathering, looks almost like durain, zones of high resin content, cleated?	2.0
3.	Siltstone, yellowish brown, shaly, slope former	1.8
2.	Shale, black, carbonaceous, fissile, coaly fragments, slope former	1.2
1.	Star Point Sandstone, Not Measured	
	Total	209.7

Measured Section No. 6: Section of the Blackhawk Formation measured in the NW 1/4 section 4, T. 19S., R. 7 E.

Castlegate Sandstone

Blackhawk Formation

Unit		METERS
62.	Shale, medium gray, weathers light gray calcareous; top .1 M is coal in irregular bands, slope former	7.6
61.	Sandstone, light olive gray, weathers grayish orange, fine to medium-grained, calcareous, massive, cross-bedded, friable, bottom .1 M contains coal, mostly durain, minor resin in stringers and pockets, top .5 M contains secondary gypsum, ledge former	8.0
60.	Covered slope	6.4
59.	Sandstone, light olive gray, weathers grayish orange, medium-grained, calcareous, salt and pepper grains, iron oxide flecks, bimodal cross-bedding, continuous laterally, ledge former	2.0
58.	Shale, medium gray, weathers light gray, calcareous, slope former	.3
57.	Sandstone, light olive gray, weathers grayish orange, fine to medium-grained, calcareous, massive, cross-bedded, convolute bedding, ledge former	8.3
56.	Shale, medium gray, weathers light gray, calcareous; with interbeds of shale, black carbonaceous, slope former	9.1
55.	Sandstone, light olive gray, weathers grayish orange, fine to medium-grained, calcareous, medium to very thick-bedded, very lenticular - the lenses appear almost to be interwoven, cross-bedded, convolute bedding; with very minor shale interbeds, ledge former	5.2
54.	Sandstone, light olive gray, weathers grayish orange, fine-grained, calcareous, thin to thick-bedded, cross-bedded; interbedded with siltstone and shale, medium gray, weathers light gray, calcareous, irregular slope former	2.3
53.	Sandstone, light olive gray, weathers grayish orange, fine to medium-grained, calcareous, cross-bedded, convolute bedding, ledge former	1.5
52.	Covered slope	4.0
51.	Sandstone, light olive gray, weathers grayish orange, fine to medium-grained, calcareous, massive. cross-bedded, convolute bedding, ledge former	4.8
50.	Covered slope	6.4
49.	Sandstone, light olive gray, weathers grayish orange, fine to medium-grained, becomes finer toward the top, calcareous, massive, becomes thinner bedded toward the top, cross-bedded, convolute bedding, ledge former	8.3
48.	Shale, medium gray, weathers light gray, calcareous, slope former	5.0
47.	Sandstone, light olive gray, weathers grayish orange, fine-grained, calcareous, medium to thick-bedded, cross-bedded, ledge former	2.4
46.	Covered slope	14.1
45.	Sandstone, light olive gray, weathers reddish brown to grayish orange, fine to medium-grained, calcareous, iron oxide flecks, medium to thick-bedded, cross-bedded, ledge former	1.0
44.	Covered slope	3.4
43.	Sandstone, light olive gray, weathers grayish orange, fine to medium-grained, calcareous, massive, cross-bedded, convolute bedding, ledge former	6.1
42.	Coal, mostly vitrain, weathered dull, resin, cleated	.1
41.	Shale, dark gray, carbonaceous	.3
40.	Sandstone, light olive gray, weathers grayish orange, fine-grained, calcareous, thin to thick-bedded, cross-bedded, wavy bedding; interbedded with siltstone and shale, medium gray, weathers light gray, calcareous, irregular slope former	7.2
39.	Shale, medium gray, weathers light gray, calcareous, slope former	.8
38.	Sandstone, light olive gray, weathers grayish orange, fine to medium-grained, calcareous, massive, cross-bedded, convolute bedding, ledge former	5.7
37.	Covered slope	4.6
36.	Sandstone, light olive gray, weathers grayish orange, fine to medium-grained, calcareous, cross-bedded, highly lenticular, grades laterally into massive and thicker sandstone to the south, ledge former	1.2
35.	Shale, black, carbonaceous, coaly fragments in pockets	.5
34.	Sandstone, light olive gray, weathers grayish orange, fine-grained, calcareous, thin-bedded, platy; with shale interbeds, irregular slope former	14.8
33.	Shale, medium gray, weathers light gray, calcareous, slope former	1.3
32.	Sandstone, light olive gray, weathers grayish orange, fine to medium-grained, calcareous, cross-bedded, convolute bedding, ledge former; interbedded with .1 M shale, medium gray, weathers light gray, calcareous, 1.1 M above base of unit	1.3
31.	Covered slope	1.9

Unit		Meters
30.	Sandstone, light olive gray, weathers grayish orange, fine-grained, calcareous, thin to medium-bedded, wavy bedding, small scale cross-bedding, ripples, minor convolute bedding; minor shale interbeds. This unit grades laterally into massive sandstone channel that was observed on other side of canyon at same stratigraphic position.	7.6
29.	Shale, medium gray, weathers light gray, calcareous, slope former	1.5
28.	Shale, black, carbonaceous, coaly bands, resin inclusions, fissile, slope former	.2
27.	Coal, mostly vitrian, weathered dull, resin, cleated?	.8
26.	Sandstone, light olive gray, weathers grayish orange, fine-grained, calcareous, thin-bedded, lenticular, ledge former	.6
25.	Shale, medium gray, weathers light gray, calcareous, slope former	.3
24.	Coal, mostly vitrain, resin, cleated?	.4
23.	Shale, dusky yellowish brown, carbonaceous, coaly fragments, fissile, slope former	.1
22.	Shale, medium gray, weathers light gray, calcareous, slope former	1.7
21.	Sandstone, light olive gray, weathers grayish orange, fine-grained, calcareous, thin to thick-bedded, lenses up to .5 M thick at center within thinner bedded strata, all are cross-bedded and have convolute bedding, ripples and ripple drift noted	1.3
20.	Shale, light to medium gray, weathers grayish orange, calcareous, fissile, with thin interbeds of sandstone, slope former	1.2
19.	Shale, black, carbonaceous, fissile, slope former	.4
18.	Sandstone, light olive gray, weathers grayish orange, grades laterally into outcrops weathered medium to dark reddish brown possibly due to burn, very fine to fine-grained, calcareous, thin to medium-bedded, cross-bedded, erodes to platy chips, interbedded with siltstone and shale, medium gray, weathers light gray, calcareous, irregular slope former, 1.2 M sandstone 9.7 M above base of unit, 1.5 M sandstone 13.6 M above base, 2.8 M sandstone 17.7 M above base, .4 M sandstone 22.4 M above base, .1 M sandstone 24.5 M above base.	26.7
17.	Sandstone, weathers dark reddish brown, fine-grained, calcareous, cross-bedded, minor convolute bedding, lenticular, ledge former	.9
16.	Sandstone, very pale orange, weathers grayish orange, becomes weathered dark reddish brown upwards, very fine to fine-grained, calcareous, medium to thick-bedded becoming thinner bedded toward the top, breaks with conchoidal fracture; interbedded limestone, very pale orange, weathers grayish orange, micritic, silty; minor shale interbeds; unit is a ledge former	3.3
15.	Covered slope	1.9
14.	Sandstone, light olive gray, weathers grayish orange, fine to medium-grained, calcareous, massive, cross-bedded, ledge former	3.3
13.	Covered slope	10.7
12.	Sandstone, light olive gray, weathers grayish orange, fine to very fine-grained, calcareous, thin-bedded; interbedded with siltstone and shale, medium gray, weathers light gray, calcareous, slope former	3.7
11.	Shale, medium gray, weathers light gray, calcareous; slope former	1.8
10.	Sandstone, light olive gray, weathers grayish orange, fine-grained, calcareous, thin to medium-bedded, cross-bedded, convolute bedding; minor shale interbeds; ledge former	2.2
9.	Shale, medium gray, weathers light gray, calcareous; slope former	2.2
8.	Shale, dusky yellowish brown to black, carbonaceous, fissile, coaly fragments, slope former	.1
7.	Sandstone, light olive gray, weathers grayish orange, fine to medium-grained, calcareous, thick-bedded; minor shale interbeds; ledge former	1.6
6.	Shale, medium gray, weathers light gray, calcareous, minor sandstone interbeds; slope former	3.1
5.	Sandstone, light olive gray, weathers grayish orange, fine-grained, calcareous, thin-bedded, small scale cross beds, wavy bedding; ledge former	2.5
4.	Sandstone, light olive gray, weathers grayish orange, fine to medium-grained, calcareous, thinner bedded toward the top, cross-bedded, convolute bedding, undulatory lower surface. possibly linguoid ripples; ledge former	1.8
3.	Coal, mostly vitrain, weathers dull, resin, minor durain increasing in top .2 M, cleated?	2.6
2.	Shale, dusky yellowish brown, carbonaceous, woody fragments	.1
1.	Star Point Sandstone, pale yellowish brown, weathers light gray to white, fine to medium-grained, calcareous, massive to medium bedding, ledge former Not Measured	
	Total	239.4

Measured Section No. 7: Section of the Blackhawk Formation measured in the NW 1/4 section 7, T. 19 S., R. 7 E.

Castlegate Sandstone

Blackhawk Formation

93.	Covered slope	4.4
92.	Sandstone, weathers grayish orange to dark yellowish orange to dusky red, fine-grained, calcareous; erodes to platy chips	3.1
91.	Shale, medium gray, weathers light gray, calcareous	3.6
90.	Sandstone, weathers grayish orange to dark yellowish orange to light brown to dusky red, fine-grained, calcareous, erodes to platy chips, laminated	1.6
89.	Shale, medium gray, weathers light gray, calcareous	1.5
88.	Sandstone, light olive gray, weathers grayish orange, fine to medium-grained, calcareous, massive, cross-bedded, convolute bedding, iron oxide flecks	3.0

Unit		Meters
87.	Shale, medium to light gray, weathers light gray, calcareous	1.2
86.	Sandstone, light olive gray, weathers grayish orange, fine to medium-grained, calcareous, massive, cross-bedded, convolute bedding, iron oxide flecks	7.1
85.	Shale, black, carbonaceous, vitrain bands, fissile	0.6
84.	Sandstone, weathers grayish orange to moderate yellowish brown, fine-grained, coarsening slightly upward, calcareous, thin-bedded, erodes into platy chips; less platy toward the top of the unit	2.4
83.	Covered slope	3.1
82.	Sandstone, light olive gray, weathers grayish orange, fine to medium-grained, calcareous, cross-bedded	0.6
81.	Covered slope	1.2
80.	Sandstone, light olive gray, weathers grayish orange, fine-grained, calcareous, thin-bedded; erodes into platy chips that range in color from dark yellowish orange to light brown to dusky red that could be iron staining or burn	0.9
79.	Shale, medium gray, weathers light gray, calcareous	3.3
78.	Sandstone, light olive gray, weathers grayish orange fine to medium-grained, calcareous, massive, crossbedded, convolute bedding	12.2
77.	Shale, medium gray, weathers light gray, calcareous, interbedded with sandstone and siltstone, light olive gray, weathers to a grayish orange, fine-grained, calcareous, thin to thick-bedded, cross-bedded, ripples noted .6 meters above base of unit; also minor shale, black, carbonaceous	6.7
76.	Sandstone, light olive gray, weathers to grayish orange, fine to medium-grained, calcareous, massive, cross-bedded, convolute bedding	8.7
75.	Shale, dusky yellowish brown, carbonaceous, vitrain bands	0.2
74.	Shale, light to medium gray, weathers light gray, slightly silty, calcareous, fossil plant imprints	1.2
73.	Sandstone, light olive gray, weathers grayish orange, fine-grained, calcareous	1.2
72.	Shale, medium gray, weathers light gray, calcareous	2.5
71.	Sandstone, light olive gray, weathers grayisn orange, fine-grained, calcareous, thin-bedded, erodes into thin platy chips.	2.4
70.	Shale, medium gray, weathers light gray, calcareous	2.7
69.	Sandstone, light olive gray, weathers grayish orange, fine to medium-grained, calcareous, massive, cross-bedded, convolute bedding	7.1
68.	Sandstone, light olive gray, weathers grayish orange, fine-grained, thin-bedded, calcareous, erodes to platy fragments; interbeds of shale, medium gray, calcareous	2.7
67.	Covered slope	1.5
66.	Sandstone, light olive gray, weathers grayish orange fine to medium-grained, calcareous, massive, cross-bedded, convolute bedding	3.8
65.	Shale, black, silty, carbonaceous, coaly fragments, vitrain bands	1.2
64.	Sandstone, weathers grayish orange, fine-grained, calcareous, thin-bedded, laminated	0.5
63.	Sandstone, light olive gray, weathers grayish orange, fine to medium-grained, calcareous, cross-bedded, convolute bedding, massive, mostly quartz grains, ledge former	2.9
62.	Sandstone, light olive gray, weathers grayish orange, calcareous, thin-bedded, very fine-grained, breaks into thin platy fragments; with shale, medium gray, calcareous	3.2
61.	Shale, medium gray, weathers light gray; interbedded with siltstone and sandstone, light olive gray, weathers grayish orange, fine-grained, calcareous, thin-to medium-bedded	2.1
60.	Sandstone, light olive gray, weathers grayish orange, fine to medium-grained, calcareous massive, cross-bedded	4.6
59.	Shale, medium gray, weathers light gray, calcareous; interbedded with sandstone, light olive gray, weathers grayish orange, thick-bedded, some cross-bedded, some with silt or clay lamina	10.5
58.	Sandstone, light olive gray, weathers grayish orange, fine to medium-grained, calcareous, cross-bedded	1.4
57.	Covered slope	3.3
56.	Sandstone, light olive gray, fine to medium-grained calcareous; silt or clay lamina	1.6
55.	Siltstone, medium to light gray, weathers pale yellowish orange, calcareous	0.3
54.	Sandstone, light olive gray, weathers grayish orange, medium-grained, calcareous	1.2
53.	Sandstone, light olive gray, weathers grayish orange, fine-grained, calcareous; interbedded with siltstone and shale, medium gray, calcareous	4.6
52.	Sandstone, light olive gray, weathers grayish orange, fine to medium-grained, calcareous, massive, cross-bedded, convolute bedding	11.5
51.	Sandstone, light olive gray, weathers grayish orange, fine to medium-grained, calcareous, cross-bedded, medium to thick-bedded; interbedded with siltstone and shale, medium gray, weathers light gray, calcareous; and a few beds of shale, black, carbonaceous; ledge former	2.5
50.	Shale, black, carbonaceous, vitrain bands, coaly fragment	0.9
49.	Covered slope	1.9
48.	Sandstone, light olive gray, weathers grayish orange, fine to medium-grained, calcareous, cross-bedded	1.5
47.	Covered slope	1.9
46.	Shale, black, carbonaceous, vitrain bands, coaly fragments	1.1
45.	Shale, dark gray to black, carbonaceous	1.2
44.	Sandstone, light olive gray, weathers grayish orange, medium-grained, calcareous	1.5

Unit		Meters
43.	Shale, medium gray, weathers light gray, calcareous	0.6
42.	Shale, black, carbonaceous, fissile, crumbly	1.2
41.	Sandstone, light olive gray, weathers grayish orange, fine to medium-grained, calcareous, massive, cross-bedded; with some shale interbeds	8.3
40.	Sandstone, light olive gray, weathers grayish orange, fine to medium-grained, calcareous, thin- to thick-to massive-bedded; interbedded with siltstone, and shale, medium gray, calcareous; and shale, black to dark brown, carbonaceous, fissile	6.7
39.	Shale, dark brown, carbonaceous, woody fragments, crumbly	0.6
38.	Sandstone, light olive gray, weathers grayish orange, fine-grained, calcareous	1.5
37.	Shale, medium gray, weathers light gray, calcareous, slope former	2.7
36.	Sandstone, weathers dark yellowish brown, fine-grained, calcareous	0.3
35.	Coal, vitrain and durain, resin, cleated?	1.0
34.	Sandstone, light olive gray, weathers grayish orange, fine to medium-grained, calcareous, cross-bedded; interbeds of shale, medium gray, weathers light gray, calcareous	2.2
33.	Shale, medium gray, weathers light gray, calcareous, fissile; interbedded with siltstone and sandstone, light olive gray, weathers grayish orange, fine- grained, calcareous; and shale, black, carbonaceous	1.6
32.	Coal, durain and clarain, resin, cleated?	0.4
31.	Shale, medium gray, weathers light gray, calcareous	0.6
30.	Shale, black, carbonaceous, very fissile, coaly fragments, plant fossils and woody fragments	0.5
29.	Shale, medium gray, weathers light gray, calcareous	3.2
28.	Sandstone, light olive gray, weathers grayish orange, fine to medium-grained, calcareous	1.8
27.	Shale, medium gray, weathers light gray, calcareous; interbedded with siltstone and sandstone, light olive gray, weathers grayish orange, fine-grained, calcareous; and shale, dark gray to black, carbonaceous	3.7
26.	Sandstone, light olive gray, weathers grayish orange, fine-grained, calcareous, thin to medium-bedded	2.6
25.	Shale, dusky yellowish brown, carbonaceous, fissile, vitrain bands	0.1
24.	Sandstone, light olive gray, weathers pale yellowish orange, fine-grained, calcareous, friable, with thin, black, carbonaceous shale and medium gray, calcareous shale interbeds	1.2
23.	Shale, medium gray, weathers light gray, calcareous, interbedded with siltstone and sandstone, light olive gray, weathers grayish orange, fine-grained, calcareous	1.8
22.	Shale, black, carbonaceous	0.4
21.	Sandstone, light olive gray, weathers grayish orange, fine to medium-grained, calcareous, cross-bedded, thin to medium beds	4.1
20.	Shale, medium gray, weathers light gray, calcareous; with some interbeds of siltstone and sandstone, light olive gray, weathers grayish orange, fine- grained, calcareous; and shale, black carbonaceous	6.4
19.	Shale, black, carbonaceous	0.3
18.	Covered slope -	1.9
17.	Sandstone, weathers yellowish brown, fine-grained, calcareous	0.6
16.	Shale, medium gray, weathers light gray, calcareous, interbedded with sandstone and siltstone, light olive gray, weathers grayish orange, fine-grained, calcareous; and shale, black, carbonaceous	3.3
15.	Shale, black, carbonaceous, very fissile, coaly fragments, abundant plant and woody fragments	0.5
14.	Covered slope	4.1
13.	Shale, black, carbonaceous, fissile, coaly fragments	0.3
12.	Covered slope	0.9
11.	Sandstone, yellowish brown, weathers grayish orange, very fine-grained, calcareous, well-cemented	2.4
10.	Shale, black, carbonaceous, fissile, coaly fragments	0.7
9.	Shale, medium gray, weathers light gray, calcareous	0.3
8.	Sandstone, light olive gray, weathers grayish orange, fine to medium-grained, calcareous, cross-bedded	0.9
7.	Sandstone, light olive gray, weathers grayish orange, fine-grained, calcareous; interbedded with siltstone and shale, medium gray, weathers light gray, calcareous, fissile	6.4
6.	Shale, medium gray, weathers light gray, calcareous; interbedded with siltstone and sandstone, light olive gray, weathers grayish orange, fine-grained, calcareous, thin to medium-bedded	2.4
5.	Sandstone, light olive gray, weathers grayish orange; fine to medium-grained, calcareous; interbedded with shale, medium gray, calcareous, fissile; overall thin-bedded	4.1
4.	Sandstone, pale yellowish brown, weathers reddish brown, fine-grained, calcareous, thin-bedded	0.5
3.	Covered slope -	
2.	Coal, mostly vitrain, weathered dull, resin, cleated?	2.8
1.	Star Point Sandstone - Not Measured	
	Total	237.7

Measured Section No. 8. Section of the Blackhawk Formation measured in the NE 1/4 section 12, T. 19 S., R. 6 E.

Castlegate Sandstone

Blackhawk Formation

37.	Covered slope	3.8
36.	Sandstone, light olive gray, weathers grayish orange, fine to medium-grained, calcareous, massive, cross-bedded, convolute bedding; ledge former	4.6

Unit		Meters
35.	Sandstone, light olive gray, weathers grayish orange, fine-grained, calcareous, thin to thick-bedded, cross-bedded, wavy bedding; interbedded with siltstone and shale, medium gray, weathers light gray, calcareous; irregular slope former	3.1
34.	Sandstone, light olive gray, weathers grayish orange, fine to medium-grained, calcareous, massive, cross-bedded, convolute bedding; ledge former	7.9
33.	Sandstone, light olive gray, weathers grayish orange, fine-grained, calcareous, thin to medium-bedded, cross-bedded, convolute bedding, wavy bedding; minor shale interbeds; grades laterally into massive sandstone; ledge former	4.5
32.	Covered slope	4.3
31.	Sandstone, light olive gray, weathers grayish orange, fine to medium-grained, calcareous, massive, bimodal cross-bedding up to about 1 M across with some as much as 2 M; some look almost festoon; ledge former	8.0
30.	Shale, medium gray, weathers light gray, calcareous; with interbedded siltstone and sandstone, light olive gray, weathers grayish orange, fine-grained, calcareous, thin to thick-bedded, wavy bedding, cross-bedding, slope former	6.8
29.	Sandstone, light olive gray, weathers grayish orange, fine to medium-grained, calcareous, lenticular, cross-bedded, convolute bedding; ledge former	2.1
28.	Shale, medium gray, weathers light gray, calcareous; slope former	3.4
27.	Sandstone, light olive gray, weathers grayish orange, fine to medium-grained, calcareous, massive, cross-bedded, convolute bedding; ledge former	6.4
26.	Sandstone, light olive gray, weathers grayish orange, fine to medium-grained, calcareous, thin-bedded to massive, highly lenticular, (channelled?); interbedded with siltstone, and shale, medium gray, weathers light gray, calcareous; thin shale, black, carbonaceous, 1.2 M above base; irregular slope former	8.2
25.	Sandstone, light olive gray, weathers grayish orange, fine to medium-grained, calcareous, massive, cross-bedded, ripple marks on lower surface, convolute bedding; ledge former	8.0
24.	Shale, dark gray, weathers medium gray, carbonaceous, calcareous, carbonized plant fragments and fossils, woody fragments, fissile	0.9
23.	Shale, medium gray, weathers light gray, calcareous; with interbedded sandstone, light olive gray, weathers grayish orange, fine-grained, calcareous, thin to thick-bedded, cross-bedding, wavy bedding; slope former	12.2
22.	Sandstone, light olive gray, weathers grayish orange, fine to medium-grained, calcareous, cross-bedded, convolute bedding; ledge former	2.1
21.	Shale, medium gray, weathers light gray, calcareous; with interbeds of siltstone and sandstone, light olive gray, weathers grayish orange, fine-grained, calcareous, thin to thick-bedded, cross-bedded, wavy bedding; slope former	1.6
20.	Sandstone, light olive gray, weathers grayish orange, fine to medium-grained, calcareous, cross-bedded, convolute bedding; ledge former	1.4
19.	Shale, medium gray, weathers light gray, calcareous; slope former	13.2
18.	Sandstone, light olive gray, weathers grayish orange, fine to medium-grained, calcareous, massive, bimodal cross-bedding, convolute bedding; ledge former	5.4
17.	Shale, medium gray, weathers light gray, calcareous; with interbedded sandstone, light olive gray, weathers grayish orange, fine to medium-grained, calcareous, thin to thick-bedded, cross-bedded, wavy bedding; about 50 percent of each lithology; irregular slope former	9.8
16.	Sandstone, light olive gray, weathers grayish orange, fine to medium-grained, calcareous, massive, cross-bedded, convolute bedding; ledge former	5.5
15.	Covered slope	3.0
14.	Sandstone, light olive gray, weathers grayish orange, fine to medium-grained, calcareous, massive, cross-bedded, convolute bedding, 3M shale lens about 1.6M above base of unit; ledge former	6.1
13.	Covered slope	13.1
12.	Sandstone, light olive gray, weathers grayish orange, fine to medium-grained, becomes finer grained toward the top, calcareous, massive, becomes thinner bedded toward the top, cross-bedded, convolute bedding; ledge former	10.4
11.	Sandstone, light olive gray, weathers grayish orange, fine-grained, calcareous, thin to thick-bedded, cross-bedded, wavy bedding; interbedded with siltstone and shale, medium gray, weathers light gray, calcareous; irregular slope former	16.5
10.	Sandstone, light olive gray, weathers grayish orange, fine to medium-grained, calcareous, massive, cross-bedded, convolute bedding, .3 M shale 10.9 M above base of unit, .6 M sandstone lens 10.6 M above base, .6 M shale 10.3 M above base; ledge former	21.3
9.	Shale, black, carbonaceous, vitrain bands, resin inclusions, fissile	0.3
8.	Sandstone, light olive gray, weathers grayish orange, very fine-grained, calcareous, thin to medium-bedded, carbonized plant fossils; ledge former	0.9
7.	Shale, medium gray, weathers light gray, calcareous; with interbedded sandstone, light olive gray, weathers grayish orange, fine-grained, calcareous, thin to thick-bedded, cross-bedded, 1.4 M sandstone 9.2 M above base, 1.2 M shale, black, carbonaceous, woody fragments 11.9 M above base, .5 M sandstone 13.4 M above base; slope former	14.9
6.	Sandstone, light olive gray, weathers grayish orange, fine to medium-grained, calcareous, massive, cross-bedded, convolute bedding; minor shale interbeds; ledge former	6.4
5.	Shale, medium gray, weathers light gray, calcareous; with interbedded sandstone, light olive gray, weathers grayish orange, fine to medium-grained, calcareous, thin to thick-bedded, cross-bedded, wavy bedding, convolute bedding; slope is partially covered, but across wash near stream bed is about 3 to 4 M coal with a .6 M split with the top about 11 M above the base of this unit; irregular slope former	14.4

Unit		Meters
4.	Sandstone, light olive gray, weathers grayish orange, fine to medium-grained, calcareous, minor iron oxide, thin to thick-bedded, thin shale interbeds, cross-bedded, wavy bedding, convolute bedding; intermittant ledge former	4.5
3.	Sandstone, light olive gray, weathers grayish orange, fine to medium-grained, calcareous, massive, cross-bedded, convolute bedding; some shale interbeds; ledge former	15.3
2.	Covered; at least 1.5 M coal, vitrain, weathers dull, resin, cleated?; with too much rubble to determine how much more there is: the rest is probably shale, medium gray, weathers light gray, calcareous; slope former	7.6
1.	Star Point Sandstone - Not Measured	
	Total	257.9

The largest block of coal ever mined in Utah, from the Hiawatha Mine near Price, Carbon County, Utah. It was brought to the State Capitol Building about 1920, where for about 40 years it was on display in the basement (insert photo). At present it is stashed in a parking lot, protected by a tarpaulin. United States Fuel Company photos.

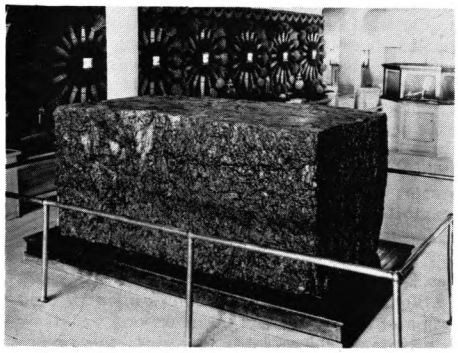

EARTHQUAKE EPICENTERS IN UTAH JANUARY - JUNE 1977

by Kenneth L. Cook[1]

EARTHQUAKES

Earthquake epicenters in and near Utah for January through June 1977, with dates of occurrences and approximate Richter magnitudes, are listed below. Known blasts have been excluded from the list of seismic events, but to discriminate man-made events from real earthquakes is often problematical; and a few events included in the list may in fact be artificial. All times are Coordinated Universal Time (UTC, same as Greenwich Mean Time, GMT), which is seven hours later than Mountain Standard Time (MST, in effect from 2:00 a.m. on October 31, 1976, MDT, until 2:00 am April 24, 1977, MST) and six hours later than Mountain Daylight Time (MDT, in effect from 2:00 a.m. on April 24, 1977, MST, until 2:00 a.m. on October 30, 1977, MDT). Therefore, some UTC dates are one day later than MST or MDT dates. All locations and magnitudes are preliminary determinations. Unless otherwise indicated, localities are in Utah. The final locations and magnitudes will be printed in the University of Utah Seismological Bulletins.

During the period January 1, 1977 through June 30, 1977, thirty-two high-gain telemetered stations (supported chiefly by the U.S. Geological Survey and the National Science Foundation) were operational along the Wasatch Front in addition to the permanent Utah seismograph network. Telemetered stations on the northern part of Stansbury Island (NSU), in Hansel Valley (HVU), and near Portage (PTU) first became operative during October 1976, November 1976, and December 1976, respectively.

Throughout the report period for southern Utah, seismic signals were received at the permanent seismograph station at Cedar City (CCU) and the telemetered stations at Marysvale (MSU, operative since October 1975), Kanab, Utah (KNB), and Glen Canyon, Arizona (GCA). Telemetered signals from KNB and GCA, which are operated by the U.S. Geological Survey, were first received at the University of Utah during November 1976. Also, in south-central and southern Utah during early 1977, the following new high-gain telemetered stations became first operative: 1) Piute Reservoir (PUU), during January 1977; 2) Richfield (RFU), during January 1977; 3) Roosevelt Hot Springs (RHU), during January 1977; 4) Milford North (MNU), during January 1977; and 5) Cove Fort (CFU), during March 1977.

Earthquake locations on a state-wide basis are only complete above approximately magnitude 2.5. A greater density of stations in north-central Utah, compared to other parts of the state, accounts for the recording and location of a greater number of small-magnitude eathquakes in that area. During the first half of 1977, a relative increase in the number of events in south-central and southern Utah is explained principally by the expansion of the University of Utah seismic network in these areas.

During the report period, earthquake activity continued to be prominent in areas adjacent to the aftershock zone of the March 1975 Pocatello Valley (Idaho-Utah border) earthquake. These include areas in Utah to the southwest (northern Hansel Valley and North Promontory Mountains), south (Blue Creek Valley), and southeast (Blue Springs Hills and West Hills). During the report period, the largest earthquake in these areas was in the north end of Blue Springs Hills (magnitude 2.4), and the largest earthquake in the adjacent Pocatello Valley area (in Idaho) was magnitude 2.3. Also, earthquake activity continued to be prominent in the Cove Fort-Sulphurdale area, and minor earthquake activity occurred repeatedly in the Levan-Mills, Marysvale, and Beaver-Manderfield areas. Some of the seismic events observed west of Cedar City may be caused by blasting in the iron mines there. There was an increase of both the number and magnitude of seismic events in the Huntington-Orangeville coal-mining area, and the largest seismic event (M = 3.2) during the report period was felt in that area.

January		Magnitude
1.	North end of Blue Springs Hills (about 10 km northeast of Blue Creek and 13 km west-southwest of Washakie and 5 km north of east-west road)	<1.0
3.	Bear River Range (4 km south of Blacksmith Fork and 12 km east-northeast of Paradise)	1.4
4.	Bear River Range (5 km east-southeast of Logan)	<1.0
4.	4 km south of Porterville	1.3
7.	Great Salt Lake (10 km east-southeast of Lakeside and 2 km south of Southern Pacific Railroad causeway)	1.2
8.	San Rafael Swell (31 km east-southeast of Emery and 3 km north of Interstate highway 70 and 8 km north-northwest of The San Rafael Knob)	1.5
9.	West margin of Hansel Valley (18 km south of Snowville)	<1.0
9.	North end of Blue Springs Hills (same location as event on January 1)	1.8
9.	Ditto--a second event	1.1
10.	Ditto	<1.0
10.	Blue Springs Hills (on east-west road, 6 km east of Blue Creek)	<1.0
10.	Great Salt Lake (18 km southwest of Cedar Springs and 15 km northwest of the south end of the road at Rozel Point).	<1.0
10.	9 km south of Nephi	1.2
10.	4 km southeast of Flux [2] [3]	<1.0
11.	8 km south of Nephi	1.4
11.	14 km north-northeast of Burrville and 9 km north of the north end of Koosharem Reservoir and 3 km northeast of Utah highway 24	1.7
11.	11 km west-northwest of Huntington[2]	1.5
12.	3 km northwest of Trenton	<1.0
12.	North end of Blue Springs Hills (same location as event on January 1)	<1.0
14.	West margin of Hansel Mountains (11 km northeast of Locomotive Springs and 22 km south-southwest of Snowville and 2 km east of Locomotive Springs-Snowville road)	<1.0

[1] Professor of Geophysics, Department of Geology and Geophysics, University of Utah, and Former Director, University of Utah Seismograph Stations, Salt Lake City, Utah 84112.

[2] Possible mine or quarry blast.

[3] Flux is 12 km southeast of Timpie and 11 km northwest of Grantsville. Timpie is also designated Rowley Junction on some maps of Utah

Magnitude

14. North end of Blue Springs Hills (same location as event on January 1) ..... <1.0
15. Lakeside Mountains[2] (12 km northeast of Low and 8 km east of north-south Low-Lakeside road) 1.3
16. 5 km east of North Ogden ..... <1.0
17. North Promontory Mountains (15 km east of Snowville and 4-5 km south of Utah-Idaho border) ..... <1.0
18. 1 km northeast of Huntsville 2.2
18. 5 km east of Sulphurdale 1.7
19. 16 km west of Price and 6 km north-northeast of Wattis[2] 1.3
19. 2 km northwest of Orangeville[2] 1.2
19. 12 km west of Huntington[2] 1.3
20. 13 km west-northwest of Huntington[2] 2.2
21. North end of Blue Springs Hills (same location as event on January 1) ..... <1.0
21. Ditto--a second event ..... <1.0
21. 12 km south-southeast of Levan and 17 km east-southeast of Mills 1.3
22. 1 km northwest of Roy 1.5
22. 3 km northeast of Henefer 1.0
22. 11 km west-southwest of Huntington and 10 km north-northwest of Orangeville[2] 2.1
23. Bear River Range (12 km southeast of Logan) 1.1
23. North end of Blue Springs Hills (same location as event on January 1) ..... <1.0
23. Ditto--a second event ..... <1.0
24. 5 km west of Fayette 1.3
24. 8 km south-southwest of Levan and 11 km east of Mills 2.1
24. 7 km southwest of Levan 1.6
24. 11 km southwest of Levan and 8 km east-southeast of Mills 1.1
24. 8 km south-southwest of Levan and 11 km east of Mills 1.7
24. 6 km southwest of Levan 1.5
24. West margin of Hansel Valley (18 km south of Snowville) ..... <1.0
24. 7 km southwest of Manti and 4 km northwest of Sterling 1.5
25. 9 km southwest of Levan 1.3
25. 8 km southwest of Levan and 9 km east of Mills 2.5
25. 9 km north-northeast of Beaver and 4 km east-southeast of Manderfield ..... <1.0
25. 1 km west of Beaver ..... <1.0
25. 3 km east-northeast of Beaver ..... <1.0
25. 3 km west-northwest of Lakeside[2] ..... <1.0
25. North end of Hansel Valley (11 km west-northwest of Blue Creek) ..... <1.0
25. 9 km northwest of Junction ..... <1.0
25. 8 km north-northwest of Junction ... <1.0
25. 10 km east-southeast of Sulphurdale 1.4
25. 5 km north of Orangeville[2] 1.4
26. North Promontory Mountains (15 km east of Snowville) ..... <1.0
26. 3 km southwest of Flux[2] 1.1
26. North Promontory Mountains (13 km east of Snowville and 4-5 km south of Utah-Idaho border) ..... <1.0

Magnitude

26. Ditto-- a second event ..... <1.0
26. Ditto--a third event ..... <1.0
26. Ditto--a fourth event ..... <1.0
26. Ditto--a fifth event ..... <1.0
27. 5 km north-northeast of Manti 1.6
27. North Promontory Mountains (13 km east of Snowville and 4-5 km south of Utah-Idaho border) ..... <1.0
27. North end of Hansel Valley (on U.S. highway 30S, 10 km northwest of Blue Creek and 14 km southeast of Snowville) 1.1
27. North Promontory Mountains (6 km northwest of Blue Creek and 1 km south of U.S. highway 30S) . 1.7
27. North Promontory Mountains (13 km east of Snowville and 4-5 km south of Utah-Idaho border) . <1.0
27. Ditto--a second event 2.1
27. North end of Hansel Valley (1 km south of U.S. highway 30S and 10 km northwest of Blue Creek and 14 km southeast of Snowville) 1.0
27. North Promontory Mountains (13 km east of Snowville and 4-5 km south of Utah-Idaho border) ..... <1.0
27. Ditto--a second event ..... <1.0
27. Ditto-a third event ..... <1.0
27. Ditto-a fourth event ..... <1.0
27. 2 km west of Lakeside[2] ..... <1.0
27. North Promontory Mountains (13 km east of Snowville and 4-5 km south of Utah-Idaho border) 1.2
27. Ditto--a second event 1.1
27. Ditto--a third event 1.1
27. Ditto--a fourth event 1.0
27. Ditto--a fifth event ..... <1.0
28. Ditto ..... <1.0
28. 7 km east of Huntsville 1.8
28. North Promontory Mountains (13 km east of Snowville and 4-5 km south of Utah-Idaho border) 1.2
28. Ditto--a second event ..... <1.0
28. 9 km west of Snowville and 2 km south of Utah-Idaho border ..... <1.0
28. 9 km east-southeast of Sulphurdale 1.6
29. North Promontory Mountains (same location as event on January 28) 1.0
29. 5 km north of Orangeville[2] 2.1
29. North Promontory Mountains (same location as event on January 28) .... <1.0
30. Northwest margin of Hansel Valley (17 km south of Snowville) 1.1
30. North end of Blue Springs Hills (same location as event on January 1) ..... <1.0
30. 2 km northeast of Porterville ..... <1.0
30. Blue Springs Hills (9 km east of Howell and 2 km south of U.S. highway 30S) 2.2
31. Bear River Range (3 km north of Blacksmith Fork and 4 km southeast of Nibley) ..... <1.0
31. Bear River Range (4 km south of Blacksmith Fork and 12 km east-northeast of Paradise) 1.2

Magnitude

31. Bear River Range (2 km south of Blacksmith Fork and 12 km east-northeast of Paradise) ..... <1.0
31. 8 km west-northwest of Huntington[2] 1.6

February Magnitude

1. Blue Springs Hills (8 km east-southeast of Howell and 4 km south of U.S. highway 30S) ... <1.0
2. Blue Springs Hills (1 km north of the east-west road and 9 km east-northeast of Blue Creek) ..... <1.0
2. 14 km west of Huntington[2] 1.2
3. North end of Blue Springs Hills (same location as event on January 1). Felt in Blue Creek and Portage. (15:26 UTC) 2.4
3. North Promontory Mountains (same location as event on January 28) ..... <1.0
3. North end of Blue Springs Hills (same location as event on January 1) ..... <1.0
3. Ditto--a second event ..... <1.0
3. Ditto--a third event 1.5
3. Ditto--a fourth event ..... <1.0
4. Ditto ..... <1.0
4. South end of Pocatello Valley (about 4 km south of Utah-Idaho border) ..... <1.0
4. North Promontory Mountains (same location as event on January 28) ..... <1.0
4. 4 km west-southwest of Flux[2] ..... <1.0
4. North Promontory Mountains (same location as event on January 28) 1.7
4. 10 km east of Cove Fort 1.5
5. Circleville Mountain (16 km southeast of Beaver and 20 km west-northwest of Circleville) ..... <1.0
5. North Promontory Mountains (same location as event on January 28) ..... <1.0
5. Ditto--a second event ..... <1.0
5. Bear River Range (12 km southeast of Logan) 1.5
5. North end of Hansel Valley (16 km east of Snowville and 5 km south of Utah-Idaho border) ..... <1.0
5. North end of Blue Springs Hills (same location as event on January 1) 1.3
5. 3 km south of Draper 1.7
6. 4 km northwest of Orangeville[2] 1.3
6. North end of Blue Springs Hills (same location as event on January 1) ..... <1.0

Magnitude

6. Utah highway 83 (6 km southwest of Penrose) ....<1.0
6. North end of Blue Springs Hills (same location as event on January 1) ....<1.0
7. North end of Hansel Valley (1 km south of U.S. highway 30S and 10 km northwest of Blue Creek and 14 km southeast of Snowville) ..<1.0
7. North end of Blue Springs Hills (same location as event on January 1) ....<1.0
7. North Bay of Bear River Bay (13 km west-southwest of Corinne) ... 1.6
8. 11 km south-southeast of Levan and 17 km east-southeast of Mills 1.6
8. North end of Blue Springs Hills (same location as event on January 1) 1.6
8. Ditto--a second event ....<1.0
8. North Promontory Mountains (same location as event on January 28) ....<1.0
8. Ditto--a second event ....<1.0
8. Ditto--a third event ....<1.0
8. Bear River Range (5 km east of Millville) ....<1.0
8. North Promontory Mountains (same location as event on January 28) ....<1.0
8. Crest of Traverse Mountains (7 km south-southeast of Draper and 8 km east-southeast of Bluffdale) 1.8
9. 13 km west-southwest of Huntington and 8 km northwest of Orangeville. Felt in American Coal Company Beehive mines (located 12 km northwest of Orangeville) and in Castle Dale, Cleveland, and Elmo. (00:42 UTC).... 3.2
9. North end of Blue Springs Hills (same location as event on January 1) ....<1.0
10. 10 km south-southeast of Porterville and 4 km west of East Canyon Reservoir ....<1.0
10. 11 km east of Cove Fort 1.8
11. 1 km west of Sulphurdale ....<1.0
12. Northeast margin of Little Mountain (9 km west of Bear River City) ....<1.0
12. North Promontory Mountains (12 km east of Snowville) ....<1.0
12. West Hills (8 km northwest of Riverside and 8 km southwest of Plymouth) ....<1.0
12. North end of Blue Springs Hills (same location as event on January 1) ....<1.0
13. Northeast margin of Little Mountain (9 km west of Bear River City) 1.1
13. West margin of Hansel Mountains (13 km northeast of Locomotive Springs and 21 km south-southwest of Snowville and 3 km east of Locomotive Springs – Snowville road) . 1.0
13. North end of Hansel Valley (10 km east-southeast of Snowville) ....<1.0

Magnitude

15. West edge of Bear Lake (1 km south of Pickleville) ....<1.0
15. 4 km south-southwest of Porterville 1.8
15. 13 km west-southwest of Huntington and 9 km northwest of Orangeville[2] .. 1.0
15. North Promontory Mountains (same location as event on January 28) ....<1.0
15. Blue Springs Hills (5 km northeast of Blue Creek and 1 km north of the east-west road) ....<1.0
16. North end of Blue Creek Valley (9 km north of Blue Creek and 6 km south of Utah-Idaho border) ...<1.0
16. North end of Blue Springs Hills (same location as event on January 1) ....<1.0
16. Ditto--a second event ....<1.0
16. Ditto--a third event ....<1.0
16. Ditto--a fourth event ....<1.0
16. 13 km east of Sulphurdale 1.5
17. 30 km south-southwest of Kelton and 18 km west of north-south road along east margin of Hogup Mountain ....<1.0
17. 11 km southeast of Beaver 1.1
17. 13 km east-southeast of Sulphurdale ....<1.0
17. 8 km northwest of Long Valley Junction 1.2
18. 8 km west of Pickleville ....<1.0
18. Crest of Stansbury Mountains (5 km west-southwest of Dolomite[4] and 8 km south-southeast of Timpie[2] ...<1.0
18. 8 km east-southeast of Cove Fort and 8 km east-northeast of Sulphurdale 1.7
19. 9 km northwest of Long Valley Junction 2.0
21. 10 km west-southwest of Spry 1.3
21. 11 km east of Beaver 2.0
22. 10 km east of Beaver 1.4
22. 11 km east-northeast of Beaver ....<1.0
22. North end of Blue Springs Hills (same location as event on January 1) 1.0
22. 10 km northeast of Cove Fort 1.3
23. 8 km north-northeast of Cove Fort ..<1.0
23. North end of Blue Springs Hills (same location as event on January 1) ....<1.0
23. Ditto--a second event ....<1.0
23. 12 km northeast of Scipio 1.7
23. 5 km south-southeast of Levan 1.8
24. 12 km west-southwest of Huntington[2] 1.2
24. 10 km north of Mill Fork 1.3
25. 9 km east-northeast of Cove Fort 1.8
27. 5 km north of Orangeville[2] 1.8
27. 2 km northwest of Sulphurdale 1.2
28. Lakeside Mountains (11 km northeast of Low and 6 km east of north-south Low-Lakeside road)[2] ...<1.0

[4] Dolomite is 8 km southeast of Timpie.

March

Magnitude

2. West margin of Stansbury Mountains (5 km south of Timpie and 1 km east of north-south Timpie-Iosepa road ....<1.0
2. 6 km east of Beaver and 2 km south of Utah highway 153 ....<1.0
2. 1 km east of Lakeside[2] ....<1.0
3. North Hansel Valley–area A (13 km southeast of Snowville and 3 km southwest of the intersection of the north-south Hansel Valley road and U.S. highway 30S) 1.1
3. Ditto--a second event ....<1.0
3. Ditto--a third event ....<1.0
3. North Hansel Valley–area B (14 km southeast of Snowville and 4 km southwest of the intersection of north-south Hansel Valley road and U.S. highway 30S) ... 1.1
3. North Hansel Valley–area A (same location as event in area A on March 3) ....<1.0
3. North Hansel Valley–area B (same location as event in area B on March 3) 1.2
4. 11 km east of Cove Fort 1.4
5. 9 km northeast of Cove Fort ....<1.0
5. North Hansel Valley–area A (same location as event in area A on March 3) ....<1.0
5. West branch of Logan River (16 km west of Garden City and 5 km south of Utah-Idaho border) ....<1.0
5. Cotton wood Creek (21 km west-northwest of Orangeville)[2] 2.5
6. East margin of Hansel Valley (12 km north-northeast of Cedar Springs) ....<1.0
8. 11 km east-northeast of Scipio and 12 km northwest of Fayette 1.6
8. 8 km east-southeast of Sulphurdale 1.9
8. 4 km southeast of Mount Pleasant 1.6
9. 12 km north-northwest of Devils Slide and 14 km north-northeast of Morgan 2.1
9. Tushar Mountains (8 km north-northwest of Signal Peak and 13 km east-southeast of Sulphurdale) ....<1.0
9. East margin of Stansbury Mountains (8 km northwest of Grantsville and 5 km south of Flux) ....<1.0
11. 10 km east of Cove Fort 1.5
11. 11 km south of Grantsville and 1 km east of St. John-Grantsville north-south road 1.1
11. Skull Valley (16 km north of Dugway and 1 km west of main north-south Dugway-Timpie road) ....<1.0
11. South end of Tooele Valley (9 km south of Grantsville and 2 km east of the St. John-Grantsville north-south road) 1.2
13. 8 km east of Blue Creek ....<1.0
14. 6 km east of Venice 1.3
15. North Stansbury Mountains

Magnitude

(3 km southwest of Flux)[2] 1.1
15. Beaver River (10 km east-southeast of Beaver) .....<1.0
15. South end of Pocatello Valley (16 km east of Snowville and 2 km south of Utah-Idaho border) 1.1
15. South end of Pocatello Valley (18 km east of Snowville and 2 km south of Utah-Idaho border) 1.7
15. 4 km south of Heber City .....<1.0
17. Hansel Valley (15 km north of Cedar Springs) 1.0
17. Ditto--a second event .....<1.0
17. 5 km north of Orangeville and 10 km southwest of Huntington[2] 2.2
17. 11 km east of Cove Fort 1.7
18. 8 km west of Royal[2] 2.6
18. 12 km west-southwest of Pickleville .....<1.0
19. 4 km north of Cottonwood Creek and 13 km northwest of Orangeville and 18 km west-southwest of Huntington[2] 1.8
20. North Promontory Mountains (13 km east of Snowville) .....<1.0
21. 9 km east of Sulphurdale 2.0
23. Blue Springs Hills (10 km northeast of Howell and 4 km north of U.S. highway 30S) .....<1.0
23. On U.S. highway 91 (4 km south-southwest of Sulphurdale) .....<1.0
24. Northern Blue Springs Hills (10 km northeast of Blue Creek) 1.2
24. Fremont Wash area (20 km south-southwest of Beaver and 2 km west of U.S. highway 91) ... 1.4
24. Blue Springs Hills (10 km northeast of Howell and 4 km north of U.S. highway 30S) .....<1.0
25. 9 km east-southeast of Cove Fort and 9 km east-northeast of Sulphurdale 1.9
25. 5 km north of Orangeville and 10 km southwest of Huntington[2] 1.6
25. Blue Springs Hills (10 km northeast of Howell and 4 km north of U.S. highway 30S) .....<1.0
25. 5 km northeast of Castle Gate[2] 2.8
26. 11 km east-southeast of Spring City .. 2.1
27. East margin of Canyon Mountains (3 km northeast of Williams Peak and 10 km northwest of Scipio) .....<1.0
28. 14 km east-northeast of Cove Fort ... 1.1
29. At Lakeside[2] .....<1.0
30. Tushar Mountains (4 km north-northwest of Mt. Belnap and 17 km west of Marysvale) 1.5
30. Blue Creek Valley (2 km south of Howell) .....<1.0
30. 4 km south-southwest of Howell and 11 km north of Thiokol and 1 km west of the north-south Howell-Thiokol road 1.0
30. 3 km southwest of Howell 1.5
31. Northern Stansbury Mountains (3 km southwest of Flux)[2] .....<1.0
31. Keg Mountains area (14 km east-northeast of Topaz Mountain and 18 km northwest of Fumerole Butte and 7 km northeast of the intersection of the east-west Trout Creek-Jericho road and the road going north to Dugway) 1.2
31. 9 km east of Sulphurdale 1.5

April Magnitude

1. East margin of Hansel Mountains (9 km southeast of Snowville and 1 km southwest of U.S. highway 30S) .....<1.0
1. Lakeside Mountains (11 km north-northeast of Low and 4 km east of north-south Low-Lakeside road)[2] 1.8
1. 9 km east of Sulphurdale 1.1
2. 4 km north-northeast of Manderfield .....<1.0
2. Hansel Mountains (16 km south-southwest of Snowville and 6 km southeast of Snowville-Locomotive Springs road) 1.2
2. 3 km north of Herriman and 6 km east-northeast of Lark .....<1.0
2. West Traverse Mountains (5 km southwest of Bluffdale) 1.7
2. Ditto--a second event .....<1.0
2. Ditto--a third event 1.0
3. Tushar Mountains--City Creek Peak area (11 km northwest of Junction and 7 km south-southwest of Alunite) 1.7
3. 4 km west-southwest of Echo .....<1.0
4. 11 km west of Huntington[2] 1.8
4. 1 km east of Lakeside[2] .....<1.0
5. East margin of Stansbury Mountains (7 km northwest of Grantsville and 5 km south of Flux) .<1.0
5. Blue Creek Valley (2 km east of Blue Creek) .....<1.0
5. 2 km northeast of Devils Slide[2] 1.2
6. Blue Springs Hills (7 km northeast of Blue Creek) .....<1.0
6. West margin of West Hills (11 km northeast of Blue Creek) .....<1.0
6. 11 km east of Cove Fort 1.8
7. Blue Springs Hills (6 km northeast of Blue Creek) .....<1.0
7. 10 km east-northeast of Cove Fort 1.9
8. 18 km east of Manderfield .....<1.0
10. 8 km west-southwest of Echo and 8 km south-southwest of Henefer 1.1
11. 20 km south of Minersville 1.4
12. Blue Springs Hills (9 km east of Howell and 2 km south of U.S. highway 30S) .....<1.0
12. 11 km east of Cove Fort 1.6
12. East margin of Stansbury Mountains (11 km south-southwest of Grantsville and 3 km west of St. John-Grantsville north-south road) 1.0
13. 11 km east of Cove Fort .....<1.0
14. 3 km east-northeast of Genola 1.1
15. 11 km east of Cove Fort 1.4
15. 1 km west of Devils Slide[2] 1.3
17. 4 km east of Sevier .....<1.0
18. 15 km south-southwest of Levan and 1 km east of Utah highway 28 ... 1.6
18. West Hills (8 km west-southwest of Portage and 5 km south of Utah-Idaho border) .....<1.0
19. 11 km east of Cove Fort 1.4
20. Utah highway 40 (6 km southeast of Timpie and 3 km northwest of Dolomite)[2] .....<1.0
20. 15 km west of Huntington[2] 1.9
20. 10 km east of Sulphurdale 1.4
22. Eastern Mineral Mountains (14 km northwest of Manderfield) ...<1.0
22. 1 km west of Devils Slide[2] .....<1.0
22. 11 km east of Cove Fort 1.5
23. 2 km southwest of Hatch 1.8
23. Tushar Mountains (17 km east-southeast of Manderfield) .....<1.0
24. West margin of Mineral Mountains--Roosevelt Hot Springs area (19 km northeast of Milford) 1.0
24. Eastern Mineral Mountains (13 km northwest of Manderfield) 1.0
25. 4 km northwest of Garfield .....<1.0
25. Lakeside Mountains (11 km north-northeast of Low and 6 km east of the Low-Lakeside road)[2] 1.3
26. On Union Pacific Railroad (2 km southwest of Latimer) 1.2
26. 14 km east of Sulphurdale 1.6
27. 2 km west of Lakeside[2] 1.2
27. 21 km south-southeast of Beaver and 6 km east of U.S. highway 91 and 3 km north of Utah highway 20 ..... 2.2
27. Fremont Wash (16 km south-southeast of Beaver and 3 km east of U.S. highway 91) 1.3
28. 7 km northeast of Magna .....<1.0
28. 8 km northeast of Milford 1.1
28. 9 km north-northeast of Cove Fort ..<1.0
28. 12 km east of Sulphurdale 1.6
28. 10 km east of Cove Fort .....<1.0
29 7 km east of Mount Pleasant 1.4
29. Eastern Stansbury Mountains (2 km south of Flux)[2] 1.2
29. 8 km southwest of Wanship 1.2
29. Weber River Canyon (5 km east of Morgan)[2] .....<1.0
29. 10 km east of Cove Fort 1.3
30. 10 km north-northwest of Milford .....<1.0

May Magnitude

2. North Promontory Mountains (14 km east of Snowville and 4 km south of Utah-Idaho border) ...<1.0
2. 10 km north of Central 1.4
3. West margin of Hansel Valley (18 km south of Snowville) 1.3
3. Tushar Mountains (13 km east of Sulphurdale) .....<1.0
3. 5 km northeast of Cove Fort .....<1.0
4. 12 km north-northeast of Cove Fort 1.7
4. 10 km east of Cove Fort 1.8
4. East margin of Stansbury Mountains (9 km west-northwest of Grantsville and 7 km south of Flux) 1.1

Magnitude

5. Northern Hansel Valley (11 km west of Blue Creek and 16 km southeast of Snowville; on north-south road 4 km south of the intersection of north-south road and U.S. highway 30S) 1.0
5. Great Salt Lake (13 km west-northwest of south end of north-south road at Rozel Point and 17 km east of middle of Dolphin Island) 1.5
5. 2 km southwest of Cornish 1.2
6. 4 km south of Porterville ..... <1.0
6. Tushar Mountains (11 km east of Sulphurdale) 1.5
7. Northern East Canyon Reservoir (9 km southeast of Porterville) ..... <1.0
7. 11 km north-northeast of Cove Fort ..... <1.0
7. 2 km south of Cove Fort ..... <1.0
7. Antelope Range (11 km northeast of Newcastle) 1.9
7. 3 km east of Cove Fort ..... <1.0
7. 3 km east of Cove Fort 1.3
8. 11 km north-northeast of Cove Fort ..... <1.0
9. Hansel Mountains (12 km south of Snowville) 1.5
9. 12 km west-northwest of Huntington[2] 2.5
9. 13 km east-northeast of Alunite 1.3
9. 6 km east of Marysvale 1.1
10. 1 km southeast of Lakeside[2] 1.1
11. 3 km southwest of Joseph ..... <1.0
11. East margin of Tushar Mountains (4 km southwest of Marysvale) ..... <1.0
11. 10 km east of Cove Fort 1.6
12. Southern Blue Springs Hills (6 km east-northeast of Thiokol) 1.3
12. Northern Valley Mountains (9 km northeast of Scipio) 1.1
12. 2 km north-northwest of Devils Slide[2] 1.3
12. 11 km east-northeast of Liberty ..... <1.0
12. 11 km east-northeast of Liberty 1.5
13. Blue Springs Hills (7 km northeast of Blue Creek) ..... <1.0
13. Circleville Mountain (20 km east-southeast of Beaver) 1.1
14. 11 km north-northeast of Cove Fort ..... <1.0
14. 17 km northwest of Huntington[2] 2.1
14. 2 km north of Ruins and 6 km northwest of Mills 1.0
14. 1 km south of Ruins and 4 km west-northwest of Mills 1.7
14. East branch of Logan River (12 km west-northwest of Garden City and 2 km south of Utah-Idaho border) ..... <1.0
14. West margin of San Pitch Mountains (15 km southeast of Mills and 4 km east of Utah highway 28) 1.1

Magnitude

15. West Hills (11 km east-northeast of Blue Creek) ..... <1.0
15. Blue Springs Hills (6 km east-northeast of Blue Creek) ..... <1.0
16. 8 km east of Cove Fort 1.0
18. North end of Blue Springs Hills (8 km northeast of Blue Creek) 1.4
19. The Three Peaks area (10 km north of Iron Springs and 4 km west-southwest of Cedar City-Lund road)[2] 1.4
20. Southern Blue Springs Hills (6 km east-northeast of Thiokol ..... <1.0
20. 9 km east-northeast of Sulphurdale and 9 km east-southeast of Cove Fort 1.6
21. Paunsaugunt Plateau (19 km east-northeast of Long Valley Junction and 15 km southeast of Hatch) 1.3
22. Blue Springs Hills (6 km east-northeast of Blue Creek) ..... <1.0
22. Blue Springs Hills (4 km east of Blue Creek) ..... <1.0
22. 6 km west of East Canyon Reservoir and 10 km south of Porterville 1.8
23. Blue Springs Hills (9 km east-southeast of Howell and 4 km south of U.S. highway 30S) <1.0
24. 8 km north-northwest of Mill Fork and 14 km east-northeast of Thistle 1.2
25. 5 km north-northwest of Orangeville[2] 2.0
25. Lakeside Mountains (13 km north-northeast of Low and 5 km east of north-south Low-Lakeside road)[2] 1.6
26. Blue Creek Valley–on U.S. highway 30S (4 km northeast of Howell) ..... <1.0
27. Bear River Range (10 km east-northeast of Richmond and 10 km east-southeast of Cove) ..... <1.0
27. 13 km east of Cove Fort 1.8
27. East margin of Iron Mountain (21 km west-southwest of Cedar City and 15 km east-southeast of Newcastle and 2 km north of the east-west Utah highway 56)[2] 1.2
28. West margin of Bear River Range (6 km east-northeast of Richmond and 6 km east-southeast of Cove) 1.2
28. West margin of Bear River Range (8 km east-northeast of Richmond and 7 km east-southeast of Cove) 1.2
28. West margin of Bear River Range (7 km east-northeast of Richmond and 7 km east-southeast of Cove) ..... <1.0
28. 6 km south-southeast of Alunite and 1 km east of U.S. highway 89 ..... 1.0
28. West margin of Bear River Range (7 km east-northeast of Richmond and 7 km east-southeast of Cove) ..... <1.0
28. 2 km east of Cove Fort ..... <1.0

Magnitude

29. West margin of Bear River Range (6 km east-northeast of Richmond and 6 km east-southeast of Cove) 1.2
30. 3 km east-southeast of Cove Fort ..... <1.0
31. 8 km west of Burrville ..... <1.0
31. North margin of Granite Mountain (2 km south of Iron Springs)[2] 1.3

June

Magnitude

1. Blue Creek Valley (3 km south of Howell) ..... <1.0
1. 1 km northeast of Lakeside[2] 1.0
1. 2 km west of Devils Slide[2] ..... <1.0
2. Tushar Mountains (23 km east of Beaver) ..... <1.0
2. East margin of Tushar Mountains (7 km west-southwest of Marysvale) ..... <1.0
2. 2 km north of Santaquin 1.6
3. 11 km east-southeast of Kenilworth[2] 3.0
3. Tushar Mountains (14 km east of Sulphurdale) 1.6
4. North end of Blue Springs Hills (7 km northeast of Blue Creek) 1.8
4. At Monroe ..... <1.0
5. Bear River Range (12 km east-southeast of Logan and 5 km south of Logan River) ..... <1.0
6. South central part of Bear Lake (4 km southeast of Pickleville) ..... <1.0
7. 12 km north-northeast of Cove Fort 2.0
8. 8 km north of Cove Fort 1.0
8. Ditto--a second event ..... <1.0
8. Ditto--a third event 1.0
9. Blue Springs Hills (6 km southeast of Blue Creek) ..... <1.0
9. 13 km southeast of Beaver ..... <1.0
10. Blue Springs Hills (6 km southeast of Blue Creek) ..... <1.0
10. Ditto--a second event ..... <1.0
10. Blue Springs Hills (7 km southeast of Blue Creek) 1.0
10. Blue Springs Hills (8 km east-southeast of Blue Creek) 1.3
10. Tushar Mountains (13 km east-southeast of Sulphurdale) 1.6
11. 11 km east of Alunite 1.1
11. 3 km west of Devils Slide[2] 1.1
11. 2 km east of Sulphurdale 1.2
11. 3 km east of Cove Fort ..... <1.0
12. 12 km north of Cove Fort 1.4
12. Fremont Wash (21 km south of Beaver and 3 km northeast of junction of U.S. highway 91 and Utah highway 20) 1.3
12. North end of Hansel Valley (11 km southeast of Snowville and 2 km north of U.S. highway 30S) ..... <1.0
12. Ditto–a second event ..... <1.0
13. 2 km east-northeast of Marysvale ..... <1.0
15. 1 km north of Sulphurdale 1.3
15. Tushar Mountains--Delano Peak area (6 km west of Alunite) 1.9

Magnitude

15. 4 km southwest of Pickleville 1.0
15. 10 km east of Mills 2.0
16. North end of Hansel Valley (12 km southeast of Snowville and 2 km north of U.S. highway 30S) 1.3
16. East margin of Hansel Mountains (10 km southeast of Snowville and 2 km south of U.S. highway 30S 1.0
16. North end of Hansel Valley (2 km southeast of Snowville and 2 km north of U.S. highway 30S) 1.8
17. 13 km east of Cove Fort 2.0
18. 10 km east of Coalville 1.6
18. 6 km northwest of Cove Fort 2.3
19. East margin of Hansel Mountains (9 km southeast of Snowville and 2 km south of U.S. highway 30S) 1.8
20. North end of Hansel Valley (2 km southeast of Snowville and 2 km north of U.S. highway 30S) 1.0
21. South central Bear Lake (4 km southeast of Pickleville) .....<1.0
21. 10 km east of Cove Fort 1.3
22. East margin of San Pitch Mountains (10 km west-northwest of Ephraim) .. 1.5
22. South end of Pocatello Valley (19 km east of Snowville and 3 km south of Utah-Idaho border) .....<1.0
22. North end of Blue Creek Valley (20 km east-southeast of Snowville and 5 km south of Utah-Idaho border)<1.0
22. Lakeside Mountains (13 km north-northeast of Low and 6 km east of north-south Low-Lakeside road)[2] 1.9
23. 2 km south of Flux[2] .....<1.0
24. West edge of Bear Lake (2 km south of Garden City) .....<1.0
24. 8 km east-northeast of Cove Fort 1.3
27. North end of Hansel Valley (12 km southeast of Snowville and 2 km north of U.S. highway 30S) 1.6
28. 1 km north of Henefer[2] .....<1.0
28. West margin of Bear River Range (4 km southeast of Richmond) .....<1.0
29. 1 km north of Henefer[2] 1.1

Table 1. Number of probable rockbursts - January 1, 1977 through June 30, 1977.

Date	January	February	March	April	May	June
1	3			2	2	2
2	5	2	3	1	5	2
3		1	4	2	8	6
4	2	3	2	3	3	3
5	2	3	6	3	6	4
6	5	4	3	2	4	2
7	6	2	2		5	3
8	6		1	2	2	1
9		1	3	1	2	1
10	2	1	3	4	3	5
11	2	2	6		8	6
12	2	4	1	3	2	
13	1	1	1	2	4	
14	1	2	2	1	6	
15		1	1	5	3	4
16	1	2	3	3	6	4
17	2	2	1	1	1	3
18	3		2	4	3	1
19	3		4	1	2	5
20	1	4	7	1	1	1
21	3	2	2	1		3
22	2	2	2	1		4
23			6	1		6
24	2	3	8	1		3
25	2		2	1		2
26	2		3	1		2
27	3	1		3		4
28	2	1	1	2		2
29	5		6		4	4
30	3		3	2	5	4
31			4			
Total	71	44	92	54	85	87

PROBABLE ROCKBURSTS

Seismic events (total of 433) during January through June, 1977, in the coal-mining areas of Carbon County, Utah–in particular, the Sunnyside-East Carbon City-Columbia region– are listed separately (table 1) in terms of the number of events each day. These events are interpreted as "probable rockbursts," although some may be earthquakes; no attempt was made to distinguish these two types of events. The interpretation of these events was based on the paper seismograms of the Price, Utah (PCU) seismograph station, the nearest recording station.

ACKNOWLEDGMENTS

Seismic monitoring in Utah is carried out as part of an earthquake research program at the University of Utah involving S. H. Ward, R. B. Smith, W. J. Arabasz, W. D. Richins, K. L. Cook, and numerous staff members of the University of Utah Seismograph Stations. Earthquakes during this report period were routinely located by W. D. Richins, G. M. Hathaway, J. C. Murphey, J. G. McReynolds, and C. E. Hill. Financial support for the operation of the seismograph stations and the compilation of the data was provided by the National Science Foundation, the U.S. Geological Survey, the Utah Geological and Mineral Survey, and Utah state funds from the Utah Legislature as a line-item budget to the University of Utah.

Information concerning "felt" earthquakes in or near the Blue Creek Valley area and the Huntington-Orangeville area was provided by people residing in those areas, too numerous to mention individually, who filled out and returned questionnaires circulated to them by the University of Utah Seismograph Stations.

Appropriations No. 01-61-03
Archives Approval No. 7800091

UTAH GEOLOGICAL AND MINERAL SURVEY

606 Black Hawk Way
Salt Lake City, Utah 84108

THE UTAH GEOLOGICAL AND MINERAL SURVEY is a Division of the Utah Department of Natural Resources and operates under the guidance of a Governing Board appointed by the Governor from industry and the public-at-large. The Survey is instructed by law to collect and distribute reliable information concerning the mineral resources, topography, and geology of the state, to investigate areas of geologic and topographic hazards that could affect the citizens of Utah, and to support the development of natural resources within the state. The *Utah Code Annotated, 1953 Replacement Volume 5, Chapter 36, 53-36-1 through 12,* describes the Survey and its functions.

The Survey publishes bulletins, maps, a quarterly newsletter, and a biannual journal that describe the geology of the state. Write for the latest list of publications available.

The Survey also sells the colored geologic map of Utah (Army Map Service base, 1:250,000, in four quarters), a project of the College of Mines and Mineral Industries of the University of Utah from 1961 through 1964. It acts as sales agent for publications of the Utah Geological Association and its predecessor organizations, the Utah Geological Society, the Intermountain Association of Geologists, and the Intermountain Association of Petroleum Geologists.

THE SAMPLE LIBRARY is maintained to preserve well cuttings, drill cores, stratigraphic sections, and other geological samples. Files of lithologic, electrical, and mechanical logs of oil and gas wells drilled in the state are also maintained. The library's collections have been obtained by voluntary donation and are open to public use, free of charge.

THE UTAH GEOLOGICAL AND MINERAL SURVEY adopts as its official policy the standard proclaimed in the Governor's Code of Fair Practices that it shall not, in recruitment, appointment, assignment, promotion, and discharge of personnel, discriminate against any individual on account of race, color, religious creed, ancestry, national origin, or sex. It expects its employees to have no interest. financial or otherwise, that is in conflict with the goals and objectives of the Survey and to obtain no personal benefit from information gained through their work as employees of the Survey. For permanent employees this restriction is lifted after a one-year absence and for consultants the same restriction applies until publication of the data they have acquired.